GEOSPHERE

CORRESPONDENCE: cjbusby@ucdavis.edu

GOLD
OA
OPEN ACCESS

THE GEOLOGICAL SOCIETY
OF AMERICA®

A tale of two Walker Lane pull-apart basins in the ancestral Cascades arc, central Sierra Nevada, California

Cathy J. Busby[1], K. Putirka[2], Benjamin Melosh[3], Paul R. Renne[4,5], Jeanette C. Hagan[6], Megan Gambs[7], and Catherine Wesoloski[1]

[1]Department of Earth and Planetary Science, University of California, Davis, California 95616, USA
[2]Department of Earth and Environmental Sciences, California State University, Fresno, California 93720, USA
[3]U.S. Geological Survey, Menlo Park, California 94025, USA
[4]Berkeley Geochronology Center, 2455 Ridge Road, Berkeley, California 94709, USA
[5]Department of Earth and Planetary Science, University of California, Berkeley, California 94720, USA
[6]Exxon Mobil, Houston, Texas 77389, USA
[7]School of Oceanography, University of Washington, Seattle, Washington 98105, USA

ABSTRACT

We integrate new geochronological, petrographic, and geochemical data with previously published (Sierra Crest–Little Walker volcanic center) and new (Ebbetts Pass volcanic center) structural and stratigraphic data to describe two deeply dissected, spectacularly well-exposed Walker Lane pull-apart basins in the ancestral Cascades arc. The Miocene (ca. 12–5 Ma) Sierra Crest–Little Walker arc volcanic center and the Miocene–Pliocene (ca. 6–4.6 Ma) Ebbetts Pass arc volcanic center formed in pull-apart basins in the Walker Lane, a NNW-trending zone of dextral strike-slip and oblique normal faults at the western edge of the Basin and Range Province. The Sierra Crest–Little Walker arc volcanic center is a transtensional arc volcanic field that is as areally extensive (~4000 km²) and as long-lived (~3 m.y.) as the Pliocene to Holocene Long Valley transtensional rift volcanic field, which is also in the Walker Lane. The Ebbetts Pass volcanic center is the next major volcanic center to the north within the ancestral Cascades arc. It formed within a smaller pull-apart basin. Its estimated original volume (~270 km³) is comparable to the estimated volume for the Lassen volcanic center in the last 825 k.y. (200 km³), a major magmatic focus in the northernmost Walker Lane pull-apart basin. Postvolcanic faulting and erosion provide spectacular three-dimensional time-integrated views of the structure and stratigraphy of the Miocene to Pliocene volcanic centers described herein. The volcanic stratigraphy of this region is divided into four unconformity-bounded sequences: (1) Oligocene silicic ignimbrites erupted in central Nevada (Valley Springs Formation), (2) Miocene arc volcanic and volcaniclastic rocks (Relief Peak Formation), (3) ca. 11.5–9 Ma high-K arc volcanic rocks (Stanislaus Group), and (4) Miocene–Pliocene arc volcanic rocks (Disaster Peak Formation). We present 19 new $^{40}Ar/^{39}Ar$ ages and integrate them with previous $^{40}Ar/^{39}Ar$ ages to erect a detailed stratigraphic and intrusive chronology. For the first time, we present a systematic description of all of the volcanic and intrusive map units, using outcrop photos, photomicrographs, modal analyses, and geochemical data.

Geochemistry and modal analyses show that volcanism at the younger, smaller Ebbetts Pass volcanic center is more evolved than that of the Sierra Crest–Little Walker volcanic center. The Sierra Crest–Little Walker volcanic center is dominated by Stanislaus Group basalt, trachybasaltic andesite, trachyandesite, and andesite. Climactic eruptions at its southern end produced the Little Walker caldera and its Stanislaus Group trachydacite ignimbrites. In contrast, the Ebbetts Pass volcanic center erupted much less basalt, and an approximately equal mixture of basaltic andesite, andesite, dacite, and rhyolite. By virtue of its higher SiO_2, on average, it shows geochemical evidence for higher extents of crustal contamination. All of the volcanic rocks except the Stanislaus Group are compositionally identical to Mesozoic plutonic rocks of the Sierra Nevada Batholith, indicating a similar petrogenesis by shallow-level fractional crystallization with no evidence for deep-seated pyroxenite cumulates. Only the high-K_2O Stanislaus Group requires a significant degree of fractionation of clinopyroxene and Fe-Ti oxides. The major-oxide trends and clinopyroxene-rich modes of the Stanislaus Group may be the volcanic expression of processes that produced pyroxenite cumulates. The basal and most voluminous unit of the Stanislaus Group, the Table Mountain Latite, is a likely parent to succeeding units of the Stanislaus Group (Eureka Valley Tuff and Dardanelles Formation), but this particular liquid line of descent is otherwise rare in the Mesozoic and Cenozoic history of the Sierra Nevada.

Volcano-tectonic activity continued for a longer period (ca. 12–6 Ma) in the northern half of the Sierra Crest–Little Walker volcanic center than it did in the southern half (ca. 12–9 Ma), overlapping for ~1 m.y. with the onset of volcano-tectonic activity at the Ebbetts Pass volcanic center to the north. This provides local-scale confirmation of the regional-scale interpretation that a transtensional rift tip propagated northward with time within the arc axis, in concert with northward migration of the Mendocino triple junction. Transtensional rift magmatism followed in its wake and continues today at various points along the length of the Walker Lane. "Tectono-stratigraphic recycling" was a key geologic process throughout the development of these ancestral Cascades arc pull-apart basins, and it consisted of the transfer of megaslide slabs, up to 2 km long and tens to hundreds of meters thick, from footwall to hanging-wall blocks in the transtensional rift. A time-slice series of block diagrams is used to illustrate the structural controls on arc volcanism in the early stages of Walker Lane transtensional faulting (ca. 12–4.6 Ma).

■ INTRODUCTION

The Sierra Nevada (California) forms an asymmetrical block-faulted mountain range with a gentle western slope and a steep fault-bounded range front on the east. The steep eastern range front was previously interpreted to be the result of Basin and Range extension (Bateman and Wahraftig, 1966; Slemmons, 1953, 1966). However, it is now known to form the western boundary of the Walker Lane, an ~100-km-wide, NNW-trending zone of dextral strike-slip and oblique normal faults that lies along the western edge of the Basin and Range Province (e.g., Faulds and Henry, 2008; Jayko and Bursik, 2012; Busby, 2013). The Walker Lane accommodates ~20%–30% of the right-lateral motion between the Pacific and North American plates (Argus and Gordon, 1991; Dixon et al., 2000; Oldow, 2003; Unruh et al., 2003; John et al., 2012). This region has been described as the northernmost extension of the Gulf of California transtensional rift, where the process of continental rupture has not yet been completed, and rift initiation can be studied on land (Faulds and Henry, 2008; Jayko and Bursik, 2012; Busby, 2013). The northern and southern segments of the Walker Lane are dominated by translation along long NNW-trending dextral strike-slip faults (Faulds and Henry, 2008; Jayko and Bursik, 2012; Busby, 2013). In contrast, the central Walker Lane (Fig. 1) shows evidence of distributed dextral shear accommodated by oblique-normal faults, block rotations, and partitioning of oblique deformation between subparallel normal and strike-slip faults (e.g., Wesnousky, 2005; Dong et al., 2014; Bormann et al., 2016).

Faults of the central Walker Lane strike approximately NE, as well as approximately N-S (Fig. 1). The Carson domain, along the northern boundary of the central Walker Lane, has numerous ENE-striking faults with oblique sinistral-normal slip, and clockwise block rotations of up to 44°–90° measured on volcanic rocks (Cashman and Fontaine, 2000; Faulds and Henry, 2008; Kreemer et al., 2009). The Mina deflection, along the southern margin of the central Walker Lane, is a regional-scale releasing bend consisting of ENE-striking sinistral-oblique, sinistral, and normal faults (Ryall and Priestly, 1975; Oldow, 1992, 2003; Wesnousky, 2005; Faulds and Henry, 2008; Oldow et al., 2008; Lee et al., 2009a, 2009b; Jayko and Bursik, 2012). Series of basins have opened up along the Mina deflection from the middle Miocene to the present day (Oldow et al., 1994, 2001, 2009; Stockli et al., 2003; Lee et al., 2009a; Ferranti et al., 2009; Tincher and Stockli, 2009). Like the Carson domain, the Mina deflection shows paleomagnetic evidence of clockwise vertical-axis block rotations (Petronis et al., 2004, 2007, 2009, 2016; Gledhill et al., 2016). Clockwise block rotations of up to 55° also occur in the region between the Carson domain and the Mina deflection (Carlson et al., 2013; Carlson and Faulds, 2015, 2016). This includes clockwise rotations of ~18° in volcanic rocks on the Sierran frontal fault zone just north of the Little Walker caldera (Figs. 1 and 2A), described herein and by Pluhar et al. (2009) and Carlson et al. (2013). Geodetically determined rates of rotation (Bormann et al., 2016) appear to underestimate the contribution of vertical-axis rotation determined by paleomagnetic studies, perhaps because fault-bounded, rotated blocks are significantly smaller than the regional-scale blocks presented in geodetic models (Carlson, 2017). Additionally, the importance of vertical-axis rotations along the western boundary of the central Walker Lane has been severely underevaluated (Carlson, 2017); the stratigraphic and structural results described herein are ideal for future studies on this.

The Carson domain and Mina deflection represent very large right steps in the central Walker Lane, ~60 km and 90 km, respectively, with vertical-axis rotations described above. In this paper, we describe smaller right steps along the western edge of the central Walker Lane (Fig. 1 and 2A): an ~15 km right step, referred to herein as the Sierra Crest–Little Walker pull-apart, and an ~5 km zone of right-stepping faults, referred to herein as the Ebbetts Pass pull-apart. This paper describes Oligocene through Pliocene volcanic sections that will be appropriate for much-needed paleomagnetic assessment of the importance of vertical-axis rotations. In this paper, we demonstrate the controls of these faults on two large volcanic centers that formed in the pull-apart basins.

The central Walker Lane (Fig. 1) has more abundant Cenozoic volcanic rocks than the northern and southern Walker Lane, probably because it lies at a higher rift angle relative to the overall plate margin (Busby, 2013). The abundant volcanic rocks make the central Walker Lane ideal for detailed reconstructions of transtensional rifting and magmatism in a continental setting, because the volcanic strata are dateable by the $^{40}Ar/^{39}Ar$ method (e.g., Busby et al., 2008a, 2008b, 2013a, 2013b, 2016; Hagan et al., 2009; Nagorsen-Rinke et al., 2013; Fleck et al., 2015). Our studies have focused on the western margin of the central Walker Lane along the central Sierra Nevada range front and range crest (Fig. 1). There, Cenozoic volcanic and volcaniclastic rocks are extensive and are spectacularly well exposed in three dimensions over rugged topography with high structural relief. This provides the opportunity to study the structural controls on volcano-tectonic basins, vents, and plumbing systems as they relate to preserved eruptive units.

In this paper, we describe two volcanic centers sited in ancestral Cascades arc pull-apart basins in the central Walker Lane: (1) the ca. 12–9 Ma Sierra Crest–Little Walker volcanic center, and (2) the ca. 6–4.6 Ebbetts Pass volcanic center. The Miocene (ca. 12–9 Ma) Sierra Crest–Little Walker volcanic center is a transtensional volcanic system, and it is as areally extensive (~4000 km²) and long-lived (~3 m.y.) as the Pliocene to recent Long Valley transtensional rift volcanic center (Busby, 2012; Busby et al., 2013a, 2013b). The Sierra Crest–Little Walker volcanic center also forms the largest volcanic center recognized to date in the ancestral Cascades arc, and it records the birth of the Walker Lane "future plate boundary" within the arc at ca. 12–9 Ma (Busby, 2013). The Ebbetts Pass volcanic center is the next major ancestral Cascades arc volcanic center to the north, and we show herein that it formed within a smaller Walker Lane pull-apart basin in Miocene to Pliocene time. An estimated original volume of ~270 km³ for the Ebbetts Pass volcanic center is comparable to that estimated by Hildreth (2007) for the Lassen transtensional arc volcanic center in the last 825 k.y. (200 km³). The main difference between the Miocene to Pliocene volcanic fields described herein and the more well-studied, active volcanic fields of the Walker Lane is that the Miocene to Pliocene volcanic fields are dissected to the ideal level for viewing the structural controls on volcanism and sedimentation over a period of ~8 m.y.
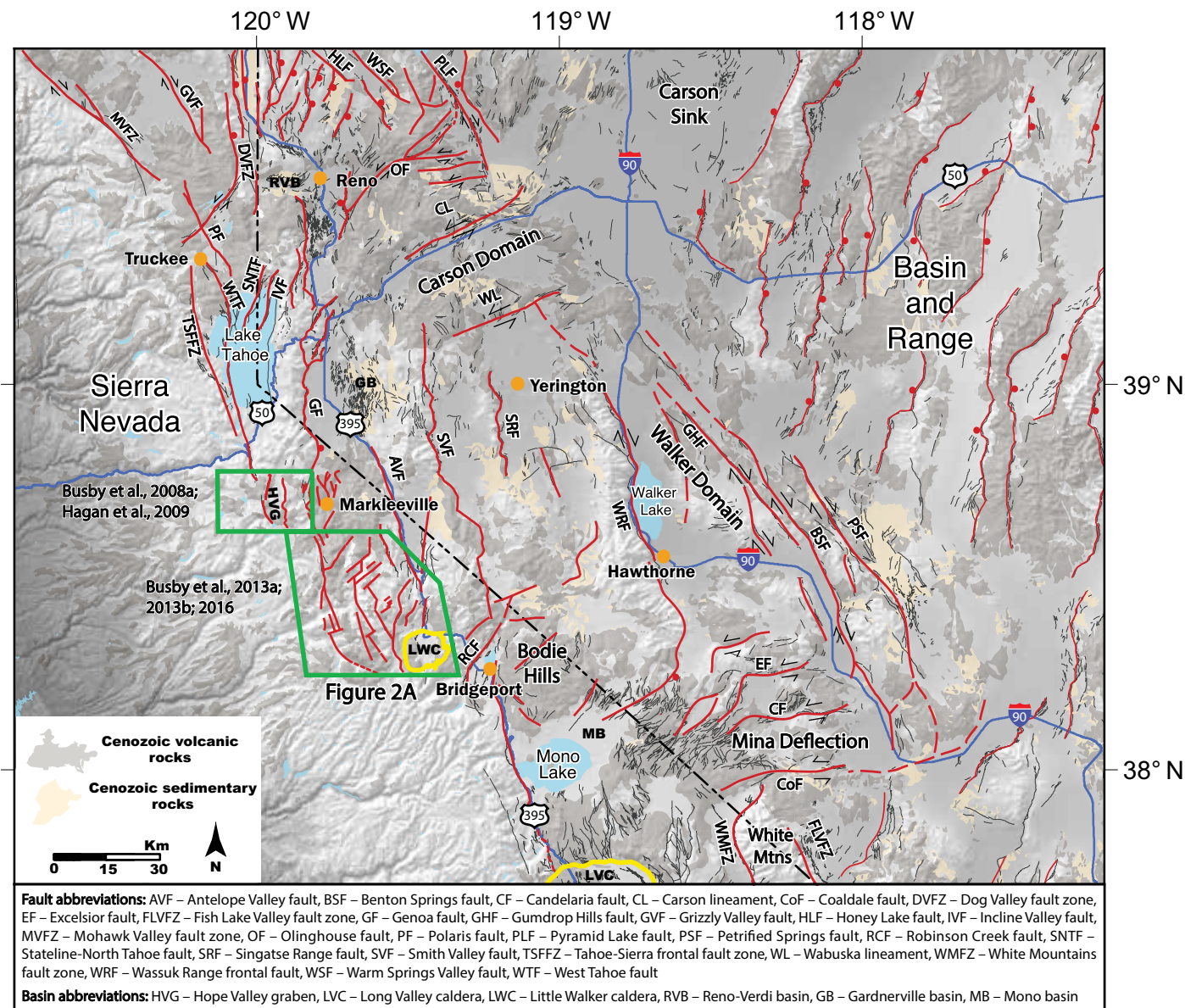
Figure 1. Central Walker Lane and adjacent areas, showing Cenozoic volcanic and sedimentary rocks and faults, modified from Faulds and Henry (2008), Wesnousky et al. (2012), and Bormann et al. (2016). Additional map data are from Kent et al. (2005), Crafford (2007), Hunter et al. (2011), Cashman et al. (2009, 2012), Jayko and Bursik (2012), John et al. (2012), Carlson et al. (2013), Nagorsen-Rinke et al. (2013), Carlson and Faulds (2014), and John et al. (2015a, 2015b). This is the first published Walker Lane compilation map to show faults of the Walker Lane pull-apart basins described in this paper, outlined in the box labeled Fig. 2A (Busby et al., 2013a, 2013b, 2016). Our compilation map also includes our Walker Lane faults mapped to the north at Carson Pass (Hagan et al., 2009), shown on Figure 4.
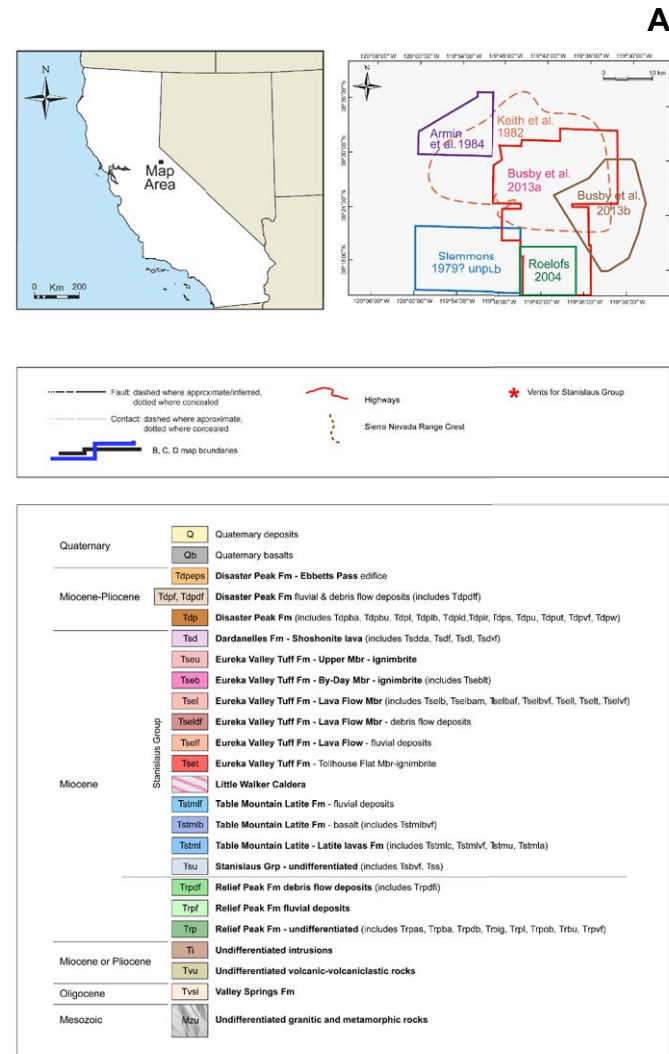
Inside figure:

Fault abbreviations: AVF – Antelope Valley fault, BSF – Benton Springs fault, CF – Candelaria fault, CL – Carson lineament, CoF – Coaldale fault, DVFZ – Dog Valley fault zone, EF – Excelsior fault, FLVFZ – Fish Lake Valley fault zone, GF – Genoa fault, GHF – Gumdrop Hills fault, GVF – Grizzly Valley fault, HLF – Honey Lake fault, IVF – Incline Valley fault, MVFZ – Mohawk Valley fault zone, OF – Olinghouse fault, PF – Polaris fault, PLF – Pyramid Lake fault, PSF – Petrified Springs fault, RCF – Robinson Creek fault, SNTF – Stateline-North Tahoe fault, SRF – Singatse Range fault, SVF – Smith Valley fault, TSFFZ – Tahoe-Sierra frontal fault zone, WL – Wabuska lineament, WMFZ – White Mountains fault zone, WRF – Wassuk Range frontal fault, WSF – Warm Springs Valley fault, WTF – West Tahoe fault

Basin abbreviations: HVG – Hope Valley graben, LVC – Long Valley caldera, LWC – Little Walker caldera, RVB – Reno-Verdi basin, GB – Gardnerville basin, MB – Mono basin
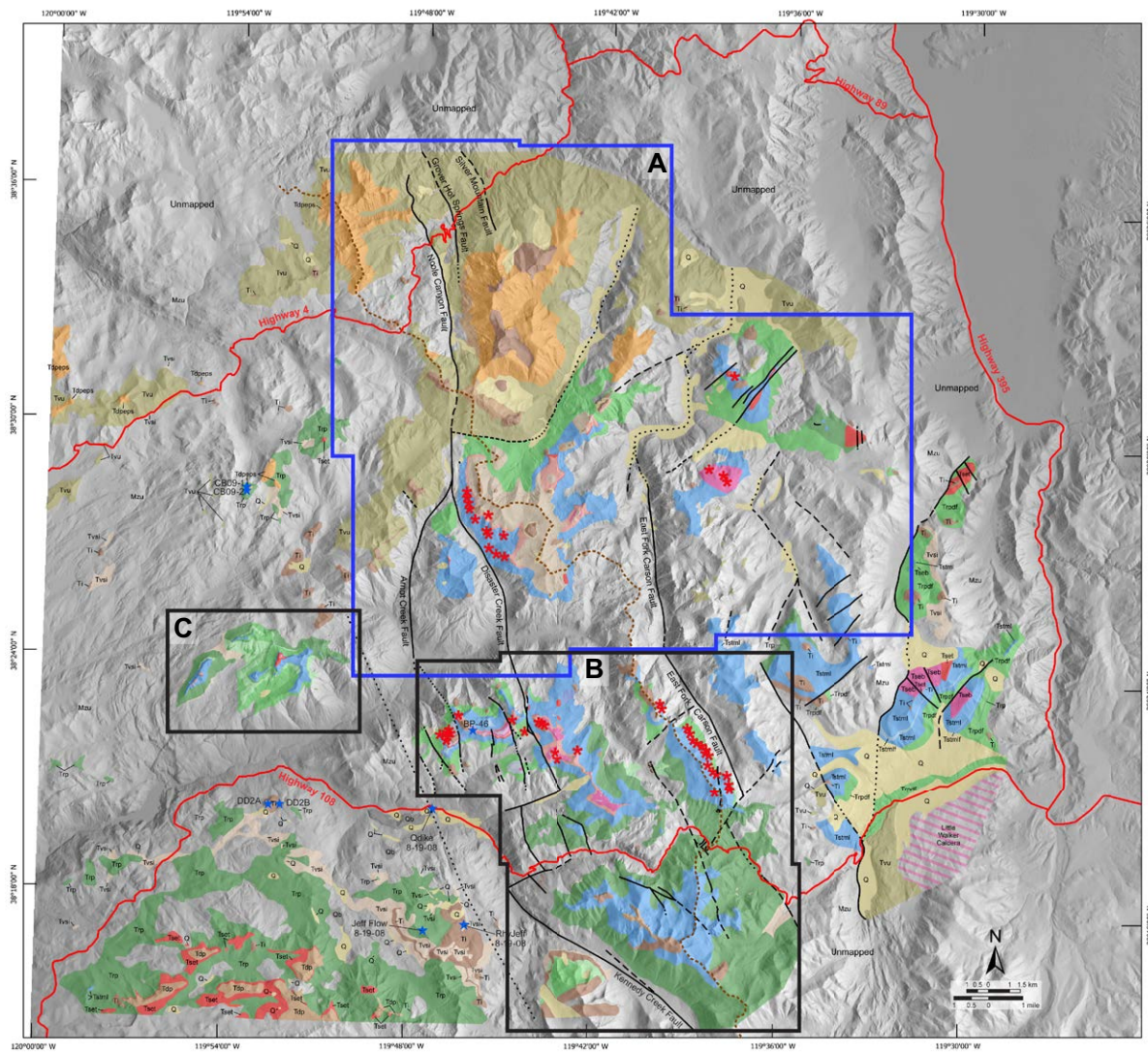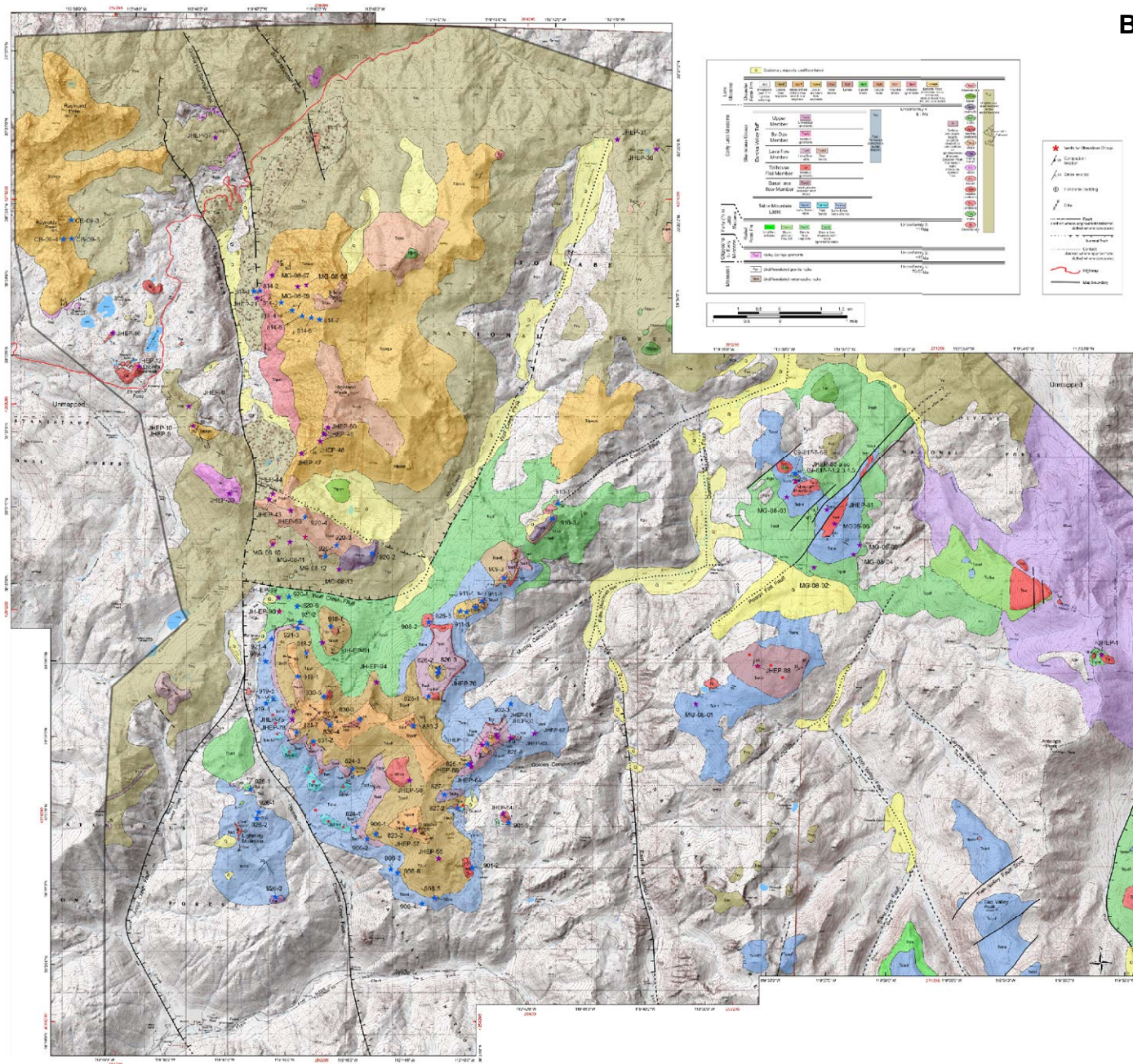
Figure 2 (*on this and following page*). (A) Generalized geologic map of Tertiary rocks of the Sonora Pass to Ebbetts Pass area, central Sierra Nevada, from Busby et al. (2016). Location is on Figure 1. All mapping was done by Busby and her graduate students (Jeanette Hagan, Alice Koerner, Ben Melosh, Dylan Rood) and her postdoctoral researcher (Graham Andrews) between 2001 and 2012, drawing on previous work by Slemmons (1953), an unpublished 1979 map provided to Busby by Slemmons, Keith et al. (1982), Huber (1983a, 1983b), Armin et al. (1984), and Roelofs (2004). Insets on upper right show location and previous mapping. Red stars highlight vents for Stanislaus Group volcanic rocks. Map unit contacts and labels are not drawn in the boxed areas of this generalized map because it is so reduced; instead, a detailed map of area A is shown in Figure 2B, and detailed maps of areas B and C were published in Busby et al. (2016). Some samples discussed in this paper lie outside the area of Map A and are plotted here. To view the full-sized version of this map, please visit https://doi.org/10.1130/GES01398.m1 or the full-text article on www.gsapubs.org.

To view the full-sized version of this map (Fig. 2A), please visit https://doi.org/10.1130/GES01398.m1 or the full-text article on www.gsapubs.org.

Figure 2 (*continued*). (B) Detailed geologic map of the Ebbetts Pass region. Location is on Figure 2A. This map plots the locations of most of the samples described in this paper, although several samples collected outside this map area are plotted on Figure 2A. The geology in the north half of the map (Highland Peak–Ebbetts Pass–Raymond Peak area) is described for the first time in this paper. The geology of the Lightning Mountain–Arnot Peak–Disaster Peak–Mineral Mountain area was described in detail by Busby et al. (2013a). This paper describes the petrography, geochemistry, and geochronology of volcanic and intrusive rocks from this map area, divided into three volcanotectonic suites: (1) the ca. 12–9 Ma Sierra Crest–Little Walker volcanic center and pull-apart basin, shown in greens, blues, lavender, and red; (2) the ca. 9–5 Ma Disaster Peak Formation in the Sierra Crest graben-vent system, shown in browns and oranges in the southern half of the map; and (3) the ca. 6.4–4.6 Ebbetts Pass pull-apart basin and volcanic center, shown in browns and oranges in the north part of the map. To view the full-sized version of this map, please visit https://doi.org/10.1130/GES01398.m2 or the full-text article on www.gsapubs.org. Red stars—samples collected by Jeanette Hagan (JHEP) and Megan Gambs (MG), respectively. Blue stars—samples collected by Ben Melosh. Black dots—samples collected by Cathy Busby. Global positioning system (GPS) coordinates of samples are given in Supplemental Files (see text footnote 1).

To view the full-sized version of this map (Fig. 2B), please visit https://doi.org/10.1130/GES01398.m2 or the full-text article on www.gsapubs.org.

For the first time, this paper presents photomicrographs and modal analyses on rocks of the Sierra Crest–Little Walker volcanic center and integrates these with whole-rock geochemical data. We also present a new map, and new structural, stratigraphic, petrographic, and geochronologic data on the Ebbetts Pass volcanic center. These are integrated into time-slice block diagrams that describe the evolution of the central Sierra segment of the ancestral Cascades arc as a series of northward-migrating, transtensional, intra-arc pull-apart basins in the Walker Lane.

Our geochemical data show that arc volcanism was most primitive where transtension was areally extensive, in the Sierra Crest–Little Walker volcanic center, and of largest volume, in the southern part of that center. A higher degree of crustal contamination at the Ebbetts Pass pull-apart is attributed to its much smaller size, with probable lower extension rates on faults that may not have all penetrated the lithosphere, leading to lower rates of basalt intrusion. Magmatism and transtension gradually migrated northward in time from the southern half of the Sierra Crest–Little Walker volcanic center into its northern half, and then northward into the Ebbetts Pass volcanic center, as part of a regional-scale northward migration of the rift tip, in concert with northward migration of the Mendocino triple junction.

■ STRATIGRAPHIC FRAMEWORK FROM PALEOCHANNEL FILLS

Prior to our mapping shown in Figures 2A and 2B, the Cenozoic stratigraphy of the region described herein was best known from paleochannel fills in the unfaulted part of the Sierra Nevada west of the crest (Fig. 3). This was described in detail by Busby et al. (2016), and we refer the reader to dozens of references to previous work cited there. In this section, we provide a brief review of Sierran paleochannels, and we describe the relatively simple stratigraphy preserved in largely unfaulted paleochannels of the region west of the pull-apart basins (Fig. 2A). This provides a basis for describing the much more complex and faulted stratigraphy in the two volcanic centers described herein.

Paleochannels of the Sierra Nevada were first exploited for placer gold deposits during the California Gold Rush that began in 1848. Then, more than a century ago, they were mapped in surveys that showed that they flowed westward, like the modern rivers of the range (Ransome, 1898; Lindgren, 1911). These studies assumed that the heads of the paleochannels lay at the modern range crest. A first paradigm shift occurred about a half century ago, when it was recognized that at least some of the paleochannel fill was sourced from Nevada, showing that the range was younger than the paleochannels (younger than 6 Ma; Slemmons, 1953; Curtis, 1954; Bateman and Wahraftig, 1966; cf. Wakabayashi, 2013). More recent work has demonstrated that Sierran paleochannels are ancient features that were carved into the shoulder of a broad high uplift formed during Late Cretaceous to Paleocene crustal shortening (the Nevadaplano). Their headwaters lay in central Nevada prior to disruption of the Nevadaplano by Basin and Range extension (cf. Henry, 2008; Henry et al., 2012).

Sierran paleochannels in the area described here (Fig. 1) contain four unconformity-bounded stratigraphic sequences (Fig. 3). Sequence 1 consists of Oligocene silicic ignimbrites erupted from arc calderas in central Nevada (Valley Springs Formation). Sequence 2 consists of andesitic arc volcaniclastic and volcanic rocks (Relief Peak Formation). Sequence 3 consists of distinctive high-K_2O arc lavas and ignimbrites (Stanislaus Group). These include Table Mountain Latite mafic to intermediate lavas, and the Eureka Valley Tuff, with three trachydacite ignimbrite members, and two lava members that range from basalt through trachydacite. Sequence 4 records a return to andesitic arc magmatism (Disaster Peak Formation). The Relief Peak Formation is defined as andesitic rocks underlying or older than the high-K_2O Stanislaus Group, and the Disaster Peak Formation is defined as andesitic rocks overlying or younger than Stanislaus Group (Slemmons, 1953, 1966; Keith et al., 1982). This division is only feasible in the area containing Stanislaus Group, from the Sonora Pass region to the Ebbetts Pass region (Fig. 2).

As described in detail by Busby et al. (2016), three paleochannels crossed what is now the Sonora Pass to Ebbetts Pass region prior to their beheading or derangement by faults and volcanoes of the Sierra Crest–Little Walker volcanic center and the Ebbetts Pass volcanic center (Fig. 4). This paper focuses on volcanic and intrusive rocks of the Sierra Crest–Little Walker volcanic center and the Ebbetts Pass volcanic center, and their structural framework.

■ STRUCTURAL FRAMEWORK

Cenozoic faults are herein identified and mapped by offsets in the Cenozoic volcanic rocks, or offsets of the contacts between volcanic rocks and underlying Mesozoic basement (Figs. 2, 4A, and 4B). Many of the faults described here were first mapped by Slemmons (1953), Keith et al. (1982), and Armin et al. (1984) on the basis of these features. However, the synvolcanic slip history of the faults described here was previously unrecognized because many of the faults were reactivated after volcanism ceased, cutting all volcanic units (Figs. 2A and 2B). Detailed volcanic lithofacies mapping was required to demonstrate synvolcanic faulting on the basis of stratal relations, such as abrupt thinning of strata onto footwalls, fanning dips, and lateral offsets across piercing points that die out up section (Busby et al., 2008a, 2013a, 2013b). In addition, Slemmons (1953, and unpublished mapping) inferred that straight canyons trending approximately N-S or NE-SW were also fault-controlled, even if they only occurred in basement rocks and were not constrained by offsets in volcanic strata. Some of those faults are also shown on Figure 2, but they are dashed and queried. Kinematic indicators are very few, because fault planes are only well exposed on the most resistant volcanic units, which are intrusions. Where faults pass from more resistant volcanic rocks into softer granitic basement, they are buried beneath stream boulders or forested areas. However, they follow straight traces and commonly reemerge to offset strata or volcanic-basement contacts along volcanic ridges.

Paleochannel Stratigraphy, Sonora Pass Area

Andesitic block-and-ash flow tuff, debris flow, and streamflow deposits (Tdp)

Sequence 4

unconformity 4

Dardanelles Formation: lava flow (Tsd)

Eureka Valley Tuff, Upper Member (Tseu)

Eureka Valley Tuff, By-Day Member (Tseb)

Eureka Valley Tuff, Lava Flow Member (Tsel)

Sequence 3

Eureka Valley Tuff, Tollhouse Flat Member (Tset)

Eureka Valley Tuff, Basal Lava Flow Member

Table Mountain Latite: lavas (Tstml)

unconformity 3

Andesitic block-and-ash flow tuff, debris flow, and streamflow deposits (Trp)

Sequence 2

unconformity 2

Rhyolite ignimbrites (Tvs)

Sequence 1

unconformity 1

Mesozoic granitic and metamorphic rocks

Late Miocene — Disaster Peak Formation — 7.28 ± 0.06 Ma

early Late Miocene — Stanislaus Group — 9.137 ± 0.017 Ma, 9.34 ± 0.04 Ma, 9.4 ± 0.3 Ma, 9.54 ± 0.04 Ma, 9.94 ± 0.03 Ma, 10.36 ± 0.06 Ma, 10.41 ± 0.08 Ma

Early (?) to Late Miocene — Relief Peak Formation — 10.39 ± 0.18 Ma, 11.33 ± 0.03 Ma, > 12.15± 0.04 Ma

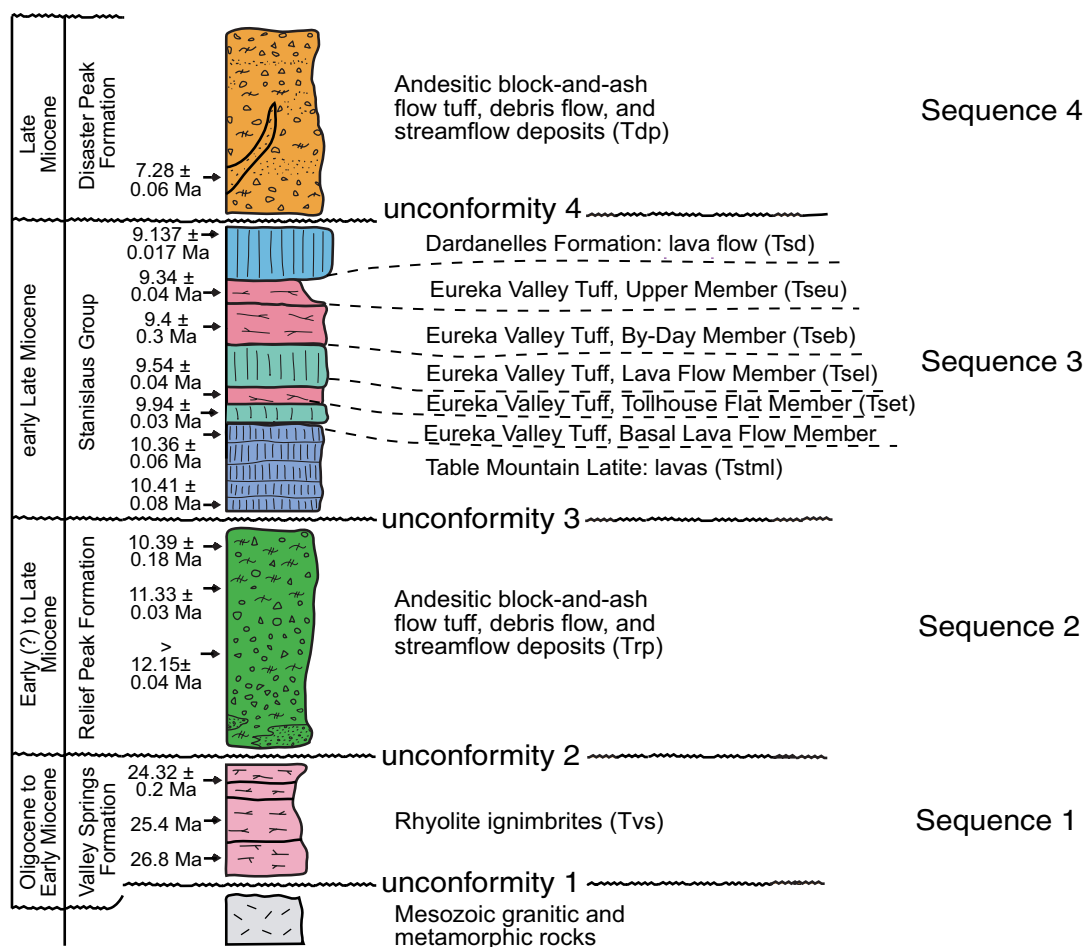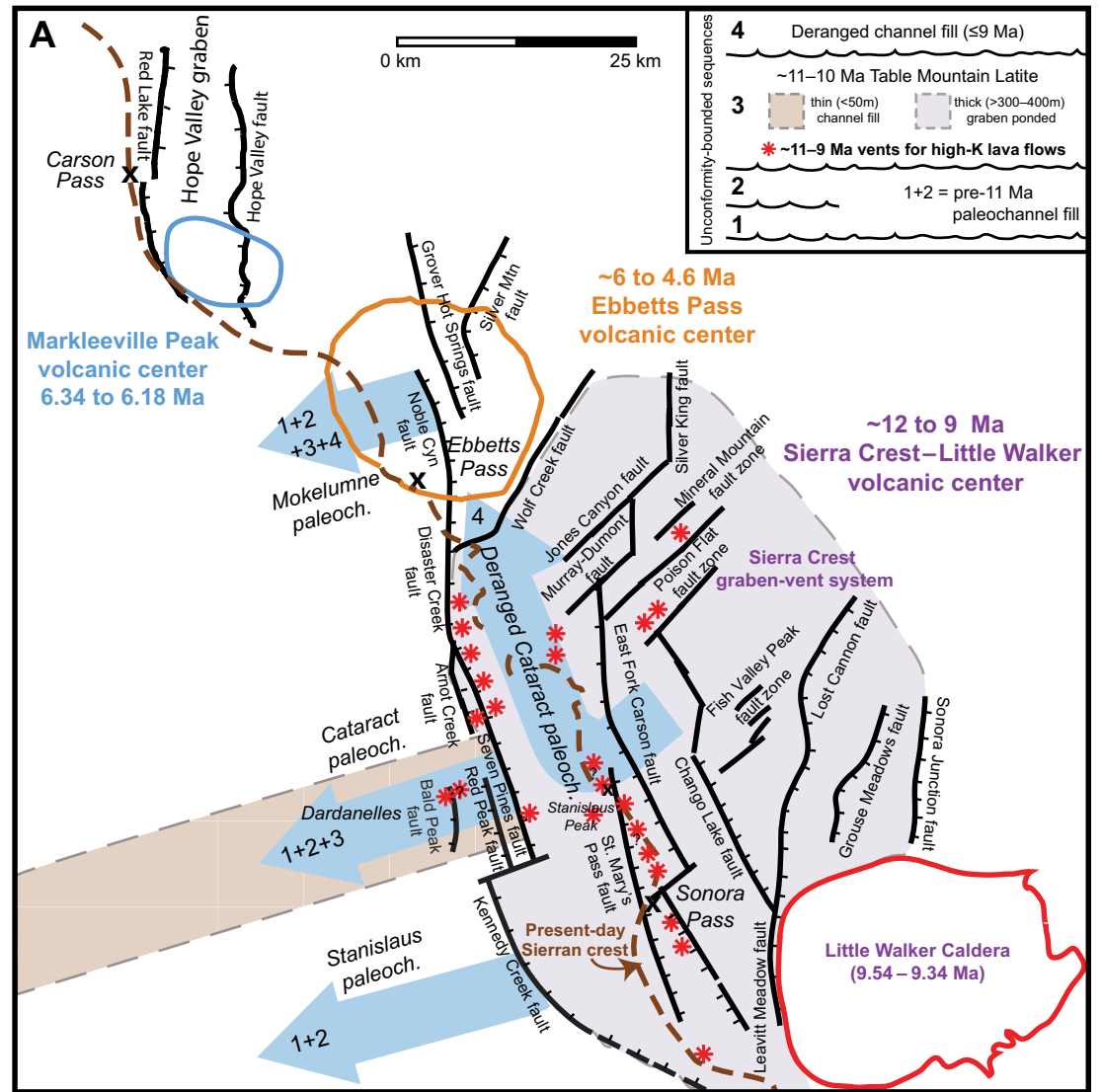Oligocene to Early Miocene — Valley Springs Formation — 24.32 ± 0.2 Ma, 25.4 Ma, 26.8 Ma

Figure 3. Generalized stratigraphy of Cenozoic paleochannel fill in the Sonora Pass region, central Sierra Nevada, California, modified from Busby et al. (2013a). Thicknesses of units are variable and not shown to scale. Mappable erosional unconformities divide the section into four sequences that have been correlated with unconformities in other central Sierra Nevada paleochannels (Busby et al., 2008a, 2008b; Busby and Putirka, 2009; Busby, 2012). Ages are from Busby et al. (2008b), Busby and Putirka (2009), Busby et al. (2013b), and this paper (Fig. 5). The two older ages on the Valley Springs Formation are based on correlations made by Chris Henry (2013, written commun.).

Sierra Crest–Little Walker Volcanic Center

The structure of the Sierra Crest–Little Walker volcanic center was described in detail by Busby et al. (2013a, 2013b), so only a brief summary is provided here. Our previous work was the first to show evidence of synvolcanic faults and their controls on vents and ponded volcanic sections, in what we term the Sierra Crest–Little Walker volcanic center. The Stanislaus Group (Fig. 3) contains distinctive widespread units that act as regional strain markers, making it much easier to document the importance and nature of synvolcanic faulting.

The Sierra Crest–Little Walker volcanic center is dominated by the Sierra Crest graben-vent system (Fig. 4A; Busby et al., 2013a, 2013b). This has a very large full graben (the Sierra Crest graben) bounded by NNW-striking oblique normal-dextral faults, and a major NE-striking transfer zone that emanates from its northern half, with dominantly sinistral oblique normal faults (Fig. 4B). Synvolcanic transtensional faults ponded high-K_2O lavas in grabens to thicknesses of >400 m. Vents occur along these faults as fissures and lesser fault-controlled point sources (red stars, Fig. 4A). These faults include (Figs. 2, 4A, and 4B):

Figure 4 (*on this and following page*). (A) Tectonic and volcanic setting of the Sonora Pass to Ebbetts Pass to Carson Pass region (green boxes, Fig. 1), modified from Busby (2013). This paper focuses on two volcanic centers sited in ancestral Cascades arc pull-apart basins in the Walker Lane: the ca. 12–6 Ma Sierra Crest–Little Walker volcanic center, and the ca. 6–4.6 Ma Ebbetts Pass volcanic center (geology shown in detail on Fig. 2). Also shown is the Hope Valley graben (Hagan et al., 2009), which formed at about the same time as the Ebbetts Pass pull-apart basin (Busby et al., 2016). Paleochannels carved in Cretaceous–Paleocene time contain four unconformity-bounded stratigraphic sequences, shown in Figure 3. The high-K$_2$O volcanic rocks of sequence 3 were erupted from the Sierra Crest–Little Walker volcanic center. This formed a Walker Lane transtensional intra-arc graben complex. High-K$_2$O lavas (mostly Table Mountain Latite, shown in lavender gray) were erupted from fissures and point sources along faults (red stars). High-K$_2$O ignimbrites were erupted from the Little Walker caldera. All three paleochannels contain sequences 1 and 2 (Fig. 3), indicating that they were not deranged prior to ca. 12 Ma (Busby et al., 2016). The Stanislaus paleochannel contains no Table Mountain Latite, so it was beheaded before Table Mountain Latite erupted (i.e., prior to deposition of sequence 3). Volcanic rocks erupted from the Sierra Crest–Little Walker volcanic center were captured by the Cataract paleochannel and funneled westward (sequence 3), but it was completely beheaded before deposition of sequence 4. Sequence 4 was deposited in a paleochannel that flowed toward the north-northwest in the Sierra Crest graben, referred to as the deranged Cataract paleochannel (ca. 9–5 Ma). This now lies along the modern range crest (brown dashed line), and it is parallel to modern drainages in the Walker Lane. The Mokelumne paleochannel was beheaded during deposition of sequence 4 at Ebbetts Pass (Busby et al., 2016). New mapping and dating presented here on the Ebbetts Pass volcanic center (Fig. 2B) show it includes ca. 6 Ma lavas and the ca. 5–4 Ma Ebbetts Pass stratovolcano, which formed in a Walker Lane pull-apart basin. The Ebbetts Pass pull-apart basin beheaded the Mokelumne paleochannel at ca. 6–5 Ma. At the same time to the north (ca. 6 Ma), the Markleeville Peak volcanic center formed in the Hope Valley graben, and the E-W Carson-Kirkwood paleochannel became tectonically deranged into the NNW-trending Hope Valley graben (Hagan et al., 2009).

(1) NNW-SSE faults that bound the 28-km-long, 8–10-km-wide Sierra Crest full graben. These include the East Fork Carson fault on the east and the Kennedy Creek–Seven Pines–Disaster Creek faults on the west. Vents lie in the hanging walls near the surface trace of these faults. This group also includes NE-SW–striking faults that accommodate right steps in the NNW-SSE graben-bounding faults.

(2) Series of small NNW-SSE half grabens on the west side of the Sierra Crest graben, including the Red Peak, Bald Peak, and Arnot Creek faults.

(3) The NE-SW transfer zone faults and grabens that extend ~20 km along the northeast side of the Sierra Crest pull-apart basin, including the Poison Flat and Mineral Mountain fault zones. This zone is inferred to
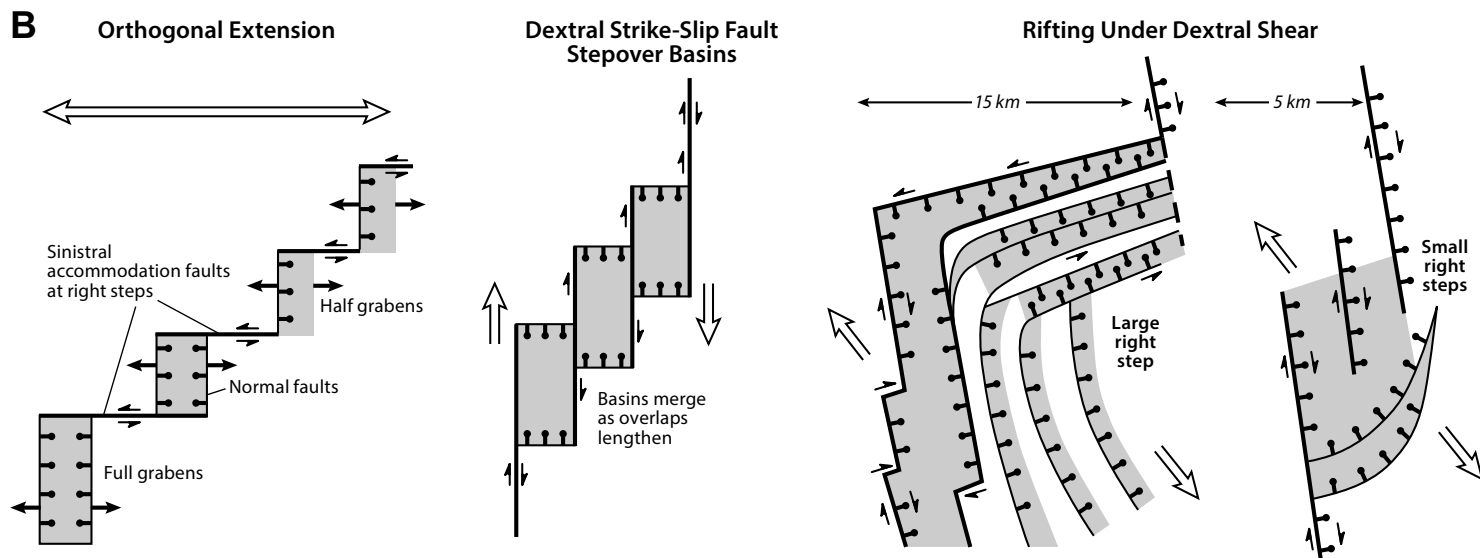
Figure 4 (*continued*). (B) Simplified depiction of faults and basins formed under orthogonal extension (panel one) and under right-stepping dextral strike-slip faults (panel two), for comparison with faults and basins formed under transtension/rifting under dextral shear. Rifting under dextral shear is illustrated for the transtensional faults and basins of the Sierra Crest–Little Walker pull-apart (panel three), and the Ebbetts Pass pull-apart (panel four). In both, obliquity between Sierra Nevada and North American microplate motion (large open arrows) and the orientation of faults resulted in approximately N-S normal-dextral faults. A large right step was accommodated by a system of approximately NE normal-sinistral faults in the Sierra Crest–Little Walker pull-apart basin (panel three). In contrast, in the Ebbetts Pass pull-apart basin, series of small right steps along approximately N-S normal-dextral faults produced a smaller pull-apart structure, with normal faults along its trailing edge (panel four).

transfer transtensional slip from the Sierra Crest graben to a fault zone that lay east and northeast of the graben (Fig. 4B), the Antelope Valley fault (Fig. 1).

Ebbetts Pass Volcanic Center

The Ebbetts Pass volcanic center formed at a much smaller pull-apart basin than that of the Sierra Crest–Little Walker volcanic center (Figs. 4A and 4B). The basin is bounded to the west and northwest by a series of right-stepping, N-S–trending, dextral-oblique, down-to-the-east normal faults that lie on the modern Sierra crest and range front (Noble Canyon, Grover Hot Springs, and Silver Mountain faults; Figs. 2B and 4). It is bounded to the southeast and south by the down-to-the-northwest Wolf Creek fault (Figs. 2B and 4). Mesozoic basement is successively dropped down to the east across the right-stepping oblique faults, and silver mines are located along them (Fig. 2B), similar to the normal fault-localized silver deposits immediately to the east and southeast (John, 2001). Our mapping of these faults is new, so a description of each fault is given here.

Noble Canyon Fault

The Noble Canyon fault (Figs. 2B and 4) forms a dramatic 410 m (1340 ft) topographic escarpment in granitic rock on the west side of Noble Canyon, dropping volcanic rocks down on the east side of the fault. It was previously mapped by Keith et al. (1982) and Armin et al. (1984). Although it clearly cuts all of the volcanic rocks south of Highway 4 (Fig. 2B), we infer that it is also synvolcanic because the contact between granitic basement and overlying volcanic rock is dropped at least 120 m (400 ft) lower on the east side of the fault (Fig. 2B). The fault strikes 330°–350°, dips 75°–90° east, and is more than 12 km long. The fault ends northward in a right step to the Grover Hot Springs fault (Figs. 2 and 4). It ends southward at the Wolf Creek fault, but it connects to the Disaster Creek fault, which together with the Arnot Creek fault forms the western boundary of the northern Sierra Crest graben (Figs. 2 and 4). The Disaster Creek fault connects southward to the Seven Pines fault, which in turn transfers westward to the Kennedy Creek fault; these form the western boundary of the southern Sierra Crest graben (Figs. 2A and 4). As discussed in the following, the faults on the west boundary of the Sierra Crest graben became active during deposition of the Relief Peak Formation, but there is no evidence for activity along the Noble Canyon until late in the deposition of the Disaster Peak Formation.

Grover Hot Springs Fault

The Grover Hot Springs fault is a long fault that extends 15 km northward past the trace shown on Figure 4 (Armin et al., 1984). It dips steeply east and strikes 340°, dropping undifferentiated andesitic volcaniclastic rocks down to the east against the Valley Springs Formation, which in turn rests on granitic basement (Fig. 2B). The fault appears to end in the south near the contact between altered basal fill and overlying unaltered 4.6–4.5 Ma volcanic rocks of the Ebbetts Pass pull-apart structure. The next fault to the east (Silver Mountain fault) also dies out southward (Fig. 2B), so we infer that the faults stepped right in a releasing stepover (Fig. 4B).

Grover Hot Springs, the Silver Peak mine, and the Pennsylvania mine are all situated along the Grover Hot Springs fault. Because Mesozoic basement does not crop out on the hanging wall, we can only say that vertical separation along the fault is >180 m (600 ft). The fault zone is well exposed for 1 km north of Highway 4, where it forms a 5-m-wide gouge zone. Within 3 m of the fault zone, the Valley Springs Formation ignimbrite (which is normally flat lying) is rotated into the fault zone, with a strong vertical foliation striking 350°. The undifferentiated volcaniclastic rocks (Tvu, Fig. 2B) are strongly altered along the fault.

Silver Mountain Fault

The Silver Mountain fault is parallel to the Grover Hot Springs and Noble Canyon faults (striking 340°; Figs. 2B and 4), but it dips more shallowly (55°–60° east). Armin et al. (1984) mapped the Silver Mountain fault, but only south of Highway 4 (highway shown on Fig. 2). Multiple silver mines are sited along this fault, including the Rippon, Gould and Curry, IXL, Lady Franklin, and Exchequer mines. This fault also passes through the "Silver Mountain site," the location of a mining town during the 1850–1870s (Curtis, 1954; Clark and Evans, 1977). The undifferentiated volcaniclastic rocks (Tvu; Fig. 2B) on both sides of the fault lack features that can be used to determine displacement.

Wolf Creek Fault

The Wolf Creek fault is a normal fault that separates the Ebbetts Pass pull-apart basin to the northwest from the Sierra Crest–Little Walker pull-apart basin to the south (Figs. 2 and 4). South of the Wolf Creek fault, there is a >1-km-thick section of Relief Peak Formation and Stanislaus Group (Fig. 2). North of the fault, altered andesitic volcaniclastic rocks form the basal fill of the Ebbetts Pass pull-apart (Tvu and Tva) basin, overlain by unaltered volcanic rocks of the lower silicic section (dacite lava [Tdpld], rhyolite welded ignimbrite [Tdpwi], and rhyolite lava [Tdplr]), and the Ebbetts Pass stratovolcano (Tdpeps; Fig. 2B).

The basal fill of the Ebbetts Pass pull-apart basin consists of undifferentiated and altered volcanic rocks (Tvu and Tva; Fig. 2B). It is a crumbly blue-gray volcanic-volcaniclastic rock that is too strongly altered to clays, micas, quartz, and pyrite to allow $^{40}Ar/^{39}Ar$ dating. Stratification is faintly visible. The basal fill was mapped as Relief Peak Formation (Trp) by Armin et al. (1984), but there is no evidence that it is older than the Stanislaus Group, since there are no dates on it, nor are there any stratigraphic relations with the Stanislaus Group. We infer that the basal fill is largely volcanic debris-flow deposits that were catastrophically deposited into the pull-apart basin as it began to form, and these were extensively altered by fluids during emplacement of the overlying unaltered volcanic section and its coeval intrusions. The basal fill is thus most likely Disaster Peak Formation (Tdp) dropped down against Relief Peak Formation along the Wolf Creek fault (Fig. 2B), although we show it as undifferentiated (Tvu, Tva) because it is undated.

The thick fill of the Sierra Crest graben-vent system ends abruptly against the Wolf Creek fault, suggesting it continues northward at depth beneath the Ebbetts Pass pull-apart basin (i.e., it was down dropped beneath it along the Wolf Creek fault). A splay of the Wolf Creek fault drops 4.6–4.5 Ma Ebbetts Pass stratovolcano basin fill down against ca. 6.4 Ma basin fill (Fig. 2B). This strand is shown as a queried normal fault that brings up a dacite lava in its footwall (Tdpld, dated at 6.367 ± 0.017 Ma; Fig. 5). The fault is partially buried by a younger rhyolite lava (Tdplr, dated at 4.73 ± 0.03 Ma; Fig. 5), where it is shown dotted through that unit. All strata north (basinward) of the queried fault are 4.6–4.5 Ma (Tdpeps, Ebbetts Pass stratovolcano; Fig. 4A) and are inferred to lie in the hanging wall of the queried normal fault strand. The fault strand is queried because the dacite lava (Tdpld) could alternatively represent a megaslide block, but its large size (>2.5 km long and >225 m thick) and the absence of associated smaller slide blocks make that seem unlikely.

Summary of Structural Framework

The Sierra Crest graben-vent system as a whole forms a very large right releasing stepover (Fig. 4B), with increasing transtensional fault offset southward (Busby et al., 2013b). This controlled the siting of the Little Walker caldera in the southeast corner of the volcanic field (Fig. 4A), which produced ignimbrites of the Eureka Valley Tuff (Fig. 3). Extreme transtension in the very large Sierra Crest–Little Walker pull-apart is inferred to have triggered rapid ascent of low-degree partial melts (Putirka and Busby, 2007), causing outpouring of high-K_2O "andesite flood lavas" (Putirka and Busby, 2007; Busby et al., 2013b). The NE-striking fault zone in the northeast part of the Sierra Crest–Little Walker volcanic center mimics the right steps and NE-striking faults of the Carson domain and Mina deflection but on a smaller scale (Fig. 1). Three models have been proposed to explain fault-slip transfer across the Mina deflection, summarized by Nagorsen-Rinke et al. (2013): (1) normal faults at a dextral strike-slip fault stepover (e.g., see panel 2, Fig. 4B), (2) oblique-slip (sinistral

Tectonic Setting	Gp/Fm/Mbr	Rock Types	Ages in Ma		Sample #
Rift	Basalt monogenetic center	Basalt plug and cinder cone erosional remnant on Disaster Peak	Plag	3.69 +/- 0.03	JHEP-57
Ebbetts Pass Volcanic Center (Ancestral Cascades Arc) — Disaster Peak Formation (Tdp) — Ebbetts Pass Stratovolcano (Tdpeps)		Dacite intrusion on Highland Peak (Tdpid)	San	4.478 +/- 0.007	JHEP-49
		Rhyolite feeder dike (to Tdpeps)	Plag	4.626 +/- 0.018	JHEP-8
		Andesite lava MEGA-SLIDE SLAB (in Tdpeps)	Hb	6.203 +/- 0.011	MG-08-08
		Basaltic andesite lava (Tdpeps)	Groundmass	4.6 +/- 0.7	JHEP-9
		Basaltic andesite lava (Tdpeps)	Plag	4.90 +/- 0.02	JHEP-47
	Lower Silicic section	Rhyolite lava (Tdplr)	Hb / Pl	4.73 +/- 0.03 / 4.53 +/- 0.03	JHEP-44
		Rhyolite welded ignimbrite (Tdpwi)	Sanidine 14 crystals	4.636 +/- 0.014	MG-08-07
		Rhyolite welded ignimbrite (Tdpwi)	Plag	4.665 +/- 0.02	JHEP-21
		Dacite lava (Tdpld)	Hb	6.367 +/- 0.017	MG-08-12
Sierra Crest - Little Walker Volcanic Center (Ancestral Cascades Arc)		Andesite block-and-ash-flow tuff (in Tdpdf)	Hb / Pl	4.96 ± 0.05 / 4.457 +/- 0.014	JEHP-55
		Basalt lavas (in Tdplb)	Plag	7.25 ± 0.01	JHEP-83
		Dacite lava MEGA-SLIDE SLAB (in Tdpld)	Hb	11.05 +/- 0.031	JHEP-70
	Stanislaus Group (Ts) — Dardanelles Fm (Tsd)	Shoshonite lava (Tsdl)	WR	9.137 +/- 0.017	BP-46
	Eureka Valley Tuff (Tse) — Upper Member (Tseu)	Previous work 9.34 +/- 0.04 Ma (trachydacite non-welded ignimbrite)[6]			
	By Day Member (Tseb)	Previous work 9.4 +/- 0.3 Ma (trachydacite welded ignimbrite)[5]			
	Lava Flow Member (Tsel)	Trachydacite lava MEGA-SLIDE SLAB in Tsel	Pl	11.66 +/- 0.07	JHEP-64
	Tollhouse Flat Member (Tsel)	Previous work 9.54 +/- 0.04 Ma (trachydacite welded ignimbrite)[4]			
	Basal Lava Flow Member (Tseblt)	Trachydacite intrusion and lava (Tselit)	Hb	9.94 +/- 0.03	JHEP-88
	Table Mtn Latite Fm (Tml)	Previous work 10.41 +/- 0.08 Ma to 10.36 +/- 0.06 Ma (trachyandesite, trachybasaltic andesite and basalt lavas)[2] Has andesite lava MEGA-SLIDE SLAB 12.95 +/- 0.09 Ma[3]			
	Relief Peak Formation (Trp)	Andesite block-and-ash-flow tuff within andesitic debris flow deposits (Trpdf) Previous work includes 10.39 ± 0.18 Ma to > 12.15 ± 0.04[1] Has rhyolite ignimbrite MEGA-SLIDE SLABS (~29-25 Ma)	Hb	11.33 +/- 0.03	JHEP-90

Figure 5. Summary of new ^{40}Ar/^{39}Ar geochronological results, placed in stratigraphic and tectonic context. For plots and interpretations of them, see Figure S1 (text footnote 1). All dates are relative to Fish Canyon Tuff sanidine with an assigned age of 28.02 Ma. Previous ^{40}Ar/^{39}Ar dates: 1—Busby et al. (2008a) and Busby et al. (2013b); 2—Busby et al. (2008a); 3—Busby et al. (2013b); 4, 5, 6—Busby and Putirka (2009). Hb—hornblende; Pl/Plag—plagioclase; WR—whole rock; San—sanidine.

and normal) faults, or (3) clockwise block rotations between sinistral faults (e.g., see Fig. 3; Nagorsen-Rinke et al., 2013). Model 2 applies to the transfer zone mapped herein (Fig. 4B, panel 3), but with faults that dip more steeply (80°–90°) than those portrayed in model 2 of Nagorsen-Rinke et al. (2013). We predict that future paleomagnetic work along the NE-striking fault zone in the Sierra Crest–Little Walker volcanic center will show evidence for clockwise block rotations, similar to those determined in the Carson domain and Mina deflection (described earlier herein). This area would be ideal for determining if block rotations are present, and whether or not they are progressive, because some structural blocks contain units that range from ca. 10.5 Ma (Table Mountain Latite), through ca. 9.54 Ma (Eureka Valley Tuff), to ca. 7.25 Ma (basalt lavas; Figs. 2B and 5).
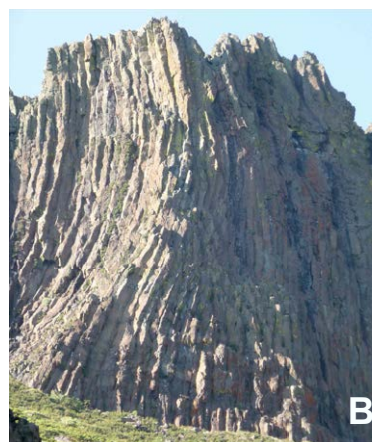
The Ebbetts Pass pull-apart represents a much smaller right step than the Sierra Crest–Little Walker pull-apart, along a series of small stepovers (Fig. 4B).

It differs from the simple pull-apart model shown in panel 2 of Figure 4B by having through-going normal faults along its southern boundary, and a volcanic fill that thins northward (Figs. 2 and 4B).

■ FIELD AND PETROGRAPHIC CHARACTERISTICS AND NEW ^{40}Ar/^{39}Ar GEOCHRONOLOGY

In this section, we present the first systematic description of all the volcanic and intrusive map units in the Sierra Crest–Little Walker and Ebbetts Pass volcanic centers, using outcrop photos, photomicrographs, modal analyses, and geochemical data, in conjunction with ^{40}Ar/^{39}Ar geochronology (Figs. 5–13). Previous papers have presented small geochemical data sets in stratigraphic context (Ransome, 1898; Noble et al., 1976; Putirka and Busby, 2007; Busby

Figure 6 (*on this and following two pages*). Outcrop photos from the Sierra Crest–Little Walker volcanic center, from oldest to youngest; see stratigraphy in Figures 2, 3, and 5. (A) Oblique aerial photo of 500-m-thick section of nearly flat-lying Table Mountain Latite (lavas), resting on Relief Peak Formation debris-avalanche deposits up to 500 m thick with chaotic bedding and megaslabs up to 2 km long. The debris-avalanche deposit is composed of megaslide blocks of andesitic debris flow and fluvial deposits and lesser block-and-ash-flow tuff. It was shed off the faults marginal to the Sierra Crest graben immediately before eruption and deposition of the Table Mountain Latite within the Sierra Crest graben (Fig. 14B; Busby et al., 2013a). Photo taken by private plane from Sonora Pass looking south along Sierra crest. (B) 100-m-high columnar joints in the "Classic" flow of the Table Mountain Latite, a lava that extends from the Sierra Crest graben down the Cataract paleochannel to the Sierra Foothills at Table Mountain; taken from the south flank of The Dardanelles (Busby et al., 2016). (C) Typical appearance of the Table Mountain Latite, with large skeletal plagioclase phenocrysts weathered out against the groundmass (photomicrographs in Figs. 9B–9E). (D) Table Mountain Latite fissure vent deposits that form red ramparts up to 6 km long (Figs. 2 and 4) and up to 300 m thick. The ramparts are composed of red, crudely stratified to massive accumulations of scoria bombs and lesser dense (nonvesiculated) Vulcanian megablocks up to 6 m in size, representing proximal, highly energetic ballistic fall accumulations. These interfinger with Table Mountain Latite lava and lie along NNW-striking faults bounding the Sierra Crest graben (Figs. 2 and 4). White granitic basement is in bottom-right foreground, and dark-brown layered Table Mountain Latite lavas are on distant ridge.

Sample #	LITHOFACIES, with notes: ** = geochronology, # = photomicrograph, ^ = modal analysis	Latitude	Longitude
Table I-I Quaternary (to Pliocene?) basalts			
JEFF Q DIKE	8-19-feeder dike to Column of the Giants	38.3403	-119.795
Table I-H I Intrusions in and around Ebbetts Pass pull-apart basin/volcanic center			
JHEP-8	**FIX:** ** ^ rhyolite dike in Tvu west of Noble Cyn fault	38.5404	-119.7988
MG-08-10	# ^dacite intrusion in altered basal fill (Tvu)	38.5107	-119.771
MG-08-13	^ andesite intrusion in altered basal fil (Tdpia)	38.5053	-109.7556
BLM 09-920-2	andesite intrusion in altered basal fil (Tdpia)	38.509	-119.746
MG-08-11	andesite intrusion in altered basal fill	38.512	-119.766
MG-08-13	andesite intrusion in altered basal fill (Tdpia)	38.50528	-119.756
JHEP-48	^ dacite intrusion of Highland Peak (Tdpid)	38.5335	-119.7617
JHEP-49	**^* dacite intrusion of Highland Pk (Tdpid)	38.5349	-119.7602
JHEP-50	# dacite intrusion of Highland Peak	38.5363	-119.7593
JHEP-37	basaltic andesite in undifferentiated volcanics (Tvu)	38.59925	-119.793
JHEP-16	basaltic andesite intrusion (Tia)	38.556	-119.820
JHEP-12	andesite intrusion (Tia)	38.548	-119.812
JHEP-8	rhyolite intrusion (in Tvdf)	38.540	-119.799

[1]Supplemental Files. Table S1: GPS coordinates for all samples. Table S2: Raw point count data, normalized to 100%. Figure S1: ^{40}Ar/^{39}Ar plots. Please visit **https://doi.org/10.1130/GES01398.S1** or the full-text article on www.gsapubs.org to view the Supplemental Files.

et al., 2008a, 2013b; Koerner et al., 2009), or used those data sets as part of a regional-scale analysis (Putirka et al., 2012; du Bray et al., 2014). However, this is the first paper to present a large geochemical data set in stratigraphic and intrusive context (Table 1), plotted on maps (Fig. 2) and located by global positioning system (GPS; see Supplemental Table S1[1]). Although abundant field photographs and descriptions have been previously published (Slemmons, 1953, 1966; Noble et al., 1974; Busby et al., 2008a; Busby and Putirka, 2009; Gorny et al., 2009; Busby et al., 2013a, 2013b, 2016), this is the first paper to link outcrop photos (Figs. 6 and 10) with photomicrographs (Figs. 9 and 13) to document textures and mineralogy. Published modal analyses were previously restricted to a very small part of the area (Busby et al., 2013b), but they are herein presented for all map units across the two volcanic centers (Figs. 7, 8, 11, and 12; raw counts in Table S2 [footnote 1]).

We also report new ^{40}Ar/^{39}Ar geochronology on 19 samples, summarized in Figure 5, with plots presented in the Supplemental Files (footnote 1). These analyses were performed on mineral separates and matrix material from lavas and intrusions, and minerals from ignimbrites, using methods and facilities described previously (Busby et al., 2013b). Ages are based on 28.02 Ma for the Fish Canyon sanidine (FCs) standard (Renne et al., 1998) and the decay constants of Steiger and Jäger (1977), to facilitate direct comparison with previous studies (e.g., Fleck et al., 2015). More recent calibrations (e.g., Renne et al., 2011) yield slightly older ages, which we consider to be more accurate.

The relationships of volcanic and intrusive rocks to structures in the Sierra Crest–Little Walker and Ebbetts Pass pull-apart basins evolved with time. A series of block diagrams are provided in Figure 14 to show the evolution of the pull-apart basins and volcanic centers.

Figure 6 (*continued*). (E) Eureka Valley Tuff, Tollhouse Flat Member, showing trachydacite welded ignimbrite with large black glassy fiamme and small white/light-gray silicic volcanic rock fragments. (F) Close-up of Eureka Valley Tuff, Tollhouse Flat Member, showing light-gray volcanic rock fragments common to all ignimbrite members of the Eureka Valley Tuff (Fig. 7C). (G) Cliff-face cross section through a cinder cone (red), in the Lava Flow Member of the Eureka Valley Tuff. This basalt cinder cone is cut by an olivine basalt feeder dike that vented olivine basalt lava flows within the Lava Flow Member of the Eureka Valley Tuff. Depositionally above the red cinder cone rocks, forming an ~10-m-thick black horizontal band, is the basal vitrophyre of the By Day Member of the Eureka Valley Tuff. This in turn is overlain by a debris-avalanche deposit shed from a graben-bounding fault during accumulation of the Stanislaus Group: Note white blocks of Upper Member Eureka Valley Tuff, including one with bedding standing on end. (H) Nonwelded upper part of the By Day Member of the Eureka Valley Tuff, showing uncompacted black pumice blocks and lapilli. Small white clasts are volcanic rock fragments common to all ignimbrites of the Eureka Valley Tuff (Fig. 7C); for photomicrograph with volcanic rock fragments, see Figure 9l. Pen for scale (resting on pumice block).

Sierra Crest–Little Walker Volcanic Center and Pull-Apart Basin

Relief Peak Formation

Figure 14A reconstructs the paleogeography of the region immediately prior to the onset of Walker Lane transtension, during deposition of Relief Peak Formation deposits in paleochannels. The Relief Peak Formation in paleochannels consists largely of stratified andesitic debris-flow and fluvial deposits, with lesser basaltic andesite to andesite block-and-ash-flow tuffs (Busby et al., 2016). Relief Peak Formation lavas in the paleochannel fills are restricted to: (1) a section of basalt lavas below The Dardanelles (samples DC001 and DC067; Table 1), and (2) a single basaltic trachyandesite lava in the Stanislaus paleochannel (sample 8–19–08; Table 1). Mafic lavas are fluid and could have been sourced from tens of kilometers to the east. Igneous rocks on Relief Peak interpreted by Roelofs (2004) to be Relief Peak Formation lavas instead are younger intrusions (Busby et al., 2016). For these reasons, we infer that arc front volcanoes lay upslope to the east (i.e., the study area lay in a forearc position), and paleochannels between the arc front and what is now the Sierra were not yet disrupted by faulting (Fig. 14A).

Relief Peak Formation rocks also occur as basal graben fill in the Sierra Crest–Little Walker pull-apart basin (Fig. 14B). The basal graben fill contrasts with the older paleochannel fill by consisting of mass-transport deposits and lacking fluvial deposits. Buried paleochannels are preserved below the graben fills in a few areas (Figs. 2 and 14B) but were mostly destroyed by faulting and avalanching. The Stanislaus paleochannel was beheaded by faulting, but the Cataract paleochannel, although faulted, was not dismembered at this time (Busby et al., 2016). The Mokelumne paleochannel lay north of the faults (Fig. 14B).

Figure 6 (*continued*). (I) Contact between nonwelded top of By Day Member of Eureka Valley Tuff (ignimbrite; under person's foot) and overlying Upper Member of Eureka Valley Tuff (ignimbrite), showing intervening white stratified pyroclastic fall deposit. See modal analysis of the pyroclastic fall deposit in Figure 7C (sample JHEP-65a) and photomicrographs in Figure 9J. (J) Close-up of Upper Member of Eureka Valley Tuff nonwelded ignimbrite, showing white uncompacted pumice, and gray to black volcanic rock fragments. Pen for scale. (K) Disaster Peak Formation within the deranged Cataract paleochannel in the Sierra Crest graben (Fig. 3). Disaster Peak Formation in the Sierra Crest–Little Walker pull-apart has abundant fluvially reworked silicic pumice, unlike all older formations. 5 pound (2.3 kg) Papillon for scale. (L) Dacite lava megaslide slab (sample JHEP-06), with flow brecciation, mapped as Disaster Peak Formation lava of dacitic composition (Tdpld; Fig. 2B) but yielding a hornblende $^{40}Ar/^{39}Ar$ age of 11.05 ± 0.031 Ma (Fig. 4). This is the same as the Relief Peak Formation, even though it lies up section from 9.54 to 9.34 Ma Eureka Valley Tuff. It thus represents a megaslide slab slide block of Relief Peak Formation derived from the faulted margin of the Sierra Crest graben-vent system (Fig. 4). It is inferred to have been derived from a lava because it has flow brecciation, shown here (hand lens for scale).

Relief Peak Formation debris-avalanche and debris-flow deposits occur as basal fill in all grabens in the southern half of the Sierra Crest–Little Walker pull-apart basin (Fig. 14B). They were redeposited from the two paleochannels that crossed that region, the Stanislaus and Cataract paleochannels (Figs. 4 and 14B). Relief Peak Formation debris-avalanche and debris-flow deposits are absent from the north part of the Sierra Crest graben (Fig. 2), because no paleochannels crossed it there (Figs. 14A and 14B).
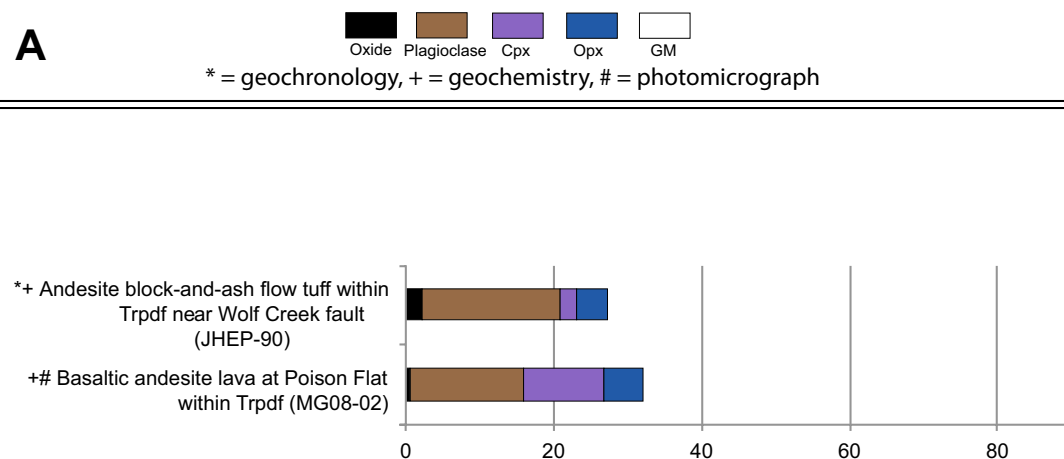
The N-S grabens have no in situ primary volcanic rocks of Relief Peak Formation, only megaslide blocks. In contrast, the NE transfer zone basins along the Wolf Creek to Poison Flat fault zones (WCF and PFFZ in Fig. 14B) contain in situ, thick sections of massive (nonstratified) debris-flow deposits with in situ interstratified primary volcanic rocks, including andesite block-and-ash-flow tuff (sample JHEP-90) and andesite to basaltic andesite lavas (samples

JHEP-89, MG-08-02, 920-5, 920-6, and 921-2; Table 1). We infer that the NE transfer zone basins acted as a funnel that extended toward the arc front, which still lay to the east during Relief Peak Formation time. This funnel captured primary eruptive products from the arc and rapidly filled the basins with massive volcanic debris-flow deposits.

The Relief Peak Formation primary volcanic rocks in the NE transfer zone basins differ from primary volcanic rocks in the younger Disaster Peak Formation by being dominated by clinopyroxene and orthopyroxene instead of hornblende (Fig. 7A). Representative photomicrographs of basaltic andesite lava show unaltered plagioclase (with sieve textures) and two pyroxenes in a glassy groundmass, with embayment and rimming of plagioclase, and clinopyroxene rimming orthopyroxene (Fig. 9A). One andesite block-and-ash-flow tuff yielded a $^{40}Ar/^{39}Ar$ hornblende age of 11.33 ± 0.03 Ma (Fig. 5), which is

A

Oxide   Plagioclase   Cpx   Opx   GM

* = geochronology, + = geochemistry, # = photomicrograph

I. Sierra Crest-Little Walker Volcanic Center

A. Relief Peak Formation

*+ Andesite block-and-ash flow tuff within Trpdf near Wolf Creek fault (JHEP-90)

+# Basaltic andesite lava at Poison Flat within Trpdf (MG08-02)

Figure 7 (*on this and following three pages*). Modal analysis of phenocrysts in volcanic strata in the Sierra Crest graben-vent system, divided into time frames: (A) Relief Peak Formation. Methods and raw counts are given in Supplemental Files (text footnote 1). Cpx—clinopyroxene, Opx—orthopyroxene, GM—groundmass.

consistent with the age of the base of the overlying Table Mountain Latite (10.41 ± 0.08 Ma; Fig. 5).

No intrusions or vent facies deposits of Relief Peak Formation age have been found in the area depicted by Figure 14B, except for an andesite sill that intrudes graben fill near the southeastern margin of the Sierra Crest–Little Walker pull-apart (Fig. 14B; Busby et al., 2013b). This has a $^{40}Ar/^{39}Ar$ hornblende age of 12.15 ± 0.04 Ma (Fig. 5; Busby et al., 2013b), providing a minimum age for the onset of faulting in the Sierra Crest–Little Walker pull-apart. Avalanching continued up to the onset of eruption of Table Mountain Latite "flood andesites," as shown by the overlap in ages (within error) between block-and-ash-flow tuff in the youngest megaslide block (10.39 ± 0.18 Ma) and the base of the Table Mountain Latite at Sonora Peak (10.41 ± 0.08 Ma; Fig. 5). Thus, the onset of Sierra Crest–Little Walker transtensional tectonism appears to have preceded the onset of voluminous arc axis volcanism of the Sierra Crest–Little Walker center by at least 1.8 m.y.

Stanislaus Group

The Stanislaus Group consists of three formations, the Table Mountain Latite, Eureka Valley Tuff, and Dardanelles Formation, with the Eureka Valley Tuff divided into five members (ignimbrites and lavas). These are all repre-

sented in paleochannels (Fig. 3), but they are much thicker and more extensive in the Sierra Crest–Little Walker volcanic center and pull-apart basin, where they were all erupted (Figs. 2 and 4A).

Detailed field descriptions of the Stanislaus Group in the Sierra Crest–Little Walker volcanic center were given in Busby et al. (2013a, 2013b). We herein provide a generalized field description, linking outcrop characteristics with new petrographic and geochemical data (Figs. 6, 7, 8, and 9; Table 1).

Table Mountain Latite. The Table Mountain Latite forms one of the most extensive and perhaps the most voluminous lavas in California, second only after the 16 Ma Lovejoy flood basalt described by Garrison et al. (2008). Its preserved volume is ~200 km³, with lavas forming sections up to 500 m thick (Fig. 6A), and single flows up to 100 m thick (Fig. 6B). One of the Table Mountain Latite trachyandesite lavas is paleomagnetically correlated to the Sierra Nevada Foothills (Pluhar et al., 2009), forming a single flow unit of >25 km³ (Gorny et al., 2009; Busby et al., 2013a, 2016). Flow-top breccias are common, but some flow tops are marked only by a vesicular horizon. Stretched vesicles are stretched parallel to the approximately N-S grabens (Busby et al., 2013b), in contrast with stretched E-W vesicles in the E-W paleochannels (Koerner et al., 2009). A section of 23 flows was measured on Sonora Peak in the Sierra Crest graben (Busby et al., 2008a), and a section of 20 flows was measured in an approximately N-S half graben on the Sierra Nevada range front just north of the Little Walker caldera (Pluhar et al., 2009; Busby et al., 2013b). In another ap-
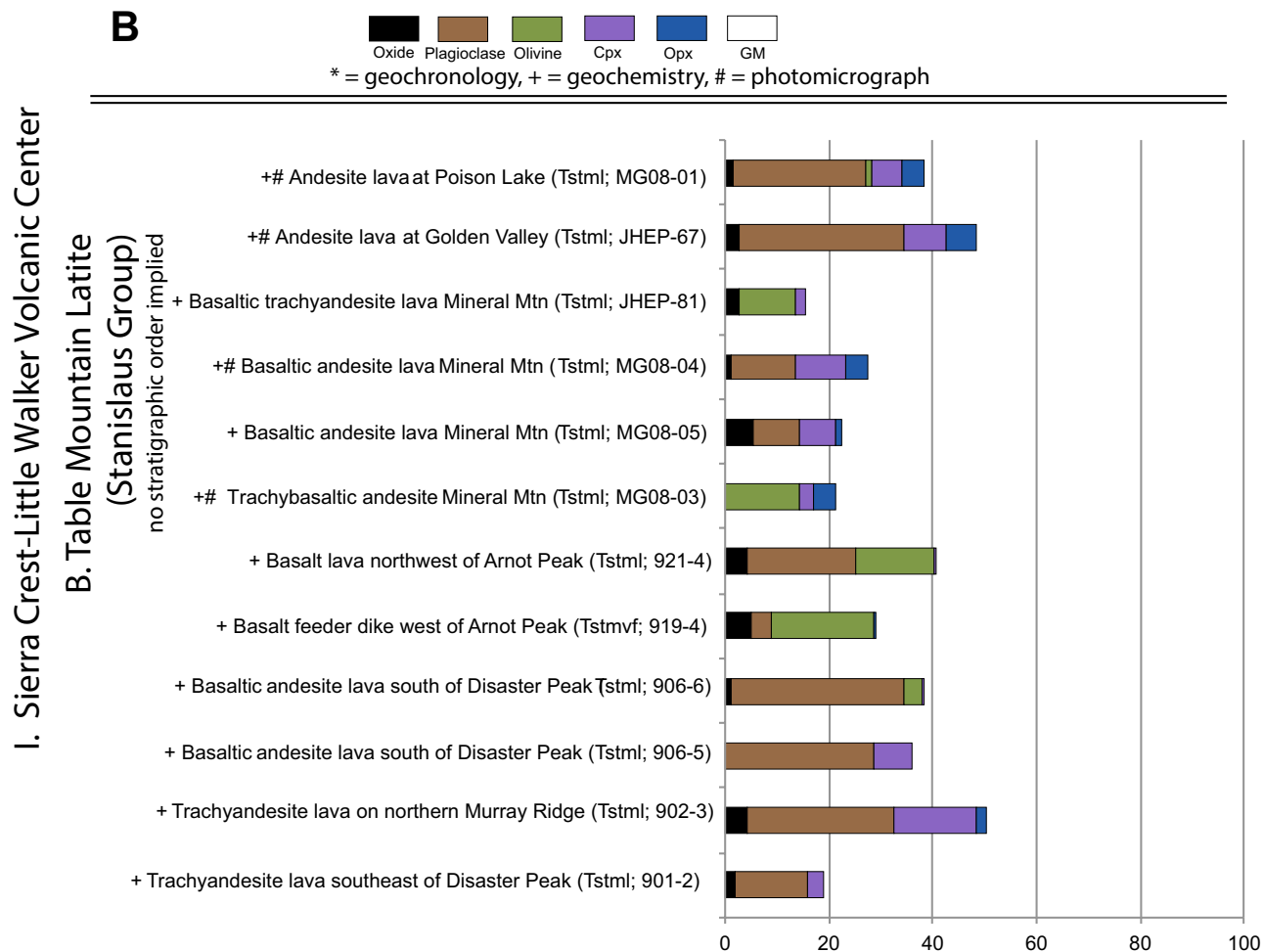
B

Oxide Plagioclase Olivine Cpx Opx GM
* = geochronology, + = geochemistry, # = photomicrograph

I. Sierra Crest-Little Walker Volcanic Center

B. Table Mountain Latite (Stanislaus Group)
no stratigraphic order implied

+# Andesite lava at Poison Lake (Tstml; MG08-01)
+# Andesite lava at Golden Valley (Tstml; JHEP-67)
+ Basaltic trachyandesite lava Mineral Mtn (Tstml; JHEP-81)
+# Basaltic andesite lava Mineral Mtn (Tstml; MG08-04)
+ Basaltic andesite lava Mineral Mtn (Tstml; MG08-05)
+# Trachybasaltic andesite Mineral Mtn (Tstml; MG08-03)
+ Basalt lava northwest of Arnot Peak (Tstml; 921-4)
+ Basalt feeder dike west of Arnot Peak (Tstmvf; 919-4)
+ Basaltic andesite lava south of Disaster Peak (Tstml; 906-6)
+ Basaltic andesite lava south of Disaster Peak (Tstml; 906-5)
+ Trachyandesite lava on northern Murray Ridge (Tstml; 902-3)
+ Trachyandesite lava southeast of Disaster Peak (Tstml; 901-2)

0   20   40   60   80   100

Figure 7 (*continued*). (B) Table Mountain Latite (Stanislaus Group).

proximately N-S range-front half graben, the Table Mountain Latite lavas have an interbedded megaslide slab of hornblende andesite lava with a ⁴⁰Ar/³⁹Ar age of 12.95 ± 0.09 Ma, derived from the Relief Peak Formation (Busby et al., 2013b; see Fig. 5). This indicates ongoing landsliding from active faults during the eruption of Table Mountain Latite.

Table Mountain Latite lavas emanate from fissure vents along faults or in the hanging walls near the surface trace of faults (Figs. 2 and 4). The vents are marked by fissure vent deposits up to 300 m thick that form ramparts up to 8 km long, formed largely of scoria bombs and lapilli, with scattered dense blocks up to 6 m in diameter (Fig. 6D). Because these are very large-volume

lavas relative to other intermediate-composition lavas described in the literature, and because they were fissure fed (Figs. 2, 4, and 6D), they are referred to as "flood andesites" (Busby et al., 2013a).

Lavas in the southern part of the Sierra Crest–Little Walker pull-apart are basalt, basaltic trachyandesite, and trachyandesite, while those in the northern part also include basaltic andesite and andesite (Table 1). The amount of extension increases southward toward the Little Walker caldera (Busby et al., 2013b), which may explain this difference.

The Table Mountain Latite is easily recognized by its distinctive large sieve-textured plagioclase phenocrysts (Figs. 6C, 9B, 9C, and 9D), which are
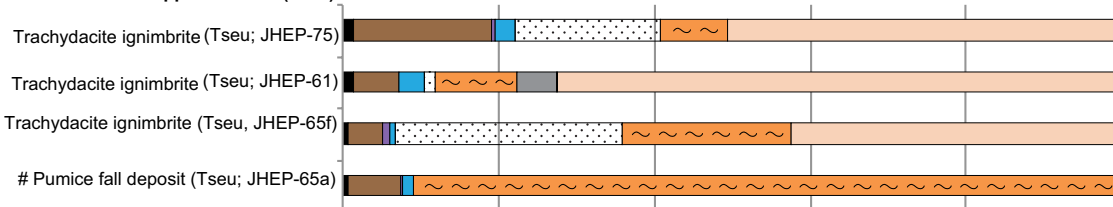
Figure 7 (*continued*). (C) Eureka Valley Tuff.

present in most, but not all, lavas (Fig. 9E). Sieve textures may be present in plagioclase cores or rims (Fig. 9B and 9D) or throughout the crystal (Fig. 9B). Many lavas have two pyroxenes, although clinopyroxene is more common and more obvious on outcrop because it forms larger phenocrysts (Figs. 7B and 9B–9E). Clinopyroxene is commonly twinned (Figs. 9B and 9D) and may occur in glomerocrysts with orthopyroxene and opaque oxides (Fig. 9B). Basalt, basaltic trachyandesite, and basaltic andesite lavas and dikes of Table Mountain Latite have phenocrysts of olivine with or without pyroxene or plagioclase (Figs. 7B and 9E), and trachyandesite lavas commonly have groundmass olivine.

The Table Mountain Latite is the most mafic stratigraphic unit of the Stanislaus Group, and it lacks silicic lavas entirely (Table 1). The only other stratigraphic unit this mafic is the youngest unit of the Stanislaus Group, the Dardanelles Formation, which is a single, small-volume, nearly aphyric shoshonite lava (Table 1). Existing ages on the base and top of the Table Mountain Latite overlap within analytical error (10.41 ± 0.08 and 10.36 ± 0.06 Ma; Figs. 3 and 5), so the flood lavas may have erupted in a short time. In contrast, the members of the Eureka Valley Tuff represent a longer time span: ca. 670–530 kyr for all members (including Basal Lava Flow Member), and ca. 280–120 kyr for the three ignimbrite members (Figs. 3 and 5).
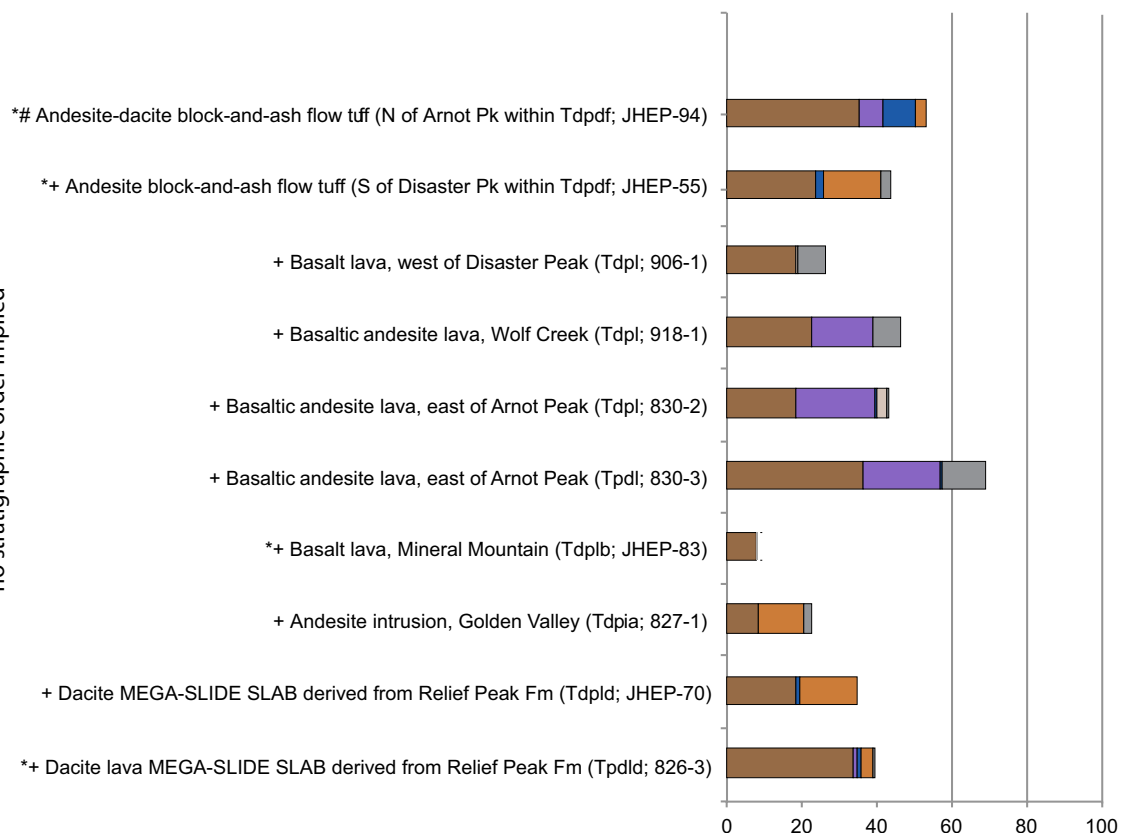
D

Plagioclase Olivine Cpx Opx Hornblende Sanidine Quartz Lithic Alteration Vesicle GM

* = geochronology, + = geochemistry, # = photomicrograph

I. Sierra Crest-Little Walker Volcanic Center
D. ~9-5 Ma Disaster Peak Formation

no stratigraphic order implied

*# Andesite-dacite block-and-ash flow tuff (N of Arnot Pk within Tdpdf; JHEP-94)

*+ Andesite block-and-ash flow tuff (S of Disaster Pk within Tdpdf; JHEP-55)

+ Basalt lava, west of Disaster Peak (Tdpl; 906-1)

+ Basaltic andesite lava, Wolf Creek (Tdpl; 918-1)

+ Basaltic andesite lava, east of Arnot Peak (Tdpl; 830-2)

+ Basaltic andesite lava, east of Arnot Peak (Tpdl; 830-3)

*+ Basalt lava, Mineral Mountain (Tdplb; JHEP-83)

+ Andesite intrusion, Golden Valley (Tdpia; 827-1)

+ Dacite MEGA-SLIDE SLAB derived from Relief Peak Fm (Tdpld; JHEP-70)

*+ Dacite lava MEGA-SLIDE SLAB derived from Relief Peak Fm (Tpdld; 826-3)

0   20   40   60   80   100

Figure 7 (*continued*). (D) Disaster Peak Formation.

Eureka Valley Tuff. The name "Eureka Valley Tuff" should ideally be modified to "Eureka Valley Tuff Formation," because it includes lava members as well as "tuff" (ignimbrite) members (Fig. 3), as first recognized by Priest (1979) and Brem (1977). However, due to historical precedent, it continues to be referred to as the Eureka Valley Tuff (King et al., 2007; Koerner et al., 2009; Pluhar et al., 2009; Carlson et al., 2013). Ignimbrites of the Eureka Valley Tuff were inferred to have been erupted from the Little Walker caldera of Priest (1979), and this was confirmed by magnetic anisotropy studies of caldera outflow ignimbrites by King et al. (2007). However, the caldera fill is too altered to determine if Eureka Valley Tuff ignimbrites are present there. Lavas were not only erupted from the Little Walker caldera margins (Priest, 1979; Brem, 1977),

but also along the length and width of the Sierra Crest–Little Walker volcanic center (Figs. 2 and 14C).

The Eureka Valley Tuff consists of three trachydacite ignimbrite members as well as two lava members (Table 1; Figs. 2, 3, and 14C). The two lava members differ from the Table Mountain Latite by having silicic lavas (trachydacite), in addition to mafic to intermediate lavas. The Eureka Valley Tuff marks the first appearance of hydrous phenocryst phases in the Stanislaus Group: Some of the trachydacite lavas and all of the trachydacite ignimbrites contain biotite, and some have hornblende in addition to pyroxenes (Figs. 7C, 9F, 9I, and 9J; also see modal analyses of Tollhouse Flat and By Day Members *in* Busby et al., 2013b). Like the Table Mountain Latite, nearly all of the ignimbrites and lavas

Figure 8. Modal analysis of intrusions in and around the Sierra Crest graben-vent system, divided by crosscutting relations; these are otherwise undated, except for the olivine basalt intrusion on Disaster Peak, which is inferred to represent a rift (rather than arc) intrusion (Fig. 5). Based on geochemistry and close spatial association with Table Mountain Latite, the trachybasalt intrusion is inferred to be one of the feeders for Table Mountain Latite. Most of the intrusions shown here are spatially closely associated with Disaster Peak Formation in the northern half of the Sierra Crest–Little Walker volcanic center, which remained tectonically and volcanically active at this time, and probably represent feeders for the volcanic rocks. Cpx—clinopyroxene, Opx—orthopyroxene, GM—groundmass.

have sieve-textured plagioclase (Figs. 9F, 9G, and 9H). Ignimbrites are massive and poorly sorted, with mixtures of pumice, glass shards, and accidental volcanic rock fragments (Figs. 6E, 6F, 6H, 6J, and 7C). Pyroclastic fall consists largely of pumice and is stratified and well sorted by size and density, with an absence of rock fragments (Figs. 6I, 7C, and 9J); it could alternatively be called pumice fall or Plinian fall. Broken crystals occur in both ignimbrites and pyroclastic fall deposits (Figs. 9I and 9J).

The lowest ignimbrite of the Eureka Valley Tuff, the Tollhouse Flat Member (Figs. 2 and 3), is by far the most voluminous of the three ignimbrites. It is also the most spatially extensive unit of the Stanislaus Group due to the much

greater mobility of pyroclastic flows relative to lavas (for its distribution, see fig. 3 in Busby et al., 2016). It forms one cooling unit throughout the Sierra Crest–Little Walker volcanic center and beyond, including the reference section several kilometers north of the Little Walker caldera measured by King et al. (2007). It has a $^{40}Ar/^{39}Ar$ biotite age of 9.54 ± 0.04 Ma (Fig. 5). The second ignimbrite, By Day Member, looks similar to the Tollhouse Flat Member in the field, with a black basal vitrophyre passing upward into dark-gray, largely welded ignimbrite (Figs. 6E–6H). However, it is easily distinguished from the Tollhouse Flat ignimbrite by the presence of larger phenocrystic biotite in the Tollhouse Flat Member (Noble et al., 1974; see also Fig. 7C). The By Day
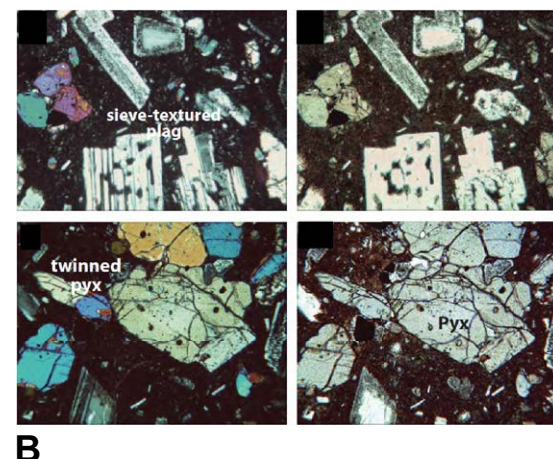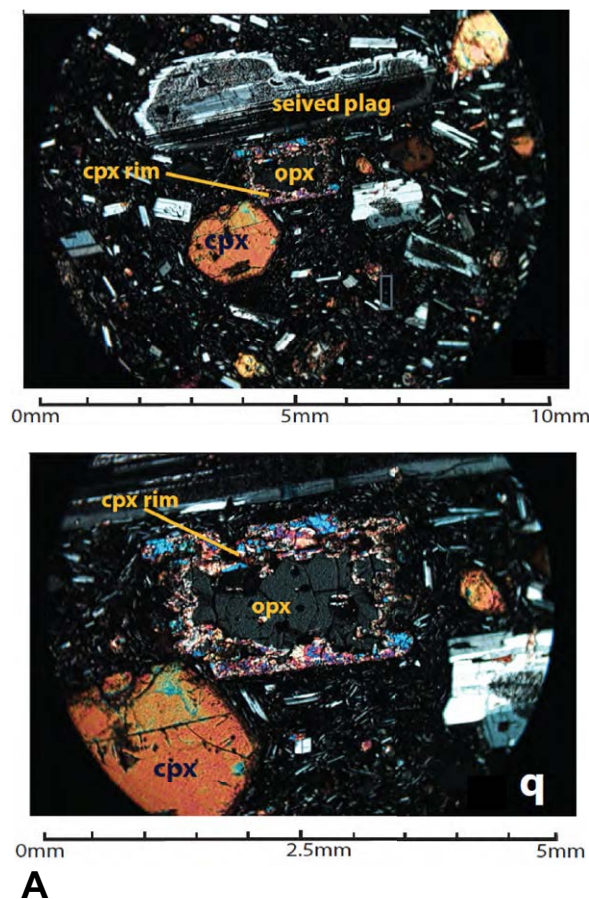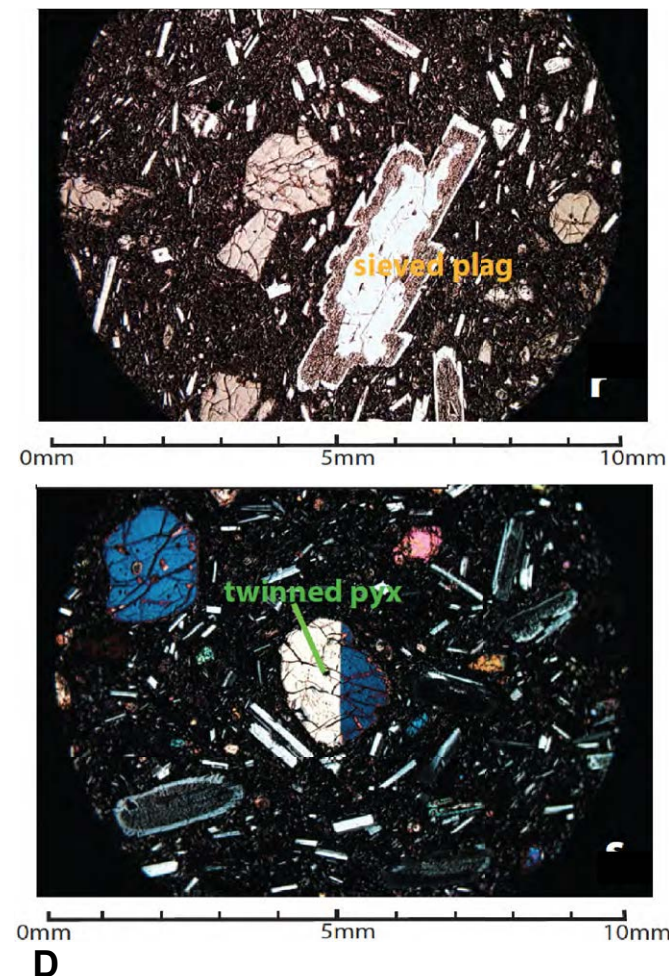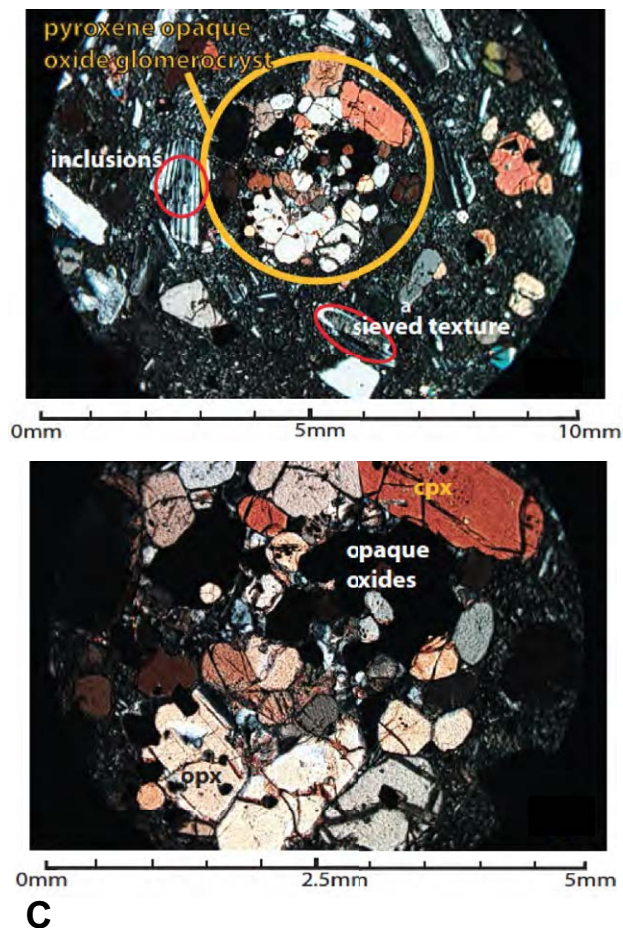
Figure 9 (*on this and following four pages*). Photomicrographs from the Sierra Crest graben-vent system (samples plotted on Fig. 2B): (A) Relief Peak Formation lava (Trpl): Two-pyroxene (pyx) basaltic andesite lava mantled with flow breccia, sample MG08–02, with modal analysis (Fig. 7A) and whole-rock geochemistry (Table 1) presented here; crossed polarizers. Top photo shows two pyroxenes and plagioclase in a glassy groundmass, and a 6-mm-long, sieve-textured, embayed, rimmed plagioclase feldspar. Lower photo shows an orthopyroxene crystal rimmed by a 0.5-mm-thick layer of clinopyroxene, adjacent to a large (2 mm) euhedral clinopyroxene crystal. (B) Table Mountain Latite (Tstml), Stanislaus Group: Two-pyroxene andesite lava (sample JHEP-67) with modal analysis (Fig. 7B) and whole-rock geochemistry (Table 1) presented here. Top photos (crossed polarizers and plane-polarized light) show sieve-textured plagioclase common to Table Mountain Latite. Bottom photos (crossed polarizers and plane-polarized light) show twinned phenocrysts of clinopyroxene.

Member forms one cooling unit in the Sierra Crest–Little Walker volcanic center and also in the Cataract paleochannel to the west, but at the reference section measured by King et al. (2007), it has three cooling units. It has a $^{40}Ar/^{30}Ar$ biotite age of 9.4 ± 0.3 Ma (Fig. 5). The third and uppermost ignimbrite (Upper Member) is by far the least extensive (Fig. 2). In the Sierra Crest–Little Walker volcanic center, the Upper Member ignimbrite is white and nonwelded (Figs. 6H and 6I), and it has interstratified pyroclastic fall deposits (Figs. 6I and 7C). At the reference section measured by King et al. (2007), the ignimbrite is welded and forms two cooling units. It has a $^{40}Ar/^{30}Ar$ biotite age of 9.34 ± 0.04 Ma (Fig. 5). All three ignimbrites have abundant volcanic rock fragments (Figs. 7C and 9I).

Lavas in the Eureka Valley Tuff occur at two stratigraphic levels (Figs. 2, 3, 5, and 14C):

(1) Basal Lava Flow Member, which is underlain by the Table Mountain Latite and locally overlain by the Tollhouse Flat Member: It is distinguished from Table Mountain Latite by its trachydacite composition and presence of hornblende and biotite (Figs. 7C and 9F; Table 1). Our new $^{40}Ar/^{30}Ar$ hornblende age of 9.94 ± 0.03 Ma (Fig. 5) shows that the Basal Lava Flow Member is intermediate in age between the Table Mountain Latite and the basal ignimbrite of the Eureka Valley Tuff. The dated locality lies along the NE-trending Poison Flat fault where a trachydacite intrusion with vertical flow banding cuts the Table Mountain Latite and passes upward into a 70-m-thick trachydacite lava with flow banding parallel to lavas in underlying Table Mountain Latite (Fig. 2). This vent area is indicated by a red star in Figures 2B and 4.
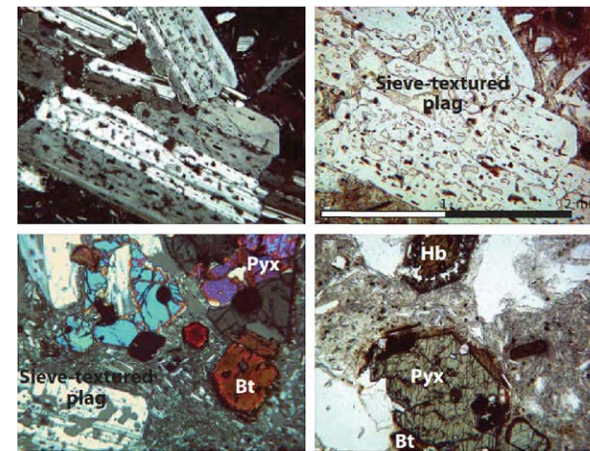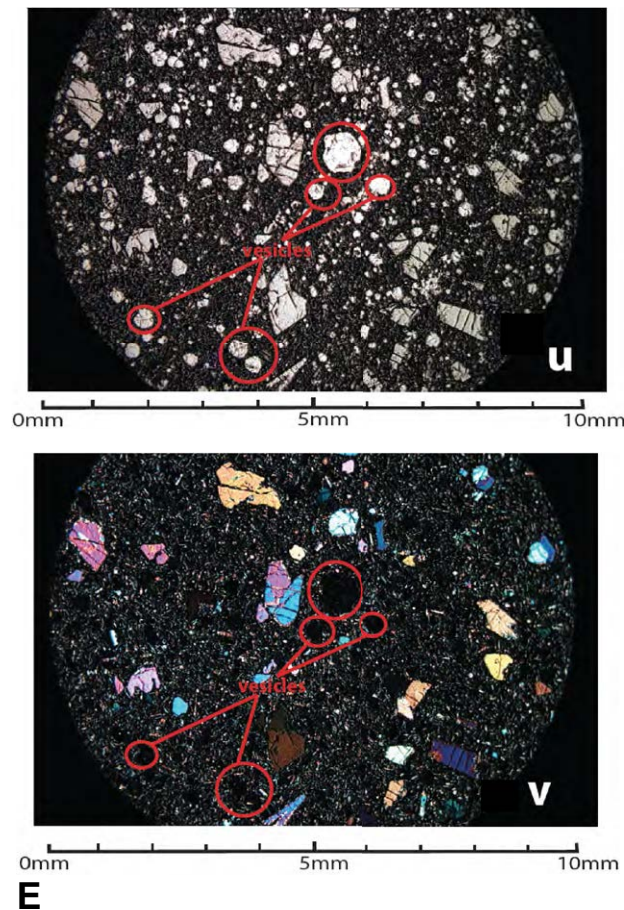
Figure 9 (*continued*). (C) Table Mountain Latite (Tstml), Stanislaus Group: Two-pyroxene olivine andesite lava (sample MG08–01), with modal analysis (Fig. 7B) and whole-rock geochemistry (Table 1) presented here. Top photo (crossed polarizers) shows glomerocryst of pyroxene and opaque oxides, as well as sieve-textured plagioclase, and plagioclase with inclusions. Bottom photo (crossed polarizers) is magnified view of two-pyroxene and opaque oxide glomerocryst, showing subrounded crystals 0.25 mm to 1.5 mm in length (cpx—clinopyroxene; opx—orthopyroxene). (D) Table Mountain Latite (Tstml), Stanislaus Group: Two-pyroxene basaltic andesite lava (sample MG08–04), with modal analysis (Fig. 7B) and whole-rock geochemistry (Table 1) presented here. Top photo (plane-polarized light) shows larger (6-mm-long) plagioclase phenocrysts with sieve textures near the rim, and clear euhedral plagioclase on the rim, with smaller phenocrysts (1–2 mm) showing sieve-textured cores and clear rims. This may indicate that there was a reaction between the crystals and one magma, followed by renewed growth in a magma of different composition. Lower photo (crossed polarizers) shows twinned and untwinned clinopyroxene.

(2) Lava Flow Member, which lies between Tollhouse Flat and By Day Member ignimbrites: Many of the lavas of the Lava Flow Member are indistinguishable from Table Mountain Latite (except by their stratigraphic position). Most lavas have basalt, basaltic trachyandesite, trachyandesite, and basaltic andesite compositions (Table 1), with large sieve-textured plagioclase phenocrysts (Fig. 9H), and many have clinopyroxene phenocrysts, which may be abundant to sparse (Figs. 7C, 9G, and 9H). However, trachydacite and trachydacite-andesite lavas also occur in the Lava Flow Member (unlike Table Mountain Latite; Table 1). Lava Flow Member rocks have large sieve-textured plagioclase (Fig. 9H), and vari-

able large (Fig. 9G) to small or absent clinopyroxene (Fig. 9H). Vent facies deposits also include trachydacite (sample 831-2; Fig. 7C). The Lava Flow Member also includes a well-preserved basalt cinder cone intruded by olivine basalt and passing laterally into olivine basalt lavas (Fig. 6G).

The Lava Flow Member lavas are tabular and concordant with bedding in underlying and overlying strata, but they appear chaotic in one small area, on the ridge between Golden Canyon and Murray Canyon (Fig. 2B). There, the Lava Flow Member shows inconsistent bedding orientations and rapid
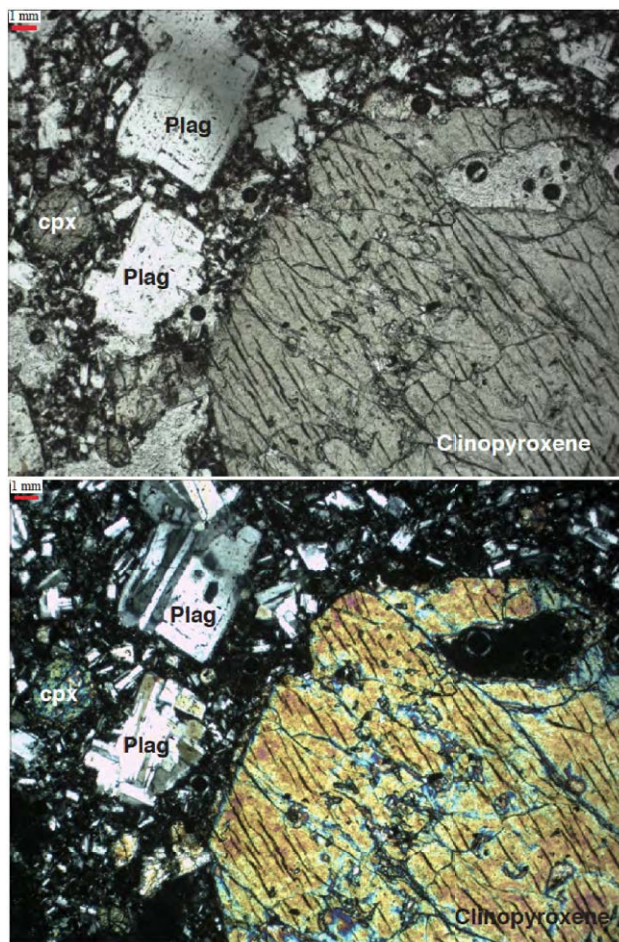
E

F

Figure 9 (*continued*). (E) Table Mountain Latite (Tstml), Stanislaus Group: Olivine (ol) two-pyroxene trachybasaltic andesite lava (sample MG08–03), with modal analysis (Fig. 7B) and whole-rock geochemistry (Table 1) presented here. Top photo is plane-polarized light, and lower photo is crossed polarizers. This sample is unusual for lacking plagioclase phenocrysts. It has small phenocrysts of olivine in addition to the larger pyroxene crystals. Vesicles are filled with chlorite. (F) Basal Lava Flow Member of the Eureka Valley Tuff (Tseblt), Stanislaus Group: Two-pyroxene hornblende biotite trachydacite intrusion that cuts Table Mountain Latite and passes upward into a lava flow that overlies Table Mountain Latite (Tselbt, sample JHEP-88), dated at 9.84 ± 0.03 Ma (Fig. 4), with modal analysis (Fig. 7B) and whole-rock geochemistry (Table 1) presented here. Top photos (crossed polarizers and plane-polarized light) show sieve-textured plagioclase phenocrysts, typical of Stanislaus Group, in a fine-grained to glassy groundmass. Bottom-left photo (crossed polarizers) shows biotite, pyroxene, and sieve-textured plagioclase (plag) crystals. Bottom-right photo (plane-polarized light) shows biotite (Bt), hornblende (Hb), pyroxene, and plagioclase phenocrysts.
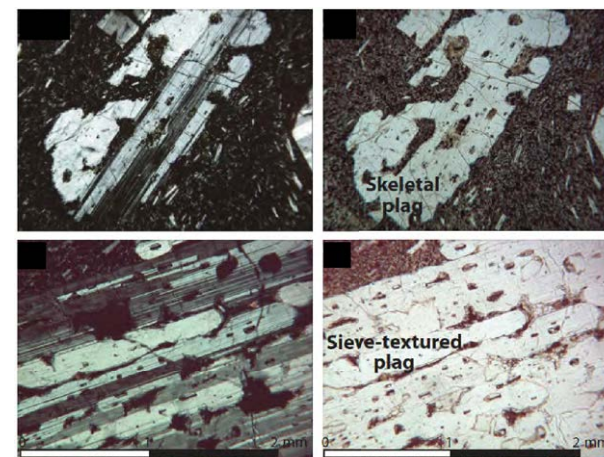
lateral juxtaposition of lavas with varying textures and compositions. A trachydacite lava with flow breccia from that section yielded a new $^{40}Ar/^{30}Ar$ plagioclase age of 11.66 ± 0.07 Ma (sample JHEP-64; Fig. 2B). Because this lava lies up section from the 9.54 ± 0.04 Ma Tollhouse Flat Member (Fig. 2B), and because the section is chaotic, this sample is interpreted to be from a megaslide block within the Lava Flow Member (Fig. 5), indicating ongoing faulting during eruption of the Lava Flow Member. The megaslide slab overlaps in age with our dates on andesites of the Relief Peak Formation (Fig. 5), and we have found no in situ high-K_2O rocks older than 10.41 ± 0.08 Ma (basal Table Mountain Latite on Sonora Peak; Fig. 5). High-K_2O rocks were erupted at this time in the Bodie Hills (John et al., 2012), but that is 55 km away from the location of the dated slide block. The source of the megaslide slab is thus unknown.

We have found no lavas between the By Day and Upper Members. The error on the $^{40}Ar/^{39}Ar$ date on the By Day Member ignimbrite is large (Figs. 3 and 5), overlapping in age with the overlying Upper Member, but it is at least ~0.17 m.y. younger than the underlying Tollhouse Flat Member (Fig. 3). Perhaps the Lava Flow Member records a greater time gap between the first two ignimbrites than the second and third ignimbrites. However, it seems more likely that the absence of lavas between the By Day and Upper Member ignimbrites records waning high-K_2O effusive volcanism across the Sierra Crest–Little Walker volcanic center, as indicated by initial rapid flood andesite eruptions (Table Mountain Latite) through eruption of progressively smaller volumes of ignimbrite alternating with small-volume lava effusions (Eureka Valley Tuff). The uppermost high-K_2O unit, the Dardanelles Formation, occurs in the type section of Stanislaus Group designated by
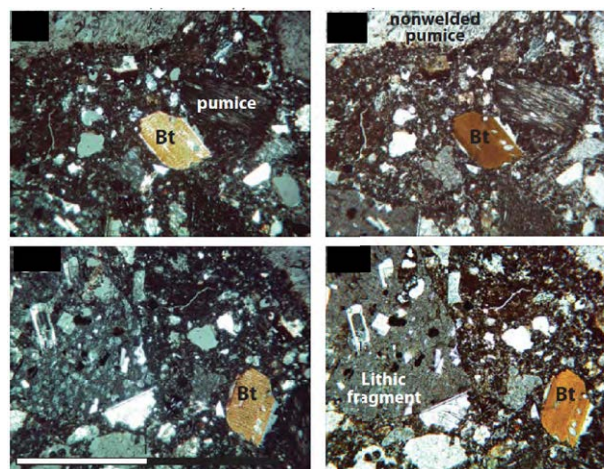
Figure 9 (*continued*). (G) Lava Flow Member of the Eureka Valley Tuff (Tsel), Stanislaus Group: Two-pyroxene basaltic andesite lava (sample BLM09–825–1), with modal analysis (Fig. 7C) and whole-rock geochemistry (Table 1) presented here. Top photo is plane-polarized light, and lower photo is crossed polarizers. Clinopyroxene is large and euhedral to embayed, and the groundmass has plagioclase crystals intergrown with an opaque mineral. **(H)** Lava Flow Member of the Eureka Valley Tuff (Tsel), Stanislaus Group: Clinopyroxene trachyandesite-trachydacite lava (sample JHEP-64), with modal analysis (Fig. 7C) and whole-rock geochemistry (Table 1) presented here. Left photos were taken with crossed polarizers, and right photos were taken with plane-polarized light. This is a variety of Lava Flow Member that is dominated by large (2 mm) skeletal and sieve-textured plagioclase with only minor mafic phenocrysts (clinopyroxene, not shown). **(I)** Eureka Valley Tuff, Upper Member (Tseu), Stanislaus Group: Two-pyroxene biotite ignimbrite (sample JHEP-65f) with modal analysis (Fig. 7C) and whole-rock geochemistry (Table 1) presented here. Left photos were taken with crossed polarizers, and right photos were taken with plane-polarized light. Upper Member of the Eureka Valley Tuff pyroclastic units are characterized by large biotite phenocrysts, with much lesser pyroxene (not shown; see modal analysis). Pumice fragments and volcanic lithics in a matrix of glass shards and broken crystals.
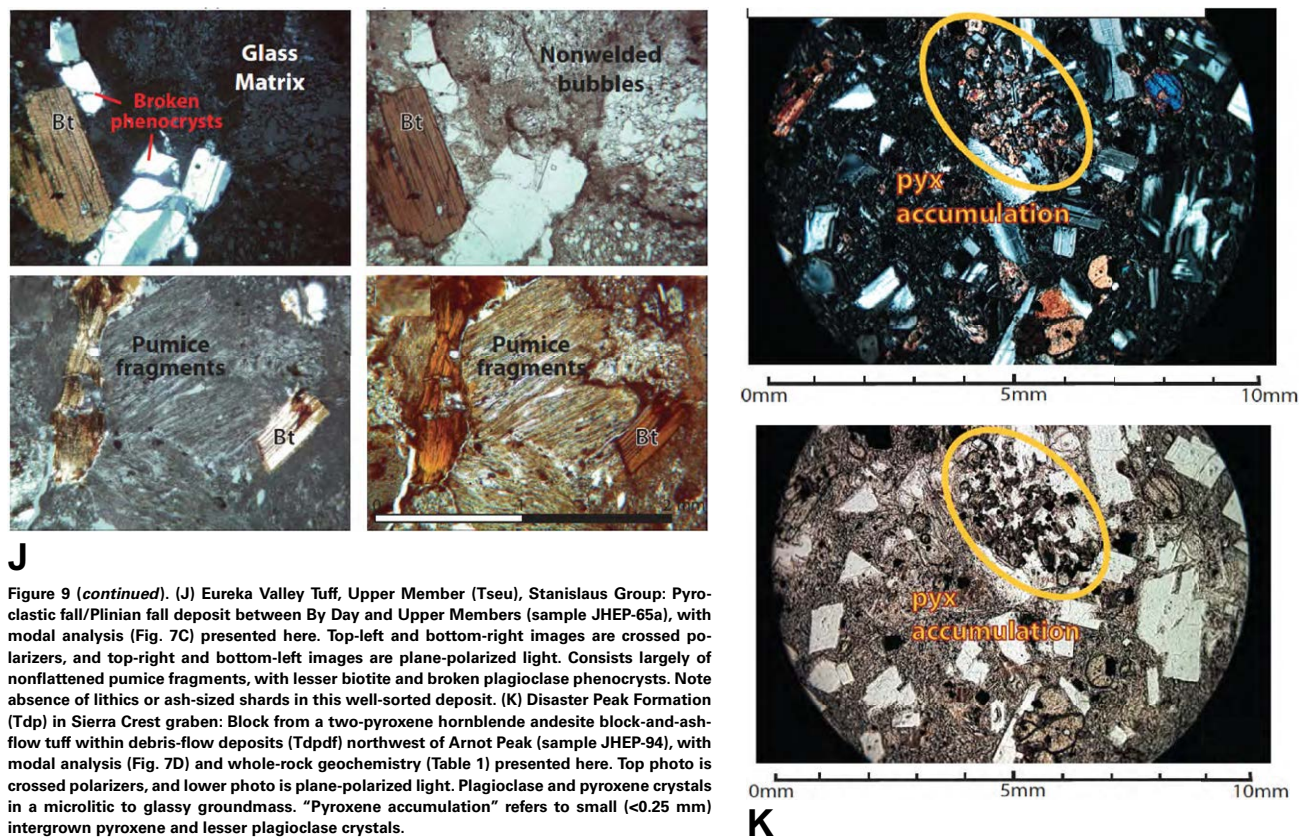
Slemmons (1953), but it is the least-extensive and least-volumetric unit (discussed next).

   Dardanelles Formation. The Dardanelles Formation consists of a single, distinctive, black glassy, nearly aphyric shoshonite lava, up to 60 m thick (top eroded), and two plugs along the western margin of the Sierra Crest graben (Busby et al., 2013a). Previous workers thought it had multiple lavas because they confused it with the Lava Flow Member (see summary in Koerner et al., 2009). The lava is discontinuously preserved for ~15 km westward down the Cataract paleochannel to Dardanelles Cone (Busby et al., 2016). One could argue that it should be included in Eureka Valley Tuff, but the other lava members include silicic (trachydacite) lavas, and we have found none above the Upper Member, so we follow the historical precedent and retain the formational name, even though it is only one lava.

   We report a new $^{40}Ar/^{39}Ar$ whole-rock age on the single Dardanelles Formation shoshonite lava of 9.137 ± 0.017 Ma (Fig. 5). This is consistent with its stratigraphic position above the Upper Member of Eureka Valley Tuff (Fig. 3; Busby et al., 2013a). It is ~150–260 k.y. younger than the Upper Member, which makes it closer in age to the ignimbrites than the Basal Lava Flow

J

Figure 9 (*continued*). (J) Eureka Valley Tuff, Upper Member (Tseu), Stanislaus Group: Pyroclastic fall/Plinian fall deposit between By Day and Upper Members (sample JHEP-65a), with modal analysis (Fig. 7C) presented here. Top-left and bottom-right images are crossed polarizers, and top-right and bottom-left images are plane-polarized light. Consists largely of nonflattened pumice fragments, with lesser biotite and broken plagioclase phenocrysts. Note absence of lithics or ash-sized shards in this well-sorted deposit. (K) Disaster Peak Formation (Tdp) in Sierra Crest graben: Block from a two-pyroxene hornblende andesite block-and-ash-flow tuff within debris-flow deposits (Tdpdf) northwest of Arnot Peak (sample JHEP-94), with modal analysis (Fig. 7D) and whole-rock geochemistry (Table 1) presented here. Top photo is crossed polarizers, and lower photo is plane-polarized light. Plagioclase and pyroxene crystals in a microlitic to glassy groundmass. "Pyroxene accumulation" refers to small (<0.25 mm) intergrown pyroxene and lesser plagioclase crystals.

K

Member, which is ~470–510 k.y. older than the basal ignimbrite (Tollhouse Flat Member).

The Dardanelles Formation is the youngest high-K_2O unit; thus, high-K_2O volcanism of the Stanislaus Group spanned ~1.2–1.4 m.y.
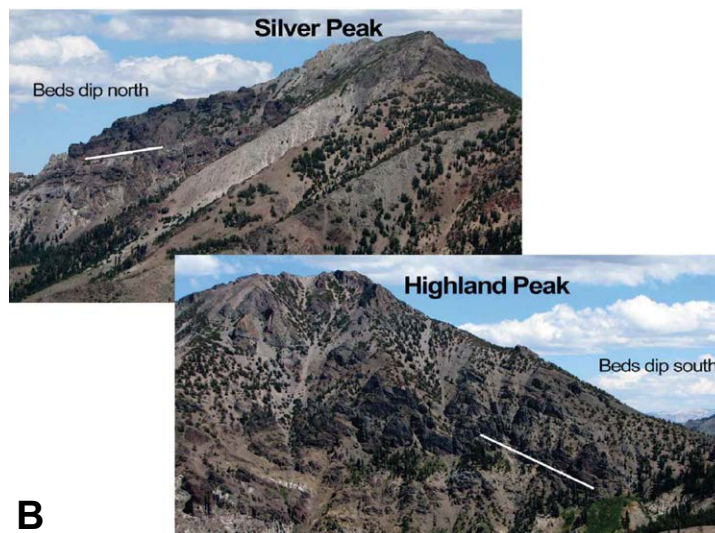
Disaster Peak Formation

The ca. 9–5 Disaster Peak Formation in the Sierra Crest–Little Walker volcanic center marks the end of high-K_2O arc magmatism in the arc axis (Fig. 14D), suggesting that the supply of low-partial melt magmas was exhausted, or that their release by transtension slowed. The southern half of the Sierra Crest–Little Walker volcanic center became magmatically and tectonically inactive, except for a few small hornblende andesite intrusions that cut the Stanislaus Group, a hornblende-bearing ignimbrite and lava preserved as erosional remnants on the ridge crest north of the Kennedy Creek fault, and a quartz dacite sill intruded along the Chango Lake fault on the range front (Busby et al., 2008a, 2013a, 2013b, 2016).

Disaster Peak Formation strata in the northern part of the Sierra Crest–Little Walker pull-apart basin form nearly half of the up to 1300 m thick fill (Figs. 2B and 14D). There, the Disaster Peak Formation is ~25% primary volcanic rock (basalt to andesite lavas and andesite to dacite block-and-ash-flow tuffs; Fig. 2B; Table 1), and the rest is debris-flow and fluvial deposits with volcanic clasts. Disaster Peak Formation in the northern part of the Sierra Crest–Little Walker pull-apart basin differs from Relief Peak Formation in the following ways: (1) It contains abundant reworked silicic pyroclastic debris in the form of pumice, crystals, and ash in debris-flow and fluvial deposits (Fig. 6K), while the Relief Peak Formation only has megaslide slabs of silicic pyroclastic rocks of the Oligocene Valley Springs Formation. The 600-m-high white cliffs on the north and east faces of Arnot Peak (Fig. 2B) are dominated by reworked silicic pyro-
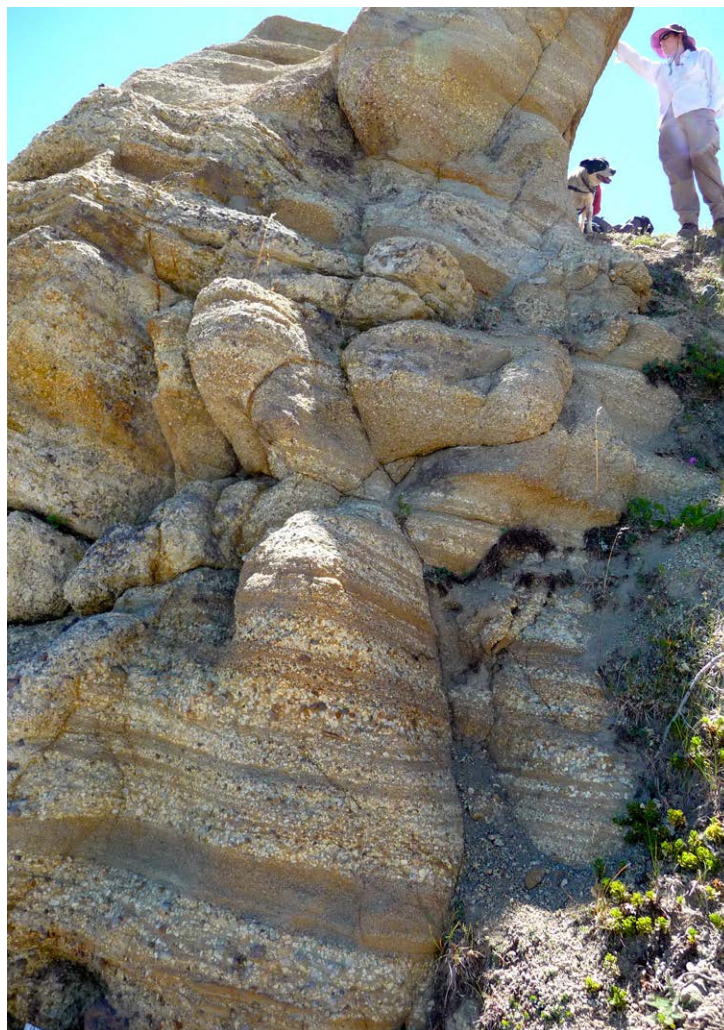
A

B

C

Figure 10 (*on this and following three pages*). Outcrop photos from the Ebbetts Pass volcanic center; see stratigraphy in Figures 2 and 5. (A) Oblique aerial photo of Ebbetts Pass stratovolcano (Tdpeps); top partially eroded. (B) View of Ebbetts Pass stratovolcano, looking eastward from the Sierra Crest on the footwall of the Noble Canyon fault (Tdpeps; Fig. 2), showing northward primary dips on the north flank of the edifice (north of Silver Peak) and southward dips on the south flank of the edifice (south of Highland Peak; see Fig. 2B). Silver Peak and Highland Peak are formed of silicic intrusions at the eroded crest of the stratovolcano. (C) Basal section of black olivine two-pyroxene basaltic andesite lavas of the Ebbetts Pass stratovolcano on the footwall of the Noble Canyon fault, along the Sierra Crest ~1.5 km south of Ebbetts Pass. Photo shows primary westward dips away from the center of the stratovolcano. See sample JHEP-9 for geochronology, geochemistry, photomicrograph, and modal analysis. At this locality, the basal basaltic andesite lava section has an underlying white clinopyroxene-orthopyroxene quartz lava (sample JHEP-10; Fig. 11A) that is flow banded, with a flow-top breccia (see text for discussion).

clastic debris, although in most places, it is subordinate to andesitic lithic clasts. (2) It has far more abundant lavas, at all stratigraphic positions. (3) Abundant basaltic andesite, andesite, and dacite intrusions are closely associated spatially with the northern part of the Sierra Crest–Little Walker volcanic center and die off away from it into granitic basement (Fig. 2). These characteristics show that the ancestral Cascades arc axis lay within the Sierra Crest–Little Walker pull-apart basin during Disaster Peak Formation time (Fig. 14D), rather than east of it, as it did during Relief Peak Formation time (Figs. 14B and 15A). The reworked silicic pyroclastic debris records silicic explosive eruptions penecontemporaneous with deposition of the fluvial and debris-flow deposits, indi-

cating that the arc was becoming more evolved. The Disaster Peak Formation also has more hornblende and less pyroxene than the Relief Peak Formation (Figs. 7A and 7D), although this is not a reliable way to distinguish between the two formations.

In the N-S Sierra Crest graben, the Disaster Peak Formation forms a N-S paleochannel cut into the Stanislaus Group (Fig. 14D), and this is filled with interstratified fluvial and debris-flow deposits, with clast imbrication and cross-bedding indicating northward transport. This paleochannel ("deranged Cataract paleochannel"; Fig. 4A) lies perpendicular to the E-W Nevadaplano paleochannels (Figs. 4A and 14A) and parallel to

Figure 10 (*continued*). (D) Small channel with beds of volcanic lithic fluvial sandstone (tan) alternating with beds rich in reworked pumice (white fragments). Ebbetts Pass stratovolcano (Tdpeps), west of the Noble Canyon fault, along the Sierra Crest 1.5 km southeast of Ebbetts Pass at the location of the strike and dip symbol (Fig. 2B; bedding dips 25° to the southwest). This body is too small to be mappable. 60 pound (27 kg) Lou Dawg (and Jeanette Hagan) for scale. (E) East-facing view of the north flank of the Ebbetts Pass stratovolcano along the ridge north of Silver Peak, which forms the light-gray silicic intrusion at the upper-right corner of photo. Red scoria fall and scoria flow deposits, dark-colored lavas and flow breccias, and white silicic tuffs and block-and-ash-flow tuffs dip northward away from the center of the stratovolcano. Discordances in bedding were produced by syndepositional slumps and faults. A 50-m-wide clastic dike cuts >180 m vertically up through the section, infilled with coarse-grained fragmental volcanic rock (outlined in white). Height of cliff face is ~300 m. (F) Mafic lava with red basal flow breccia, overlain by white rhyolite quartz biotite block-and-ash-flow tuff (sample 814–7; Table 1). Ebbetts Pass stratovolcano on the west side of Silver Peak (Fig. 2B).

D

E

F

modern Walker Lane drainages (Fig. 1), indicating tectonic reorganization of the landscape at ca. 9–5 Ma (Busby et al., 2016). We infer that it fed into the Mokelumne paleochannel, which remained undisrupted in this time frame (Fig. 14D). This section includes a hornblende orthopyroxene andesite block-and-ash-flow tuff (JHEP-55; Fig. 2B; Table 1), which yielded a $^{40}Ar/^{39}Ar$ hornblende age of 4.96 ± 0.05 Ma (Fig. 5). In contrast, the NE

transfer zone basins lack fluvial deposits and are dominated by massive debris-flow deposits, similar in appearance to Relief Peak Formation; however, they differ from Relief Peak Formation by having far more interstratified lavas (Figs. 2B and 14D).

Lavas in the Sierra Crest graben include clinopyroxene basaltic andesite lavas (samples 830-3, 830-2, and 918-1; Fig. 7D; Table 1) and a basalt lava

G

H

I

Figure 10 (*continued*). (G) Close-up of the white rhyolite quartz biotite block-and-ash-flow tuff, showing two flow units: a lower ash matrix-supported flow unit and an upper blocky flow unit. (H) Westernmost flank and highest stratigraphic level of the Ebbetts Pass stratovolcano (Tdpeps), on the footwall of the Noble Canyon fault south of Reynolds Peak (Fig. 2B). Primary dips are westward, formed of block-and-ash-flow tuffs (see parts J and K) and lesser volcanic debris-flow deposits. (I) Lateral equivalent of the Ebbetts Pass stratovolcano section shown in Figure 10H, to the north at Reynolds Peak (Fig. 2B), showing slump-folded strata. The slump folding indicates partial sector collapse, perhaps triggered by movements on the Noble Canyon fault, which has a synvolcanic to postvolcanic slip history (see text).

with plagioclase and trace olivine (sample 906-1; Figs. 2B and 7D; Table 1). Samples 827-1 and 827-2 (andesite and basaltic andesite, respectively; Table 1) are tentatively mapped as intrusions on Figure 2B (Tdpia and Tiba, east of Disaster Peak), but they may instead be lavas. Basal contacts on lavas within the deranged Cataract paleochannel locally exhibit complex mixing with the sedimentary rock below, indicating eruption onto wet and unconsolidated sands (peperites). Block-and-ash-flow tuffs in the Sierra Crest graben are generally too lenticular to map individually within Disaster Peak Formation, but one mappable body lies at the base of the Disaster Peak Formation along the Paradise Valley trail south-southeast of Arnot Peak (Tdpba; Fig. 2B), consisting of an andesite block-and-ash-flow tuff (sample 824-3; Table 1). Smaller lenses of block-and-ash-flow tuff within Disaster Peak Formation include (Fig. 2B;

Table 1): (1) an andesite block-and-ash-flow tuff along the ridge north of Murray (sample 911-4); (2) an andesite-dacite block-and-ash-flow tuff northwest of Arnot Peak, with phenocrysts of clinopyroxene, orthopyroxene, and hornblende in roughly equal proportions (sample JHEP-94; Fig. 7D; Table 1), and local fine-grained clots of pyroxene intergrown with plagioclase (Fig. 9K); and (3) an andesite block-and-ash-flow tuff south of Disaster Peak with hornblende and minor orthopyroxene (sample JHEP-55; Fig. 7D). It yielded a new $^{40}Ar/^{39}Ar$ hornblende age of 4.96 ± 0.05 Ma (Fig. 5).

Lavas in the NE transfer zone basins include a section of seven olivine basalt lavas along the Mineral Mountain–Poison Flat fault zone (sample JHEP-83, and samples 817–1, 2, 3, 4, 5; Fig. 2B; Table 1). These have plagioclase and trace olivine (Fig. 7D).

Figure 10 (*continued*). (J) Lower reddish black andesite block-and-ash-flow tuff (sample CB09–04; Table 1), Ebbetts Pass stratovolcano (Tdpeps) on the footwall of the Noble Canyon fault at Reynolds Peak. (K) Upper light-gray andesite block-and-ash-flow tuff (sample CB09–05; Table 1), Ebbetts Pass stratovolcano (Tdpeps), on the footwall of the Noble Canyon fault at Reynolds Peak. (L–M) Andesite lava of Bull Run in the Mokelumne paleochannel west of the Ebbetts Pass stratovolcano (samples CB09–1 and CB09–2; Table 1), erupted from the Ebbetts Pass stratovolcano (Fig. 14E). The basal several meters of the andesite lava contain thin, wispy accumulations of plagioclase-rich andesite oriented both subhorizontally (L) and subvertically (M), perhaps indicating some magma mingling, although whole-rock compositions are very similar (Table 1).

Tectonic recycling continued during deposition of Disaster Peak Formation in the northern Sierra Crest–Little Walker volcanic center, as shown by the presence of a dacite lava megaslide slab in a transfer zone basin (sample JHEP-70; Fig. 2B). This lies up section from the Stanislaus Group (Fig. 2), but it yielded a $^{40}Ar/^{39}Ar$ hornblende age of 11.05 ± 0.031 Ma (Fig. 5). It is therefore recycled from Relief Peak Formation.

Numerous plugs are closely associated with the Disaster Peak Formation in the northern half of the Sierra Crest–Little Walker volcanic center and pull-apart (Fig. 2). These are mineralogically and geochemically similar to the lavas and block-and-ash-flow tuffs (Figs. 7 and 8; Table 1) and probably represent feeders for them. Some of them are localized along faults or buried faults (e.g., Jones Canyon fault; Fig. 2B).
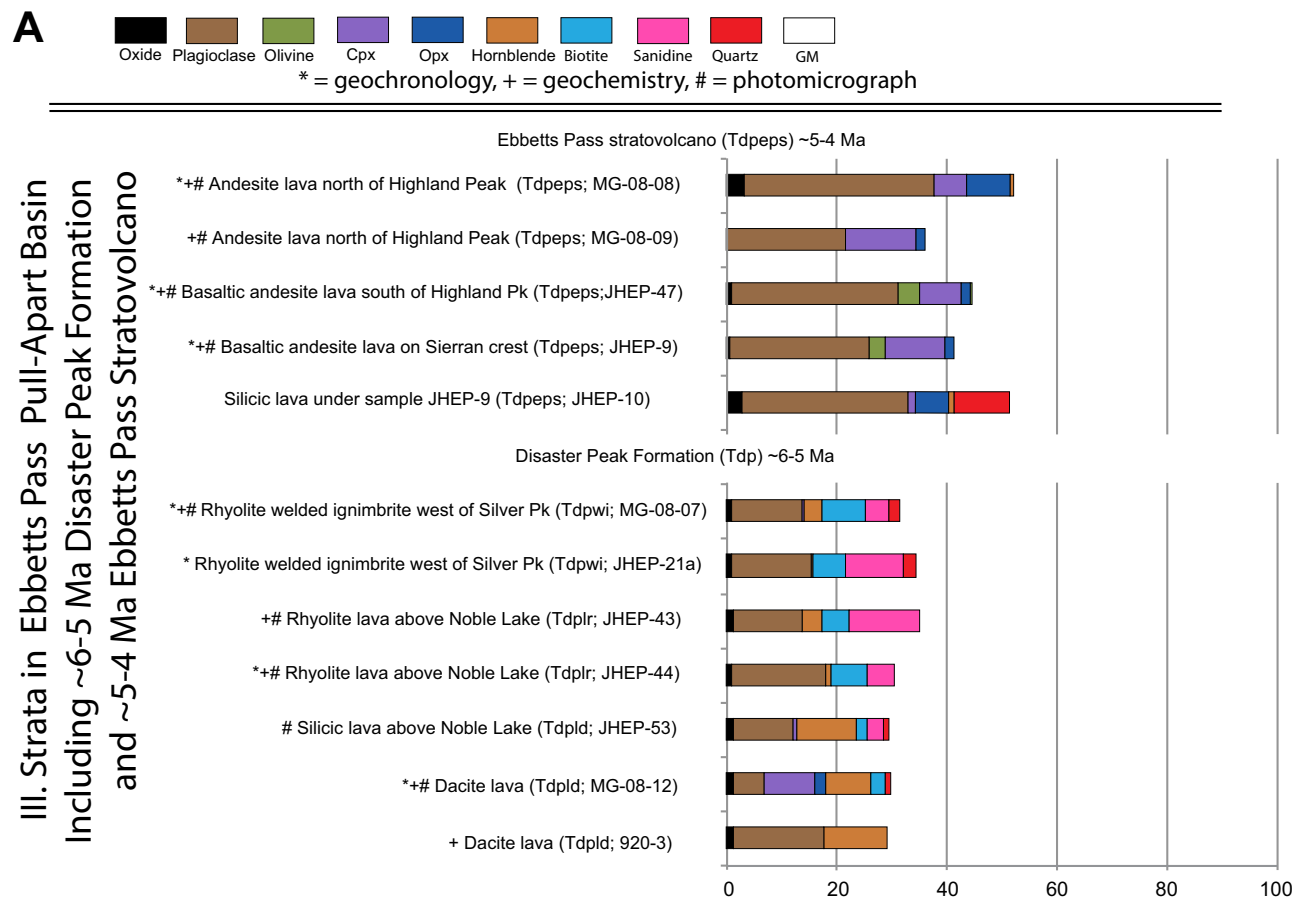
A

Oxide Plagioclase Olivine Cpx Opx Hornblende Biotite Sanidine Quartz GM

* = geochronology, + = geochemistry, # = photomicrograph

III. Strata in Ebbetts Pass Pull-Apart Basin
Including ~6-5 Ma Disaster Peak Formation
and ~5-4 Ma Ebbetts Pass Stratovolcano

Ebbetts Pass stratovolcano (Tdpeps) ~5-4 Ma

*+# Andesite lava north of Highland Peak (Tdpeps; MG-08-08)

+# Andesite lava north of Highland Peak (Tdpeps; MG-08-09)

*+# Basaltic andesite lava south of Highland Pk (Tdpeps;JHEP-47)

*+# Basaltic andesite lava on Sierran crest (Tdpeps; JHEP-9)

Silicic lava under sample JHEP-9 (Tdpeps; JHEP-10)

Disaster Peak Formation (Tdp) ~6-5 Ma

*+# Rhyolite welded ignimbrite west of Silver Pk (Tdpwi; MG-08-07)

* Rhyolite welded ignimbrite west of Silver Pk (Tdpwi; JHEP-21a)

+# Rhyolite lava above Noble Lake (Tdplr; JHEP-43)

*+# Rhyolite lava above Noble Lake (Tdplr; JHEP-44)

Silicic lava above Noble Lake (Tdpld; JHEP-53)

*+# Dacite lava (Tdpld; MG-08-12)

+ Dacite lava (Tdpld; 920-3)

0   20   40   60   80   100

Figure 11 (*on this and following page*). Modal analysis of strata in the Ebbetts Pass volcanic center and pull-apart basin. (A) Strata within the pull-apart basin divided into time frames: Disaster Peak Formation (ca. 6–5 Ma), also referred to here as the lower silicic section (Fig. 4); and Ebbetts Pass stratovolcano (ca. 5–4 Ma). (B) Lavas along the east margin of the Ebbetts Pass pull-apart basin (east of the Wolf Creek fault; Fig. 2B), tentatively inferred to have erupted from the Ebbetts Pass stratovolcano. Cpx—clinopyroxene, Opx—orthopyroxene, GM—groundmass.

In summary, the northern Sierra Crest–Little Walker pull-apart remained magmatically active from ca. 9 to ca. 5 Ma, with basalts, basaltic andesites, and andesites at all stratigraphic levels throughout the pull-apart, accompanied by emplacement of basalt to dacite intrusions. The Ebbetts Pass pull-apart basin and volcanic center began to form by 6.4 Ma (Figs. 5 and 14D), thus overlapping in time with the northern part of the Sierra Crest–Little Walker volcanic center and pull-apart by ~1.4 m.y. (Fig. 14D).

Ebbetts Pass Volcanic Center and Pull-Apart Basin

The basal fill of the Ebbetts Pass pull-apart basin (Tvu and Tva) consists of andesitic debris-flow deposits that are hydrothermally altered (Figs. 2B and 14E). In contrast, the overlying volcanic rocks in the Ebbetts Pass pull-apart ba-

sin are unaltered (Fig. 13). We infer that the altered basal debris-flow deposits record catastrophic sedimentation during initial subsidence of the pull-apart basin, similar to mass-transport deposits at the base of the Sierra Crest–Little Walker pull-apart basin. The basal fill was then altered by convective flow of heated groundwater due to emplacement of intrusions below the volcanic center that grew above it. Unaltered intrusions in the altered basal fill probably represent the last stages of this process. These include a two-pyroxene andesite intrusion (sample MG-08-13) and a two-pyroxene hornblende biotite quartz dacite intrusion (sample MG-08-10; Fig. 12; Table 1). The dacite intrusion has large quartz and plagioclase phenocrysts, hornblende with groundmass cores, and small twinned pyroxene phenocrysts or glomerocrysts set in a microcrystalline groundmass (Fig. 13F). Additional unaltered intrusions include a small unmapped andesite body (sample MG-08-11; Table 1) and a large

B

Oxide   Plagioclase   Hornblende   Alteration   GM

+ = geochemistry, # = photomicrograph

Lavas of Unknown Age tentatively assigned to Ebbetts Pass Volcanic Center

east of Wolf Creek fault

+# Andesite lava(?) along Carson River (Tvu; JHEP-36)

+# Basaltic andesite lava(?) along Carson River (Tvu; JHEP-31)
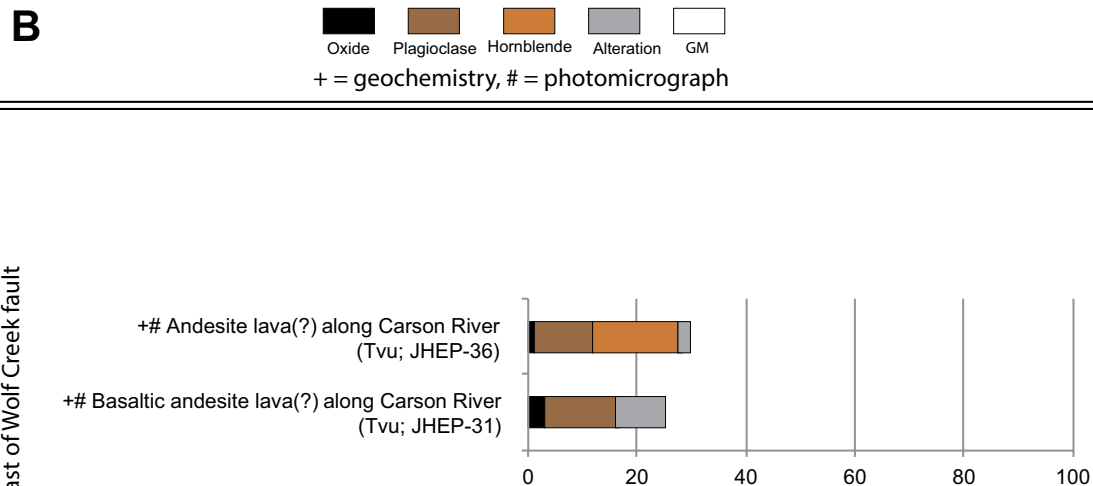
0   20   40   60   80   100

Figure 11 (*continued*). (B) Lavas along the east margin of the Ebbetts Pass pull-apart basin (east of the Wolf Creek fault; Fig. 2B), tentatively inferred to have erupted from the Ebbetts Pass stratovolcano. Cpx—clinopyroxene, Opx—orthopyroxene, GM—groundmass.

mapped andesite body with a sample at each end (Tdpia, samples MG-08-13 and 920-2; Fig. 2B). The unaltered intrusions in the altered basal fill are inferred to represent feeders to unaltered volcanic rocks and intrusions in the overlying part of the section, because they are similar in chemistry and mineralogy.

We divide the unaltered volcanic rocks of the Ebbetts Pass pull-apart basin into a lower silicic section and an upper section that we refer to as the Ebbetts Pass stratovolcano (Fig. 5).

Lower Silicic Section

Mappable bodies of the lower silicic section include an older (Miocene) dacite lava (Tdpld), and younger (Pliocene) rhyolite lavas (Tdplr) and strongly welded rhyolite ignimbrite (Tdpwi; Fig. 2B) that are ~1.6 m.y. younger than the Miocene lavas (Fig. 5).

The dacite lava forms a fault-bounded body >2.5 km long and >225 m thick in the hanging wall of a strand of the Wolf Creek fault, along the southern margin of the basin (Tdpld; Fig. 2B). This splay is partly buried by the

Pliocene rhyolite lava (Tdplr), described later, and is crosscut by the undated andesite intrusion (Tdpia) described earlier (Fig. 2B). The dacite lava has a new $^{40}Ar/^{39}Ar$ hornblende age of 6.367 ± 0.017 Ma (sample MG-08-12; Fig. 5). We interpret it to be part of a suite of andesite to dacite lavas emplaced along the margins of the incipient Ebbetts Pass pull-apart at 6.4–6.2 Ma (Fig. 14D); further evidence for this includes a Miocene andesite megaslide slab, 25 m thick and >200 m long, with a hornblende $^{40}Ar/^{39}Ar$ age of 6.203 ± 0.011 Ma (Fig. 5; sample MG-08-08; Fig. 2B). This slab was shed from the basin margin into strata of the Pliocene Ebbetts Pass stratovolcano, described later. The Miocene dacite lava varies from plagioclase hornblende dacite (sample 920-3; Fig. 11A) to plagioclase clinopyroxene orthopyroxene hornblende biotite quartz dacite (sample MG-08-12; Fig. 11A). Although most of the body is dacite (samples 920-3, 920-4, and MG-08-12; Table 1), the base of the lava is an andesite (sample 920-1; Table 1), and mafic enclaves are present near the western margin of the lava. The mineralogical and compositional heterogeneity in the dacite lava indicates that it is composed of multiple flows or records magma mingling. It differs from the Pliocene silicic volcanic rocks and intrusions by lacking sanidine (Fig. 11A).
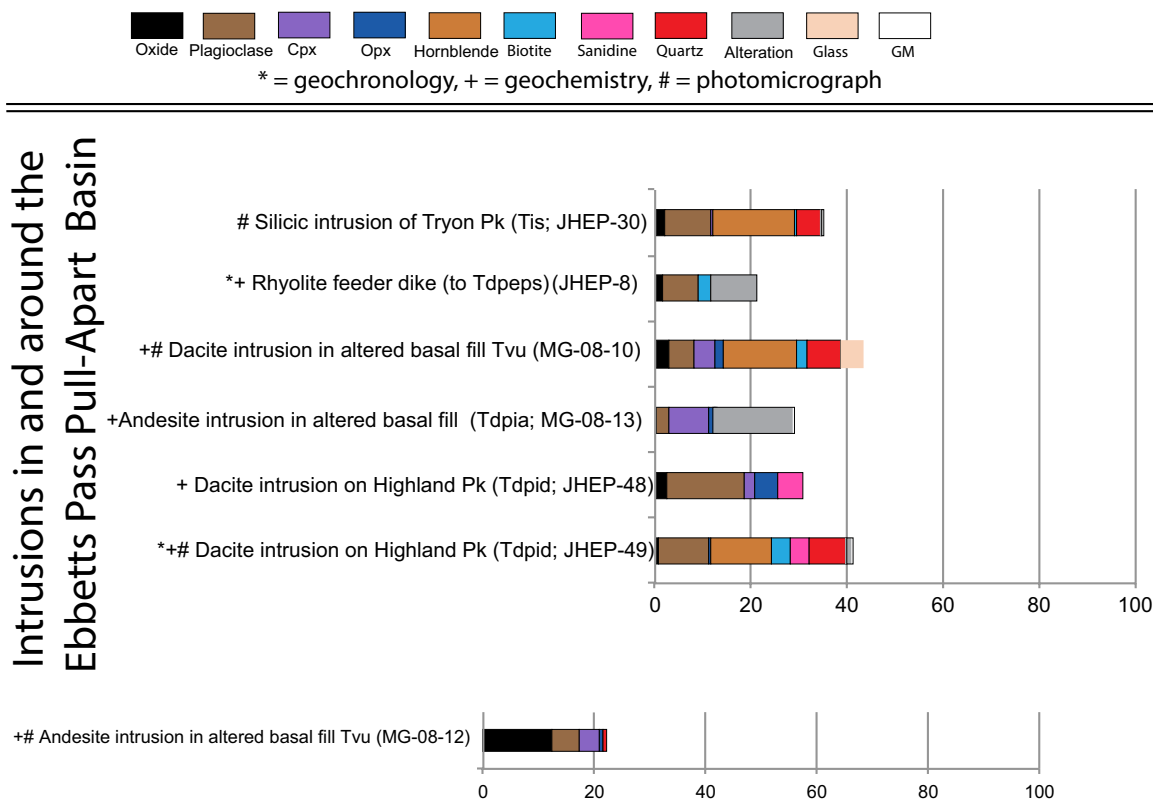
Figure 12. Modal analysis of intrusions in and around the Ebbetts Pass volcanic center and pull-apart basin. Cpx—clinopyroxene, Opx—orthopyroxene, GM—groundmass.

Our new dates on the Pliocene rhyolite lavas and the rhyolite welded ignimbrite are very similar in age, perhaps within 60 k.y. of each other using the analytical errors (Fig. 5), and they lie along strike of each other (Tdplr and Tdpwi, respectively; Fig. 2B).

The Pliocene rhyolite welded ignimbrite (Tdpwi; Fig. 2B; Table 1) has a new ^{40}Ar/^{39}Ar sanidine single-crystal age of 4.636 ± 0.011 Ma (Fig. 5). It consists largely of sintered bubble-wall shards and collapsed pumice (Fig. 13A), with 30% phenocrysts, including plagioclase, biotite, sanidine, and quartz ± hornblende (Fig. 11A). Quartz and plagioclase are strongly embayed, and the mafic minerals are fresh, with no inclusions or rims (Fig. 13A). The rhyolite ignimbrite has very strongly welded domains that appear banded, alternating with more weakly welded domains that are clearly vitroclastic. The orientation of pumice compaction foliation is variable, and fiamme may be attenuated to >4 m in length and deformed into complex flow folds, typical of very strongly welded ("lava-like" or "rheomorphic") ignimbrites. The glassy part of the ignimbrite has perlitic fracturing, and in the upper vapor phase-altered part, the

fiamme are altered. The Pliocene rhyolite lava map unit (Tdplr; Fig. 2B) has a new ^{40}Ar/^{39}Ar hornblende age of 4.73 ± 0.03 Ma (Tdplr, sample JHEP-44; Fig. 4). It forms a stubby map unit, >60–135 m (200–440 ft) thick and 1 km long, typical of silicic lavas. Its mineralogy is identical in two samples collected close to each other (200 m apart, JHEP-43 and JHEP-44; Figs. 2B, 11A), with plagioclase, hornblende, biotite, and sanidine. However, a third sample collected 1 km away from those (JHEP-53; Fig. 2B) also has clinopyroxene and quartz (Fig. 11A), although it is otherwise identical in the field. Thus, the rhyolite lava probably represents a composite of two or more flows, or comingled magmas. The lava is pervasively flow-banded, with gray glassy bands (Fig. 13B) and pale-red stony/devitrified bands (Fig. 13C).

The Pliocene rhyolite welded ignimbrite and rhyolite lava are overlain by the Ebbetts Pass stratovolcano (Tdpeps; Fig. 2B). The base of the Ebbetts Pass stratovolcano is marked by basaltic andesite lavas that dip away from its center and downlap onto underlying strata. It is this downlap that forms the unconformity recognized by Armin et al. (1984).
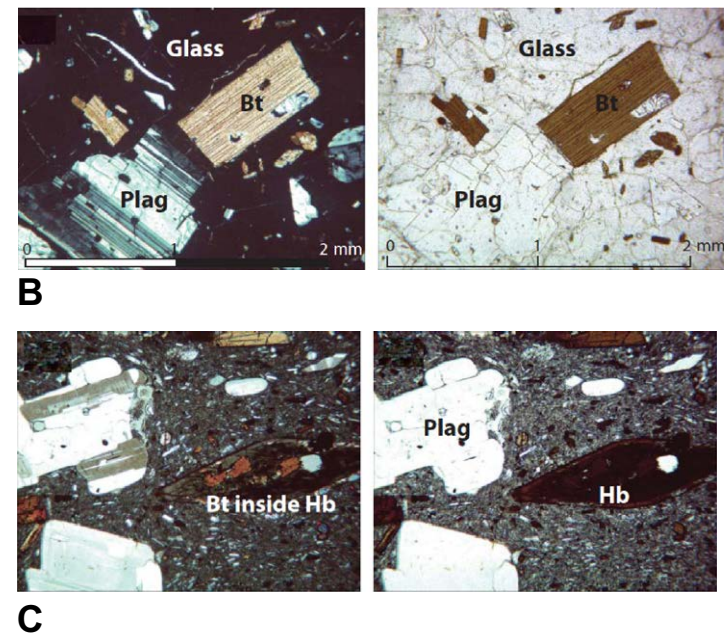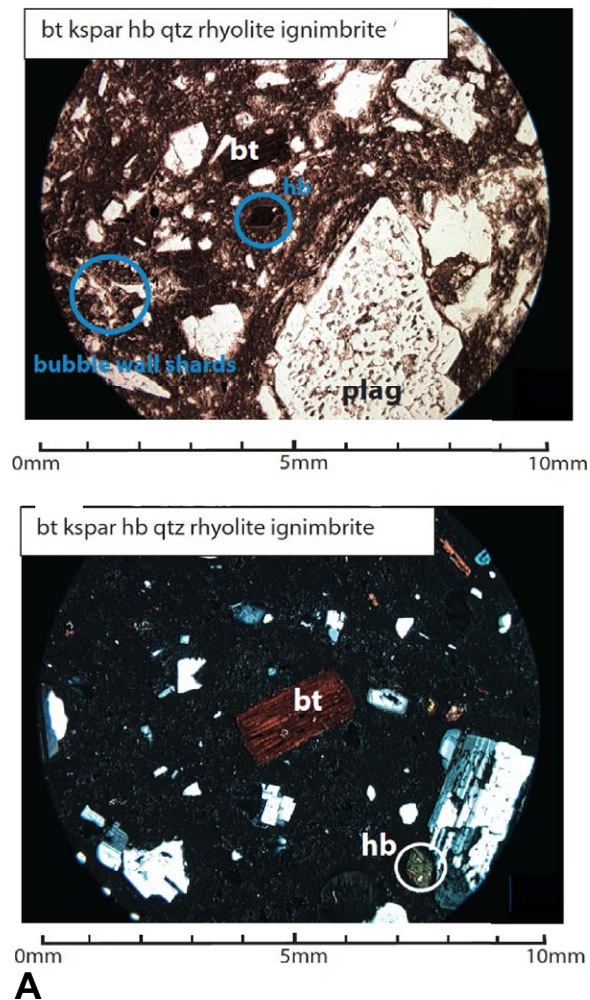
Figure 13 (*on this and following two pages*). Photomicrographs from the Ebbetts Pass volcanic center and pull-apart basin (samples plotted on Fig. 2B): (A) Lower silicic section: Biotite (bt) sanidine hornblende (hb) quartz (qtz) rhyolite welded ignimbrite (Tdpwi; Fig. 2B), sample MG08–07, with modal analysis (Fig. 11A) and whole-rock geochemistry (Table 1) and geochronology (Fig. 5) presented herein. Kspar—K-feldspar. This sample comes from a less strongly welded part of the overall very strongly welded ignimbrite, and so in plane-polarized light (upper photo), bubble-wall shards are obvious. Biotite (bt) and hornblende (hb), as well as glass matrix, are shown in crossed polarizers (lower photo). (B) Lower silicic section: Hornblende biotite rhyolite lava (Tdplr, sample JHEP-43), with modal analysis (Fig. 11A) and whole-rock geochemistry (Table 1) presented herein. Left photo (crossed polarizers) shows biotite and plagioclase in a glass groundmass. In plane light (right photo), the glass groundmass is clear and hard to distinguish from plagioclase, which is relatively free of inclusions. (C) Lower silicic section (Fig. 5): Hornblende biotite sanidine quartz silicic lava (Tdplr, sample JHEP-53), with modal analysis presented herein (Fig. 11A). Left photo (crossed polarizers) shows biotite and plagioclase enclosed by a hornblende phenocryst, with zoned plagioclase phenocrysts in a fine-grained felsitic groundmass. In plane light (right photo), the biotite crystals are barely visible within the hornblende phenocryst.
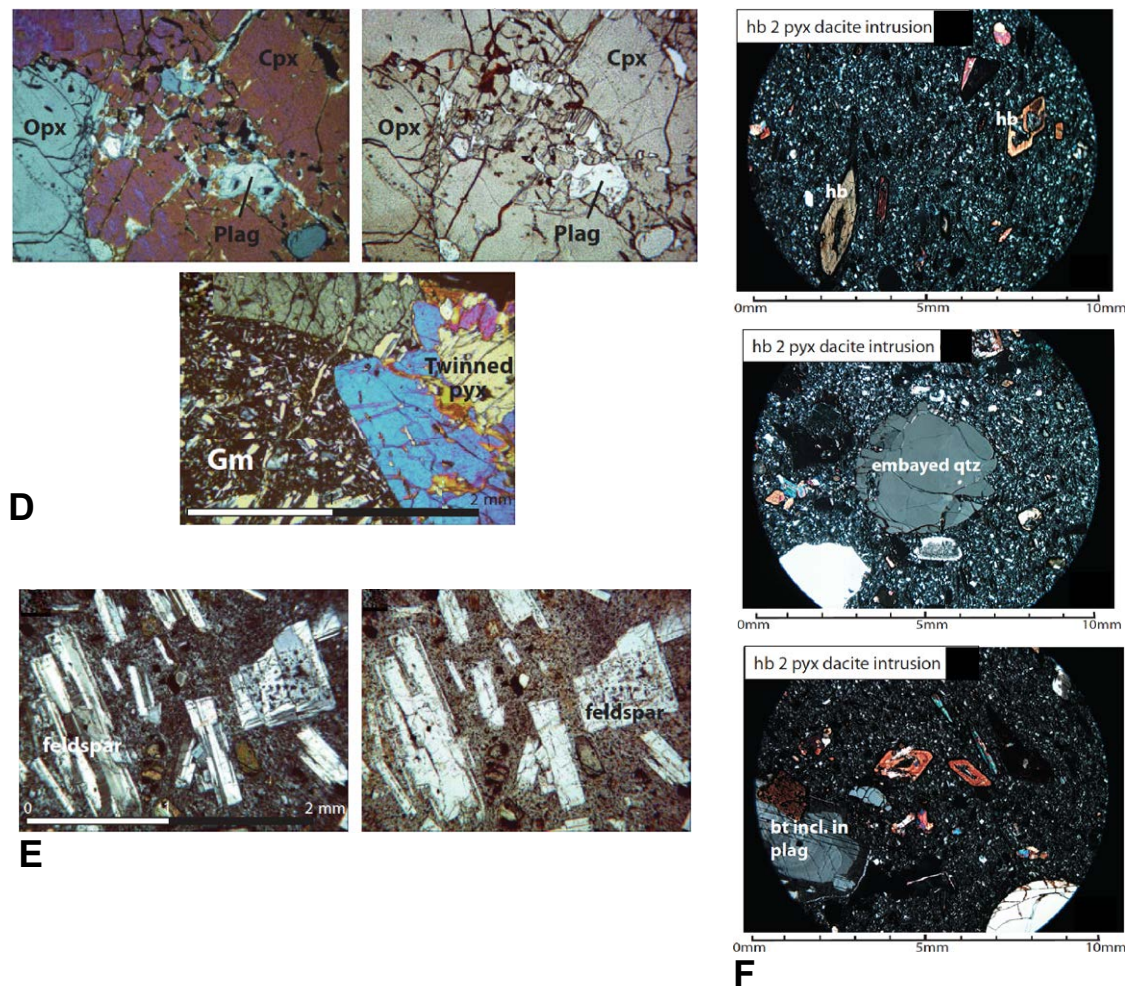
Ebbetts Pass Stratovolcano

Our Ebbetts Pass stratovolcano map unit (Tdpeps) largely corresponds to the unit that Armin et al. (1984) mapped as "Miocene Raymond and Silver Peak Andesites of Wilshire (1957) (Trs)." However, it is Pliocene (Fig. 5) in age and varies in composition from basaltic andesite through rhyolite, with one peperite basalt intrusion in the western flank, described below (Table 1). Armin et al. (1984) described what we term the "Ebbetts Pass stratovolcano" as "thick-bedded pyroxene and hornblende andesite lahars," but we find it is dominated by lavas, flow breccias, and block-and-ash-flow tuffs, with lesser

"lahars" (i.e., volcanic debris-flow deposits). They mapped this unit in the hanging wall (east of) the Noble Canyon fault, and in its footwall to the northwest, north of Ebbetts Pass in the Reynolds Peak–Raymond Peak area, and we concur (Fig. 2B). In addition, we recognized a small erosional remnant of it in the footwall of the Noble Canyon fault south of Ebbetts Pass (Fig. 2B).

The Ebbetts Pass stratovolcano is eroded, but its cone-shaped morphology and quaquaversally dipping beds are obvious in photos (Figs. 10A and 10B) and map pattern (Fig. 2B). It grew within the Ebbetts Pass pull-apart basin, and its center is occupied by the intrusions on Highland Peak and Silver Peak (Fig. 2B). It eventually filled the pull-apart and built up and out westward across the

Figure 13 (*continued*). (D) Ebbetts Pass stratovolcano (Tdeps): Orthopyroxene (opx) olivine clinopyroxene (cpx) basaltic andesite lava (sample JHEP-9), with modal analysis (Fig. 11A) and geochemistry (Table 1) and geochronology (Fig. 5) presented here. Top pair of photos (crossed polarizers and plane light) show orthopyroxene intergrown with clinopyroxene phenocrysts with small plagioclase (Plag) inclusions. Lower photo (crossed polarizers) shows a twinned pyroxene phenocryst in a groundmass with small plagioclase crystals (Gm). (E) Ebbetts Pass stratovolcano (Tdeps): Two-pyroxene andesite lava, (sample MG-08-08), inferred to form a 25-m-thick megaslide block shed from the walls of the Ebbetts Pass pull-apart (Fig. 5), with modal analysis (Fig. 11A) and geochemistry (Table 1) and geochronology (Fig. 5) presented here. Left photo (crossed polarizers) and right photo (plane light) show 2-mm-long intergrown plagioclase phenocrysts with zoning and complex growth, and small hornblende phenocrysts. (F) Disaster Peak Formation intrusion within the altered basal fill of the Ebbetts Pass pull-apart basin (Tid, sample MG-08-10): Two-pyroxene biotite hornblende quartz (qtz) dacite intrusion. Modal analysis (Fig. 12) and geochemistry (Table 1) presented here. All photos with crossed polarizers. Top photo: Hornblende crystals with groundmass cores; also, twinned pyroxene; microcrystalline groundmass. Middle photo: embayed or xenocrystic quartz and small intergrown hornblende crystals. Lower photo: Biotite intergrown with partially rimmed plagioclase; hornblende crystals with groundmass cores; and small pyroxenes.
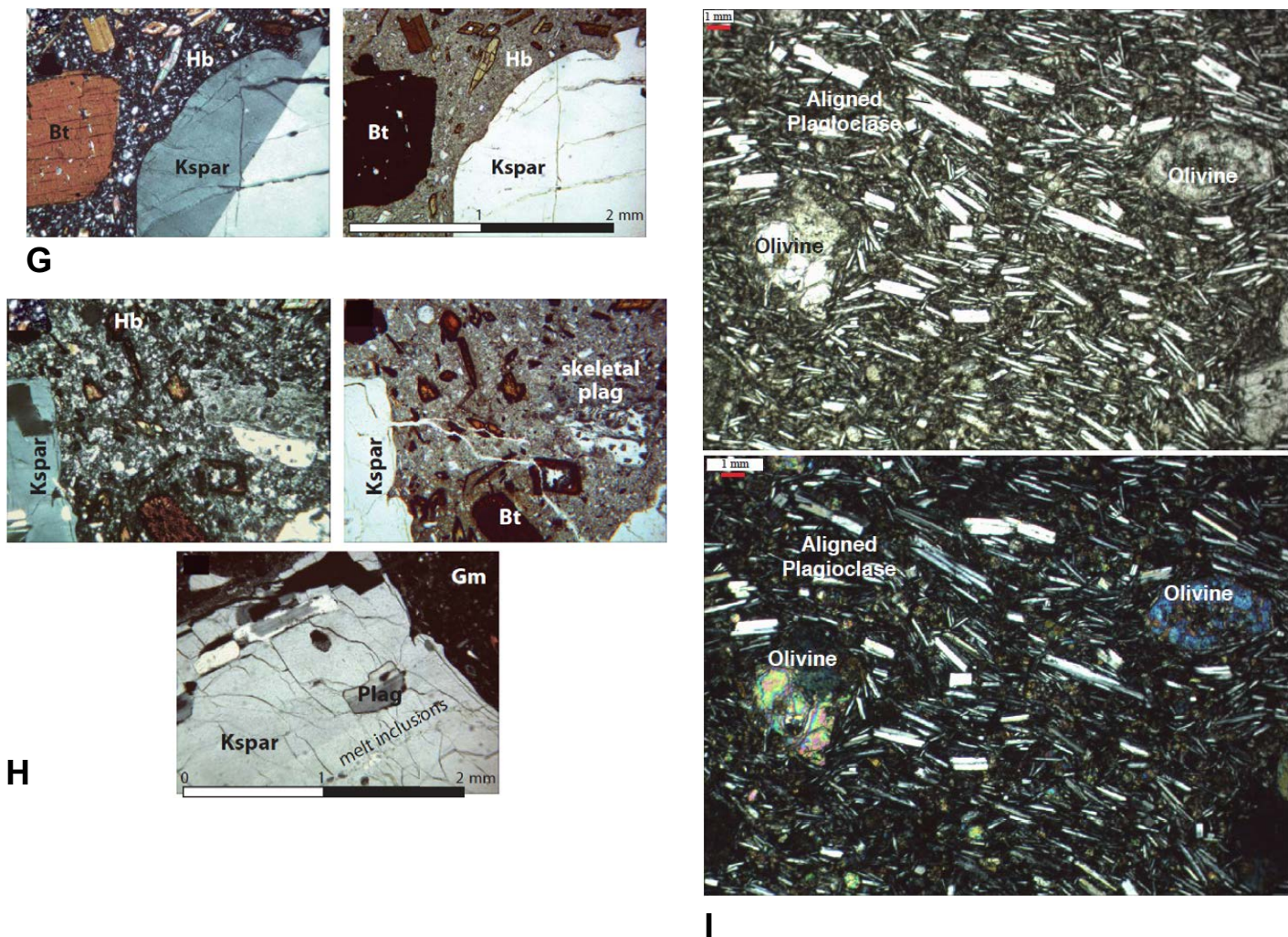
western basin-bounding fault (Noble Canyon fault), onto the footwall of the fault, where strata dip west (Fig. 2B).

The base of the Ebbetts Pass stratovolcano is a sequence of black olivine two-pyroxene basaltic andesite to basaltic trachyandesite lavas and flow breccias (samples JHEP-47 and JHEP-9; Table 1; Figs. 11A and 13D). This sequence lies largely within the pull-apart basin in the hanging wall of the Noble Canyon fault, but it is also preserved in the small erosional remnant on the footwall of the Noble Canyon fault south of Ebbetts Pass, which is close to the center of the stratovolcano. The $^{40}Ar/^{39}Ar$ groundmass age of the footwall sample is 4.6 ± 0.7 Ma, whereas the $^{40}Ar/^{39}Ar$ plagioclase age of the hanging wall sample is 4.90 ± 0.02 Ma. Because the hanging-wall lavas rest upon the welded rhyolite ignimbrite (Tdpwi), which has a very precise $^{40}Ar/^{39}Ar$ sanidine date (4.636 ± 0.014 Ma on 14 crystals; Fig. 5), we prefer the matrix age for the basal sequence. The black basaltic andesite lavas on the footwall overlie a white clinopyroxene hornblende orthopyroxene quartz silicic lava (sample JHEP-10; Figs. 2B, 10C, and 11A), and a nearby biotite rhyolite dike yielded a plagioclase $^{40}Ar/^{39}Ar$ age of 4.626 ± 0.017 Ma (sample JHEP-8; Figs. 2B, 5, and 12). The age of the rhyolite dike overlaps with the age of the Pliocene Ebbetts Pass volcanic center, so it is inferred to be a feeder for the stratovolcano. The small footwall erosional remnant south of Ebbetts Pass also has a narrow (<20-m-wide) channel filled with pumiceous fluvial sandstone (Fig. 10D).

Figure 13 (*continued*). (G) Ebbetts Pass stratovolcano: Hornblende biotite quartz dacite intrusion of Highland Peak (Tdpid, sample JHEP-49), with geochronology (Fig. 5), whole-rock geochemistry (Table 1), and modal analysis (Fig. 12) presented here, in crossed polarizers (left) and plane-polarized light (right). Biotite (Bt) is up to 1 mm long, with smaller hornblende (Hb), and twinned feldspar (Kspar). (H) Ebbetts Pass stratovolcano: Dacite intrusion of Highland Peak (Tdpid, sample JHEP-50), with geochemistry presented here (Table 1). Upper-left photo (crossed polarizers) and upper-right photo (plane light) show potassium feldspar (sanidine), skeletal plagioclase, and biotite phenocrysts. Lower photo (crossed polarizers) shows plagioclase crystals enclosed by >2-mm-long sanidine crystal with melt inclusions. (I) Postsubduction rift basaltic andesite (Fig. 5): Olivine two-pyroxene basaltic andesite intrusion (sample 901–3, same body as JHEP-54; whole-rock geochemistry in Table 1). The olivine is fresh, suggesting this is related to the young (3.65 ± 0.03 Ma plag) postsubduction rift basalt at Disaster Peak. Although age controls on this intrusion are poor because it cuts granitic basement (Fig. 5B) and is undated, we suspect that all of the olivine basalt plugs shown on Figures 2A and 2B are younger than 4 Ma in age. Top image is plane-polarized light, and bottom image is crossed polarized light.

In the hanging wall of the Noble Canyon fault (i.e., within the pull-apart basin), the stratovolcano section is 1 km thick (top eroded), and the basal sequence of black basaltic andesite lava passes upward into a much more varied section of basaltic andesite to rhyolite lavas and block-and-ash-flow tuffs (Table 1), with minor interstratified volcanic debris-flow deposits. The strata show steep depositional dips and stratal discordances caused by slumping and synvolcanic faulting (Fig. 10E). One sample traverse within the pull-apart basin includes (in stratigraphic order; Fig. 2B): (1) a 50-m-thick section of olivine pyroxene basaltic trachyandesite lavas and flow breccias (sample 814-3; Table 1); (2) an 80-m-thick section of plagioclase-bearing block-and-ash-flow tuffs, breccia, and columnar-jointed lava, where the lava is trachyandesite in composition (sample 814-4; Table 1); (3) a 50-m-thick perlitic flow-banded biotite dacite lava (sample 814-5; Table 1), which passes laterally into a non-welded silicic ignimbrite; (4) a 3-m-thick columnar-jointed biotite hornblende trachyandesite lava (sample 814-6; Table 1); and (5) a 10-m-thick mafic lava overlain by a 20-m-thick white quartz biotite rhyolite block-and-ash-flow tuff (sample 814-7; Table 1) with large blocks (Figs. 10F and 10G). Lesser volcanic debris-flow deposits intervene between the sampled primary volcanic units.

TABLE 1. LITHOFACIES AND GEOCHEMICAL DATA (IN wt%), SONORA PASS–EBBETTS PASS AREA

Sample no.	Lithofacies, with notes: **geochronology, #photomicrograph, ^modal analysis	SiO_2	TiO_2	Al_2O_3	Fe_2O_3	MnO	MgO	CaO	Na_2O	K_2O	P_2O_5	Total
Table I-I Quaternary (to Pliocene?) basalts												
JEFF Q DIKE 8-19-08	Feeder dike to Column of the Giants	51.5	1.26	18.3	9.1	0.12	4.9	9.2	3.3	1.5	0.6	99.7
Table I-H I Intrusions in and around Ebbetts Pass pull-apart basin/volcanic center												
JHEP-8	**^Rhyolite dike in Tvu west of Noble Cyn fault	74.6	0.27	14.4	1.3	0.00	0.4	1.2	3.1	4.5	0.1	99.8
MG-08-10	#^Dacite intrusion in altered basal fill (Tvu)	65.3	0.73	16.8	4.7	0.07	2.1	5.0	3.3	2.8	0.2	101.0
MG-08-13	^Andesite intrusion in altered basal fill (Tdpia)	59.6	0.94	16.4	6.7	0.07	4.0	6.6	3.4	2.1	0.4	100.1
BLM 09-920-2	Andesite intrusion in altered basal fill (Tdpia)	59.0	1.03	15.8	6.4	0.10	4.1	6.9	3.1	2.5	0.6	99.5
MG-08-11	Andesite intrusion in altered basal fill	58.3	1.03	16.9	7.0	0.08	5.5	7.5	1.9	1.8	0.3	100.3
MG-08-13	Andesite intrusion in altered basal fill (Tdpia)	60.6	1.00	16.5	6.5	0.07	4.1	6.5	2.5	1.8	0.4	100.0
JHEP-48	^Dacite intrusion of Highland Peak (Tdpid)	64.6	0.72	17.4	4.6	0.03	2.0	4.2	3.3	3.3	0.3	100.4
JHEP-49	**#^Dacite intrusion of Highland Pk (Tdpid)	67.2	0.53	16.1	3.5	0.04	1.8	3.7	3.2	3.6	0.2	99.8
JHEP-50	#Dacite intrusion of Highland Peak	67.4	0.54	16.1	3.5	0.04	1.8	3.7	3.1	3.4	0.2	99.7
JHEP-37	Basaltic andesite in undifferentiated volcanics (Tvu)	53.1	1.04	17.5	8.3	0.10	6.6	8.6	2.3	2.4	0.2	100.2
JHEP-16	Basaltic andesite intrusion (Tia)	54.7	0.88	16.0	7.8	0.09	8.4	8.1	2.4	1.6	0.2	100.1
JHEP-12	Andesite intrusion (Tia)	58.4	0.77	16.8	6.7	0.08	5.3	8.5	2.5	1.2	0.2	100.5
JHEP-8	Rhyolite intrusion (in Tvdf)	75.6	0.33	14.5	1.4	0.01	0.4	1.1	2.4	4.1	0.1	99.9
Table I-G Intrusions in and around Sierra Crest graben-vent system												
JHEP-57	**#^Basalt intrusion on Disaster Peak (Tdpib)	47.8	1.69	14.9	10.1	0.13	10.9	10.1	2.1	1.3	0.6	99.8
BLM 09-823-2	^Basalt intrusion on Disaster Peak (Tdpib)	48.0	1.95	14.7	10.2	0.16	11.2	9.6	2.2	1.7	0.6	100.2
JHEP-58	^Basaltic andesite intrusion (Tdpiba)	54.7	1.38	18.1	8.6	0.10	4.2	8.5	2.9	1.4	0.3	100.2
BLM 09-919-1	^Dacite intrusion (Tid)	63.3	0.61	18.2	4.8	0.07	1.3	5.9	3.6	2.3	0.3	100.3
BLM 09-831-7	^Dacite intrusion (Tid)	63.2	0.64	17.9	4.9	0.08	1.9	5.4	3.4	2.4	0.3	100.1
BLM 09-910-3	^Andesite intrusion (Tia)	60.6	0.85	17.4	6.1	0.09	3.2	6.2	3.1	2.7	0.3	100.4
BLM 09-826-1	Basaltic andesite intrusion (Tdpiba)	56.0	1.04	17.6	7.6	0.12	5.2	8.0	2.7	2.0	0.3	100.4
BLM 09-826-5	Andesite intrusion (Tdpba)	57.5	1.14	17.8	6.5	0.09	3.4	7.2	3.4	2.5	0.5	100.0
BLM 09-911-3	Basaltic andesite intrusion (Tdpba)	54.2	1.19	17.7	8.1	0.12	5.4	8.2	2.6	2.2	0.3	100.0
BLM 09-830-4	Andesite intrusion on Arnot Peak (Tdpia)	58.1	0.91	18.1	7.0	0.12	3.7	7.2	3.1	1.6	0.2	100.2
Dp-4A	Andesite intrusion on Arnot Peak (Tdpia)[3]	59.0	0.88	18.1	6.4	0.08	3.3	7.0	3.4	1.6	0.3	100.0
BLM 09-830-5	Basaltic andesite plug NE of Arnot Peak (Tdpiba)	56.6	0.86	17.8	7.0	0.12	5.0	7.6	2.9	1.8	0.3	99.9
BLM 09-831-7	Dacite plug W of Arnot Peak (Tdpid)	63.2	0.64	17.9	4.9	0.08	1.9	5.4	3.4	2.4	0.3	100.1
BLM 09-909-3	Basaltic andesite intrusion NW of Murray Canyon	55.4	0.91	16.3	8.0	0.12	6.6	7.8	2.7	2.3	0.3	100.3
BLM 09-908-2	^Andesite intrusion (Tia)	61.4	0.81	17.5	5.6	0.09	3.1	5.8	3.2	2.7	0.3	100.5
BLM 09-926-3	^Trachybasalt intrusion, Lightning Mtn (Tiba)	50.5	2.29	16.8	8.9	0.13	7.0	8.0	3.2	1.9	1.2	99.9
JHEP-89	^Andesite dike	60.3	0.79	17.4	6.0	0.09	2.9	6.2	2.7	2.3	0.3	99.0
BLM 09-910-1	Andesite intrusion N of Murray Canyon	58.6	0.89	17.5	6.3	0.10	3.9	6.6	3.1	2.4	0.3	99.8
JHEP-54	^Basaltic andesite intrusion (Tiba)	52.5	1.33	17.8	8.8	0.11	6.2	9.3	2.4	1.3	0.4	100.1
BLM 09-901-3	#^Basaltic andesite intrusion	54.4	1.31	16.9	8.2	0.13	5.8	8.4	2.6	1.8	0.4	99.9
BP022	Basaltic andesite plug on Bald Peak (Tdpi)[1]	57.0	0.89	17.9	6.9	0.10	4.4	7.8	3.4	1.4	0.3	100.0
BP068	Andesite plug 0.5 km NE of Bald Peak (Tdpi)[1]	58.3	0.86	18.2	6.3	0.08	3.2	6.9	3.8	1.9	0.4	100.0
PC043-2	Andesite intrusion on Stanislaus Peak (Tdpi)[1]	57.9	1.06	16.5	6.3	0.09	5.3	7.0	4.0	1.6	0.3	100.0
Table I-F Strata of Ebbetts Pass pull-apart basin												
MG-08-08	**#^Andesite lava megaslide block (Tdpeps)	62.0	0.86	18.1	5.6	0.04	2.9	5.4	2.8	3.1	0.4	101.3
MG-08-09	#^Andesite lava N of Highland Peak (Tdpeps)	62.1	0.77	18.1	5.8	0.06	2.7	6.0	2.6	2.4	0.3	100.8
JHEP-47	**^Basaltic andesite lava S of Highland Peak (Tdpeps)	53.4	1.23	18.3	8.8	0.18	4.0	9.2	2.6	1.7	0.3	99.7
BLM 09-814-3	Basaltic trachyandesite pyroxene (px) lava (Tdeps)	55.1	1.11	16.9	7.2	0.11	5.1	7.8	3.6	2.4	0.4	99.8
BLM 09-814-4	Trachyandesite px lava (Tdpeps)	60.3	0.92	17.0	5.9	0.08	3.3	6.1	3.9	2.6	0.4	100.4
BLM 09-814-5	Dacite perlitic flow-banded lava (Tdeps)	67.1	0.53	15.8	3.5	0.07	1.7	3.4	3.6	3.9	0.2	99.8

(*continued*)

TABLE 1. LITHOFACIES AND GEOCHEMICAL DATA (IN wt%), SONORA PASS–EBBETTS PASS AREA (*continued*)

Sample no.	Lithofacies, with notes: **geochronology, #photomicrograph, ^modal analysis	SiO$_2$	TiO$_2$	Al$_2$O$_3$	Fe$_2$O$_3$	MnO	MgO	CaO	Na$_2$O	K$_2$O	P$_2$O$_5$	Total
Table I-F Strata of Ebbetts Pass pull-apart basin (*continued*)												
BLM 09-814-6	Trachyandesite biotite (bi) hornblende (hb) lava (Tdpeps)	63.8	0.69	17.1	4.9	0.05	1.2	4.3	4.0	3.4	0.3	99.9
BLM 09-814-7	Rhyolite quartz (qtz) bi block-and-ash-flow tuff	73.0	0.35	14.6	2.1	0.04	0.8	1.7	3.7	4.0	0.1	100.5
JHEP-9	**#^Basaltic andesite lava (Tdpeps)	53.3	1.34	17.9	8.3	0.10	5.1	8.6	2.5	2.2	0.3	99.7
CB 09-3	Basalt peperite intrusion (Tdpeps)	50.3	1.05	14.9	9.1	0.15	9.4	10.3	2.4	1.6	0.3	99.6
CB 09-4	Andesite block-and-ash-flow tuff **(**Tdpeps)	57.4	0.93	17.6	7.0	0.12	4.2	7.2	3.1	2.1	0.3	99.9
CB 09-5	Andesite block-and-ash-flow tuff (Tdpeps)	57.5	0.89	17.9	6.8	0.12	3.6	7.0	3.5	2.2	0.3	99.9
CB 09-2	Andesite lava, Mokelumne paleoch, XL rich (Tdpeps)	60.8	0.69	17.8	5.4	0.09	2.8	6.1	4.0	1.7	0.3	99.5
CB 09-1	Andesite lava, Mokelumne paleoch, XL poor (Tdpeps)	60.1	0.76	17.8	5.6	0.11	3.2	6.7	3.6	1.8	0.3	100.1
MG-08-07	**#^Rhyolite welded ignimbrite (Tdpwi)	74.0	0.23	15.3	1.8	0.01	0.5	1.9	2.7	4.1	0.1	100.8
BLM 09-814-1	Rhyolite welded ignimbrite (Tdpwi)	73.1	0.33	14.5	1.9	0.04	0.5	1.5	4.0	4.6	0.1	100.4
BLM 09-814-2	Trachyandesite hb block-and-ash-flow tuff (under Tdpwi)	60.1	0.88	17.8	5.9	0.12	2.4	5.6	3.5	3.2	0.4	99.9
JHEP-43	#^Rhyolite lava (Tdplr)	71.1	0.36	15.8	2.3	0.02	0.8	2.4	3.3	3.9	0.1	100.1
JHEP-44	**^Rhyolite lava (Tdplr)	71.2	0.37	15.8	2.4	0.01	0.6	2.1	3.6	3.9	0.1	100.1
MG-08-12	**#^Dacite lava (Tdpld)	63.2	0.76	16.6	5.1	0.06	3.1	5.4	2.7	2.5	0.2	99.6
BLM 09-920-3	Dacite lava (Tdpld)	65.4	0.64	16.2	4.5	0.08	2.2	4.4	3.2	3.0	0.2	99.8
BLM 09-920-4	Dacite lava (Tdpld)	65.1	0.63	16.4	4.8	0.09	2.2	4.7	3.1	3.0	0.2	100.1
BLM 09-920-1	Andesite in base of the dacite lava (Tdpld)	59.3	0.80	17.4	6.5	0.10	3.2	6.8	3.1	2.1	0.2	99.5
MG-08-11	Block-and-ash-flow tuff in altered basal fill (Tvu)	57.3	1.00	16.7	7.1	0.08	5.5	7.5	2.8	2.0	0.3	100.2
JHEP-36	#^Andesite lava SW of Wolf Creek fault (Tvu)	61.4	0.79	19.0	5.4	0.05	2.2	6.5	3.3	1.4	0.3	100.4
JHEP-31	#^Basaltic andesite lava SW of Wolf Creek fault (Tvu)	56.6	0.89	19.3	9.1	0.12	3.2	7.8	2.4	0.7	0.4	100.4
Table I-E Strata of Disaster Peak Formation (Tdp) in Sierra Crest graben-vent system												
JHEP-94	Andesite-dacite block-and-ash-flow tuff Arnot Pk (in Tdpdf)	62.1	0.77	18.2	5.8	0.06	2.7	6.0	2.6	2.4	0.3	100.8
JHEP-55	**^Andesite block-and-ash-flow tuff S of Disaster Peak (in Tdpdf)	60.6	0.69	17.6	6.0	0.07	3.8	6.4	3.0	1.7	0.2	100.1
BLM 09-824-3	Andesite block-and-ash flow tuff (Tdpba)	59.7	0.68	18.2	6.2	0.11	3.1	6.4	3.0	2.1	0.3	99.8
BLM 09-906-1	^Basalt lava W of Disaster Pk (Tdpl)	49.8	1.11	13.7	9.1	0.14	12.9	8.5	1.6	2.4	0.5	99.8
BLM 09-918-1	^Basaltic andesite lava (Tdpl)	54.5	1.05	16.6	8.9	0.15	5.9	8.7	2.3	1.9	0.3	100.4
BLM 09-830-2	^Basaltic andesite lava E of Arnot Peak (Tdpl)	54.1	0.94	15.1	9.0	0.15	7.5	9.6	1.9	1.3	0.2	99.8
BLM-09-830-3	^Basaltic andesite lava E of Arnot Peak (Tdpl)	55.0	0.96	14.9	8.7	0.14	6.6	9.8	2.1	1.7	0.3	100.1
BLM 09-911-1	Basaltic andesite vent facies N of Murray Cyn (Tdpvf)	52.9	1.22	15.7	10.5	0.17	5.7	8.9	2.0	2.2	0.6	99.7
BLM 09-911-4	Andesite block-and-ash-flow tuff N of Murray Canyon (in Tdpdf)	58.3	1.06	17.5	6.6	0.10	3.7	7.1	2.9	2.6	0.4	100.3
AAK 09-817-7-7	Basalt lava #7, Mineral Mtn (Tdplb)	50.5	1.29	16.1	9.7	0.15	8.7	8.3	2.5	2.2	0.5	100.0
AAK 09-817-7-5	Basalt lava #5, Mineral Mtn (Tdplb)	48.0	1.66	16.0	10.6	0.16	8.5	9.8	2.8	1.5	0.8	99.6
AAK 09-817-7-4	Basalt lava #4, Mineral Mtn (Tdplb)	48.4	1.80	16.2	10.7	0.17	8.2	9.7	2.6	1.7	0.9	100.3
AAK 09-817-7-3	Basalt lava #3, Mineral Mtn (Tdplb)	48.2	1.71	16.3	10.9	0.16	8.5	9.7	2.4	1.9	0.8	100.4
AAK 09-817-7-2	Basalt lava #2, Mineral Mtn (Tdplb)	48.3	1.69	15.8	10.4	0.16	8.4	9.8	3.6	1.2	0.8	100.1
AAK 09-817-7-1	Basalt lava #1, Mineral Mtn (Tdplb)	49.3	1.75	15.5	9.7	0.15	8.4	9.0	3.4	1.7	0.9	99.9
JHEP-83	**^Basalt lava, Mineral Mtn (Tdplb)	51.2	1.27	16.3	9.6	0.12	8.9	8.3	2.0	2.2	0.4	100.2
BLM 09-827-1	^Andesite intrusion or lava, Golden Valley (Tdpia)	61.6	0.82	18.1	5.7	0.13	3.0	5.8	3.3	1.8	0.2	100.5
BLM 09-827-2	Basaltic andesite intrusion or lava, Golden Canyon (Tiba)	55.5	0.95	16.9	7.6	0.12	6.1	7.6	3.1	1.4	0.2	99.5
JHEP-70	**^Dacite lava avalanche slab from Relief Peak Fm (in Tdpld)	63.8	0.62	17.2	4.8	0.05	2.9	5.5	2.9	2.7	0.2	100.7
BLM 09-826-3	^Dacite lava avalanche slab from Relief Peak Fm (in Tdpld)	62.6	0.85	16.8	5.2	0.07	2.8	5.6	2.9	3.0	0.2	100.0
BLM 09-826-2	Dacite lava avalanche slab from Relief Peak Fm (in Tdpld)	62.7	0.62	16.9	4.9	0.08	3.0	5.6	3.0	2.8	0.2	99.9
Table I-D Dardanelles Formation (Tsd, Stanislaus Group), Sierra Crest graben-vent system (strata)												
BP046	Shoshonite/basaltic trachyandesite lava (Tsd)[2]	53.8	1.22	18.2	7.9	0.09	4.1	7.4	3.7	2.9	0.7	100.0
AAK-08-824-6	Basaltic andesite lava (Tsd)[2]	54.2	1.19	18.3	8.8	0.09	4.2	7.3	2.6	2.7	0.7	100.0
AAK-08-909-2	Basaltic andesite lava (Tsd)[2]	54.8	1.14	18.4	8.7	0.09	4.3	7.7	2.7	1.8	0.4	100.0

(*continued*)

TABLE 1. LITHOFACIES AND GEOCHEMICAL DATA (IN wt%), SONORA PASS–EBBETTS PASS AREA (*continued*)

Sample no.	Lithofacies, with notes: **geochronology, #photomicrograph, ^modal analysis	SiO_2	TiO_2	Al_2O_3	Fe_2O_3	MnO	MgO	CaO	Na_2O	K_2O	P_2O_5	Total
Table I-C Part 1 Eureka Valley Tuff (Tse, Stanislaus Group), Sierra Crest graben-vent system (strata)												
JHEP-65	#^Upper Member ash-fall deposit	64.6	1.03	18.1	5.0	0.10	2.3	3.4	1.9	2.9	0.3	99.6
BLM-09-825-8	Ameboid scoria block in By-Day Member ignimbrite (Tseb)	58.8	1.45	19.3	5.9	0.09	1.9	6.2	3.1	2.9	0.5	100.1
JHEP-64	#^Trachydacite lava, Lava Flow Mmbr (Tsell)	59.3	1.05	20.5	5.4	0.04	0.9	6.2	3.2	3.5	0.5	100.6
BLM-09-825-1	#^Basaltic andesite lava, Lava Flow Mmbr (Tsell)	52.8	1.23	18.0	8.5	0.15	4.5	10.4	2.3	1.4	0.2	99.5
BLM-09--824-1	^Trachyandesite lava, Lava Flow Mmbr (Tsell)	59.4	1.07	19.8	5.7	0.07	1.0	6.0	3.4	3.2	0.4	100.0
BLM-09-906-2	^Trachyandesite lava, Lava Flow Mmbr (Tsell)	58.4	1.13	20.4	5.9	0.08	1.3	6.2	3.4	2.9	0.5	100.2
BLM-09-831-2	^Trachydacite vent facies deposits, Lava Flow Mmbr (Tselvf)	62.8	1.62	17.6	5.9	0.04	0.5	3.3	3.4	4.8	0.5	100.3
BLM-09-921-3	Trachydacite lava, Lava Flow Mmbr (Tsell)	61.7	1.45	16.8	6.3	0.15	1.0	3.9	3.4	4.8	0.5	100.0
JHEP-88	**#^Trachydacite intrusion and lava, Basal Lava Flow Mmbr (Tseblt)	64.5	0.68	16.6	4.5	0.03	1.7	3.7	3.3	4.3	0.2	99.6
AAK 09-817-7-6A	Basaltic trachyandesite tuff ring, ash layer (Tss)	56.8	1.29	15.8	7.8	0.10	5.8	6.1	2.0	3.2	0.7	99.7
AAK 09-817-7-6B	basaltic trachyandesite tuff ring, scoria (Tss)	54.0	1.36	13.5	7.7	0.13	7.1	7.6	3.4	4.1	1.3	100.1
PC066	Trachyandesite lava (Tsell)[1]	59.8	0.95	19.9	4.3	0.04	1.3	6.0	4.1	3.2	0.4	100.0
PC065	Trachyandesite block-and-ash-flow tuff (Tselba)[1]	61.8	0.79	16.9	4.9	0.06	3.1	5.1	3.3	3.7	0.3	100.0
DC064-1	Trachydacite lava on The Dardanelles (Tselt)[1]	61.6	1.40	16.4	5.6	0.08	1.6	3.9	3.8	5.1	0.5	100.0
AAK-08-825-2	Trachydacite lava, Bald Pk-Red Pk (Tselt)[2]	63.5	1.12	17.1	4.9	0.04	1.2	2.9	3.5	5.3	0.4	100.0
AAK-08-830-2	Trachydacite lava, Bald Pk-Red Pk (Tselt)[2]	64.4	1.10	17.2	4.7	0.05	1.1	2.7	3.2	5.3	0.4	100.1
DC036	Basalt lava, Dardanelles Cone (Tselb)	50.3	1.15	15.9	8.5	0.13	9.8	9.2	2.6	1.9	0.5	100.0
Table I-C Part 2, EVT Tollhouse Flat Member (Tset, Stanislaus Group) pumice fragments from Long Barn, California (3)												
CMEVT2R NB	Trachydacite pumice from nonwelded ignimbrite (Tset)	66.39	0.8	16.7	3.60	0.1	1.0	2.0	3.7	5.3	0.4	100.0
CMEVT3P NB	Trachydacite pumice from nonwelded ignimbrite (Tset)	64.31	1.0	17.0	4.11	0.1	1.3	2.8	4.5	4.6	0.3	100.0
CMEVT5R NB	Trachydacite pumice from nonwelded ignimbrite (Tset)	64.98	0.9	17.5	3.84	0.1	1.3	2.6	3.7	4.6	0.5	100.0
MOEVT 2P 1NB	Trachydacite pumice from nonwelded ignimbrite (Tset)	63.90	1.0	17.0	3.99	0.1	1.3	2.9	5.1	4.5	0.3	100.0
MOEVT 4P 1NB	Trachydacite pumice from nonwelded ignimbrite (Tset)	66.48	0.7	16.7	3.10	0.1	0.8	1.8	4.7	5.3	0.2	100.0
MOEVT3P NB	Trachydacite pumice from nonwelded ignimbrite (Tset)	64.96	1.0	17.1	4.25	0.1	1.3	2.8	3.6	4.5	0.3	100.0
LTEVTP1 NB	Trachydacite pumice from nonwelded ignimbrite (Tset)	65.29	0.9	16.8	3.59	0.1	1.1	2.5	4.6	4.9	0.2	100.0
LTEVTP2 NB	Trachydacite pumice from nonwelded ignimbrite (Tset)	65.08	0.9	17.1	4.27	0.1	1.3	2.8	3.4	4.7	0.4	100.0
LTEVTP4 NB	Trachydacite pumice from nonwelded ignimbrite (Tset)	64.96	0.9	17.2	3.77	0.1	1.2	2.5	4.4	4.7	0.2	100.0
SLEVT1P NB	Trachydacite pumice from nonwelded ignimbrite (Tset)	64.80	0.9	17.1	3.56	0.1	1.2	2.6	4.7	4.8	0.3	100.0
SLEVT4P NB	Trachydacite pumice from nonwelded ignimbrite (Tset)	66.06	0.9	17.0	3.42	0.1	1.1	2.5	3.7	5.0	0.2	100.0
SLEVT5P NB	Trachydacite pumice from nonwelded ignimbrite (Tset)	66.42	0.8	16.8	3.42	0.1	1.0	2.2	3.8	5.3	0.2	100.0
Table I-B Part 1 Table Mountain Latite (Stanislaus Group), Sierra Crest graben-vent system (strata)												
MG-08-01	#^Andesite lava (Tstml)	59.5	0.90	17.3	6.5	0.06	3.8	5.9	2.8	3.2	0.3	100.2
JHEP-67	#^Andesite lava (Tstml)	59.7	0.98	17.4	6.3	0.08	3.7	6.0	2.7	3.2	0.4	100.4
JHEP-81	^Basaltic trachyandesite lava (Tstml)	50.2	1.63	15.1	8.8	0.11	8.3	8.1	2.0	5.1	1.0	100.3
MG-08-04	#^Basaltic andesite lava (Tstml)	54.4	0.92	16.0	8.1	0.09	7.4	7.8	2.1	1.9	0.3	99.0
MG-08-05	^Basaltic andesite lava (Tstml)	55.1	0.99	18.5	8.5	0.11	4.8	7.7	2.7	1.5	0.3	100.1
MG-08-03	#^Trachybasaltic andesite lava (Tstml)	51.5	1.57	14.8	8.8	0.11	9.3	8.1	1.7	5.5	0.9	102.3
BLM-09-921-4	^Basalt lava (Tstml)	50.8	1.06	16.3	9.4	0.15	9.4	8.6	2.5	1.2	0.3	99.6
BLM-09-919-4	^Basalt feeder dike (Tstml)	50.9	1.07	15.5	9.3	0.15	10.6	8.8	2.2	1.6	0.3	100.4
BLM-09-906-6	^Basaltic andesite lava (Tstml)	54.8	1.17	17.0	8.2	0.13	6.6	7.8	2.8	1.7	0.3	100.4
BLM-09-906-5	^Basaltic andesite lava (Tstml)	56.0	1.00	16.9	7.6	0.15	6.6	7.6	2.6	1.6	0.3	100.4
BLM-09-902-3	^Trachyandesite lava (Tstml)	59.5	0.99	17.3	6.2	0.10	3.6	6.1	3.0	3.4	0.4	100.5
BLM-09-901-2	^Trachyandesite lava (Tstml)	61.0	1.69	17.2	5.9	0.07	1.6	3.9	3.3	5.0	0.6	100.3
BLM-09-906-3	Basalt lava (Tstml)	51.9	1.28	17.3	9.5	0.14	7.0	9.2	2.3	1.4	0.3	100.3
BLM-09-919-4	Basalt vent facies (Tstmvf)	50.9	1.07	15.5	9.3	0.15	10.6	8.8	2.2	1.6	0.3	100.4
BLM-09-919-5	Andesite vent facies (Tstmvf)	55.0	0.98	18.6	8.2	0.13	4.2	7.9	3.0	1.4	0.3	99.8
BLM-09-919-7	Andesite lava (Tstml)	58.7	0.79	16.9	6.8	0.20	2.8	7.7	3.0	2.8	0.3	100.0

(*continued*)

TABLE 1. LITHOFACIES AND GEOCHEMICAL DATA (IN wt%), SONORA PASS–EBBETTS PASS AREA (*continued*)

Sample no.	Lithofacies, with notes: **geochronology, #photomicrograph, ^modal analysis	SiO_2	TiO_2	Al_2O_3	Fe_2O_3	MnO	MgO	CaO	Na_2O	K_2O	P_2O_5	Total
Table I-B Part 1 Table Mountain Latite (Stanislaus Group), Sierra Crest graben-vent system (strata) (*continued*)												
BLM-09-925-1	Trachyandesite lava, Lightning Mtn (Tstml)	57.5	1.73	17.3	7.4	0.06	1.9	4.8	3.4	4.6	0.9	99.6
DC016	Trachyandesite lava, East Dardanelles (Tml)[1]	58.2	1.14	17.0	6.2	0.06	3.7	6.1	3.6	3.6	0.4	100.0
DC065-1	Trachyandesite lava, The Dardanelles[1]	60.6	1.51	16.7	5.8	0.05	1.8	4.0	3.7	5.3	0.6	100.0
JHSP-41	Shoshonite/basaltic trachyandesite W of St. Mary's Pass (Tstml)[3]	56.2	1.12	17.5	7.3	0.10	3.7	7.7	3.9	2.1	0.4	100.1
BP007	Basalt lava, Bald Peak (Tstml)[1]	50.4	1.65	14.9	8.5	0.10	10.2	9.2	2.7	1.9	0.5	100.0
BP020	Basaltic andesite lava, Bald Peak (Tstml)[1]	56.5	0.89	16.6	6.4	0.07	6.6	7.4	3.7	1.6	0.3	100.0
Table I-B Part 2 Table Mountain Latite (Stanislaus Group) on Sonora Peak, 1 analysis per lava (3), measured section in (1)												
SO-P - 0107	Trachyandesite lava (Tstml)	56.30	1.3	18.4	6.40	0.1	2.1	7.8	3.7	3.3	0.7	100.0
SO-P - 0201	Trachyandesite lava (Tstml)	57.27	1.3	17.5	7.47	0.1	2.3	7.0	3.4	3.1	0.6	100.0
SO-P - 0305	Basaltic trachyandesite lava (Tstml)	55.91	1.3	16.6	7.16	0.1	4.9	7.4	3.1	3.0	0.6	100.0
SO-P - 0402	Basaltic trachyandesite lava (Tstml)	55.88	1.3	16.6	6.86	0.1	4.4	8.2	3.1	3.0	0.6	100.0
SO-P - 0505	Trachyandesite lava (Tstml)	57.11	1.3	17.1	5.96	0.1	2.4	9.3	3.2	2.9	0.6	100.0
SO-P - 0602	Trachyandesite lava (Tstml)	55.92	1.5	18.0	6.36	0.2	1.5	8.6	3.6	3.4	0.9	100.0
SO-P - 0708A	Trachyandesite lava (Tstml)	57.18	1.6	18.9	6.28	0.0	1.5	6.2	3.8	3.6	0.9	100.0
SO-P-0804B	Basaltic trachyandesite lava (Tstml)	56.14	1.2	16.7	6.87	0.1	3.7	9.0	2.8	3.0	0.5	100.0
SO-P-0902	Basaltic trachyandesite lava (Tstml)	55.34	1.2	16.6	6.92	0.1	5.4	7.9	3.1	3.0	0.6	100.0
SO-P-1001	Basaltic andesite lava (Tstml)	55.47	1.3	16.3	7.65	0.1	5.7	7.4	2.5	2.9	0.6	100.0
SO-P-1105	Trachyandesite lava (Tstml)	56.35	1.8	17.7	7.37	0.1	2.4	6.3	3.4	3.6	1.0	100.0
SO-P-1201	Trachyandesite lava (Tstml)	56.33	1.8	17.6	7.33	0.1	2.7	6.0	3.5	3.6	1.1	100.0
SO-P-1304	Trachyandesite lava (Tstml)	57.64	1.7	17.9	6.75	0.1	1.4	5.4	3.8	4.3	1.0	100.0
SO-P-1404	Trachyandesite lava (Tstml)	57.63	1.4	18.1	6.54	0.1	2.7	5.9	3.5	3.5	0.7	100.0
SO-P-1501	Trachyandesite lava (Tstml)	58.37	1.3	21.2	4.19	0.1	0.8	6.1	4.0	3.4	0.6	100.0
SO-P-1606	Trachyandesite lava (Tstml)	58.18	1.4	18.8	6.22	0.1	1.7	5.2	3.5	4.2	0.7	100.0
SO-P-1806	Trachyandesite lava (Tstml)	59.16	1.5	18.4	6.42	0.0	1.3	4.5	3.6	4.4	0.7	100.0
SO-P-1903A	Trachyandesite lava (Tstml)	57.15	1.3	17.2	7.51	0.3	2.6	6.5	3.4	3.5	0.6	100.0
SO-P-2106A	Trachyandesite lava (Tstml)	58.14	1.7	19.0	5.64	0.0	1.2	5.4	3.8	4.4	0.8	100.0
SO-P-2204A	Trachyandesite lava (Tstml)	57.52	1.2	17.7	5.99	0.2	3.6	6.3	3.3	3.7	0.6	100.0
SO-P-2301	Trachyandesite lava (Tstml)	59.17	1.4	18.3	6.26	0.0	1.3	5.2	3.6	4.2	0.6	100.0
Table I-A Relief Peak Formation (strata)												
JHEP-70	**^Dacite lava avalanche slab from Relief Peak Fm (in Tdpld)	63.8	0.62	17.2	4.8	0.05	2.9	5.5	2.9	2.7	0.2	100.7
BLM 09-826-3	^Dacite lava avalanche slab from Relief Peak Fm (in Tdpld)	62.6	0.85	16.8	5.2	0.07	2.8	5.6	2.9	3.0	0.2	100.1
BLM 09-826-2	Dacite lava avalanche slab from Relief Peak Fm (in Tdpld)	62.7	0.62	16.9	4.9	0.08	3.0	5.6	3.0	2.8	0.2	99.9
JHEP-90	**^Andesite block-and-ash-flow tuff (in Trpdf)	63.0	0.76	18.5	5.7	0.04	2.6	5.8	2.5	2.4	0.3	101.7
MG-08-02	#^Basaltic andesite lava (in Trpdf)	55.6	0.94	16.3	7.9	0.08	7.7	7.9	2.0	1.8	0.2	100.5
JHEP-89	Andesite lava (in Trpdf)	60.3	0.79	17.4	6.0	0.09	2.9	6.2	2.7	2.3	0.3	99.0
JHEP-90	**^Andesite block-and-ash-flow tuff (in Trpdf)	62.0	0.78	18.2	5.7	0.04	2.5	5.8	2.4	2.3	0.3	100.0
MG-08-02	#^Basaltic andesite lava/plug (in Trpdf)	55.6	0.94	16.3	7.9	0.08	7.7	7.9	2.0	1.8	0.2	100.5
BLM-09-920-5	Andesite lava (in Trpdf)	60.6	0.77	17.6	5.8	0.10	3.1	6.4	3.1	2.6	0.3	100.3
BLM-09-920-6	Andesite lava (in Trpdf)	61.3	0.77	17.9	6.0	0.08	1.7	5.9	3.2	2.9	0.4	100.1
BLM-09-921-2	Andesite lava (in Trpdf)	60.6	0.79	17.7	5.8	0.09	2.6	6.3	3.2	2.8	0.4	100.2
JEFF DD-2B	Andesite dome (Ti)	60.1	0.67	18.5	5.9	0.10	2.3	6.4	4.1	1.7	0.3	100.2
JEFF DD-2A	Andesite dome (Ti)	60.1	0.70	18.5	5.8	0.11	2.1	6.2	4.0	1.7	0.3	99.5
JEFF FLOW 8-19-08	Basaltic trachyandesite lava (in Trpdf)	50.0	1.24	15.9	8.0	0.12	7.3	10.0	4.5	1.8	0.9	99.8
DC001	Basalt lava, below The Dardanelles (Trpob)[1]	51.7	1.57	16.0	10.2	0.13	7.1	9.2	2.5	1.3	0.5	100.0
DC067	Basalt lava, below The Dardanelles (Trpob)[1]	50.3	1.25	16.8	10.7	0.14	7.6	9.7	2.8	0.6	0.2	100.0

Note: All sample descriptions and geochemical data are new, with samples plotted on geological maps (Figs. 2A and 2B), except where indicated for our samples described in our previous publications: 1—Busby et al. (2008a) (data presented but not with members or lithofacies); 2—Koerner et al. (2009); 3—Putirka et al. (2012). Global positioning system (GPS) locations are given in supplementary data (see text footnote 1).XL rich—crystal rich; XL poor—crystal poor.
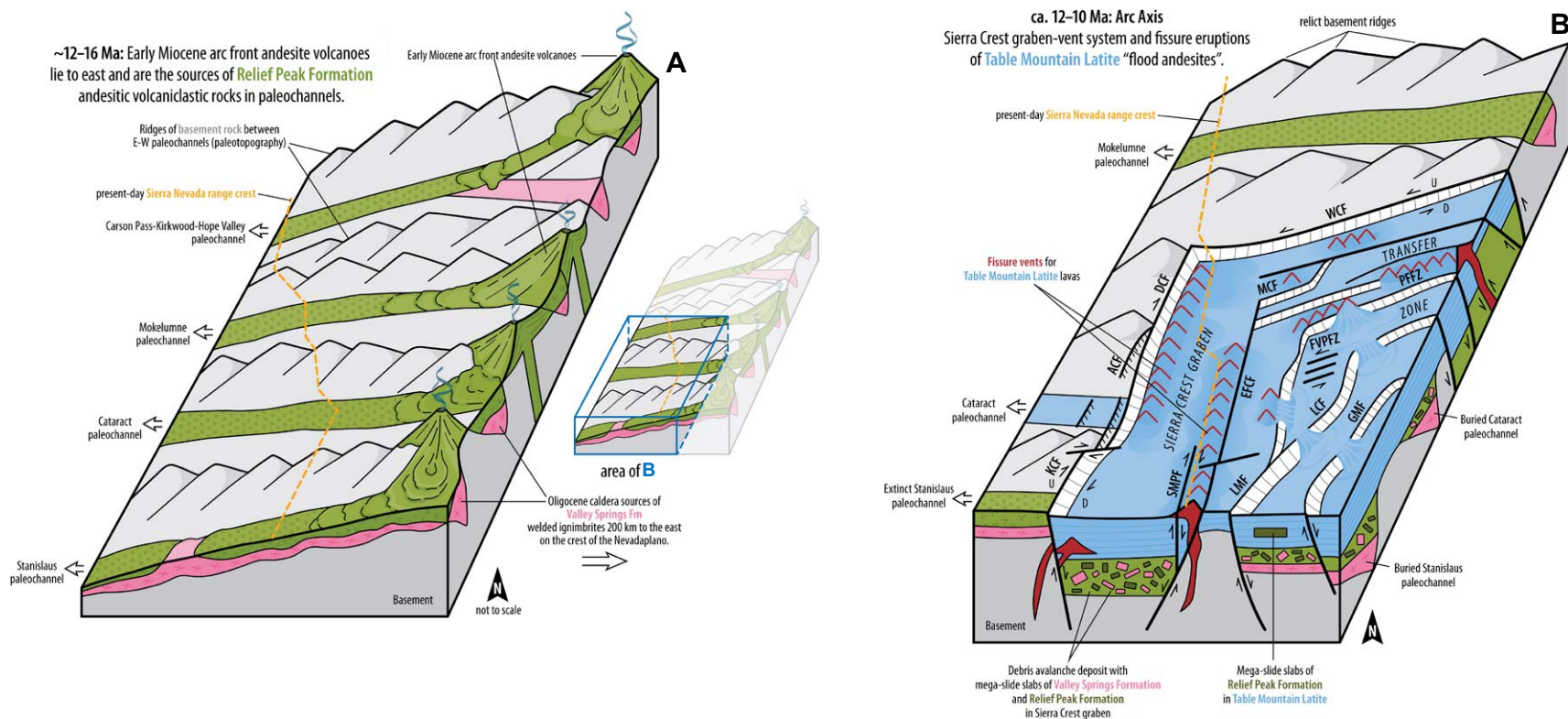
Figure 14 (*on this and following two pages*). Block diagrams illustrating the tectonic and magmatic evolution of the Sierra Crest–Little Walker volcanic center and pull-apart basin, and the Ebbetts Pass volcanic center and pull-apart basin. Data to support these interpretations are given in Figures 2 through 13, and Table 1, and the text. Faults are labeled to facilitate comparison to Figures 2 and 4: ACF—Arnot Creek fault, CLF—Chango Lake fault, DCF—Disaster Creek fault, EFCF—East Fork Carson fault, FVPFZ—Fish Valley Peak fault zone, GHSF—Grover Hot Springs fault, GMF—Grouse Meadows fault, KCF—Kennedy Creek fault, LCF—Lost Cannon fault, LMF—Leavitt Meadow fault, LWC—Little Walker caldera, MCF—Murray Canyon fault, NCF—Noble Canyon fault, PFFZ—Poison Flat fault zone, SMPF—St. Mary's Pass fault, WCF—Wolf Creek fault. Abbreviations for formations: EVT—Eureka Valley Tuff, DP—Disaster Peak Formation, R Pk—Relief Peak Formation, TML—Table Mountain Latite, VS Fm—Valley Springs Formation. (A) Main paleogeographic elements immediately prior to the onset of Walker Lane transtension (ca. 16–12 Ma), with the present-day position of Sierra Nevada range crest given for reference (also see Figs. 2A, 4). By ca. 16–12 Ma, the arc front had swept westward across Nevada into the westernmost Nevada region (see Busby and Putirka, 2009; Busby, 2012, 2013). The volcanoes lay just to the east of the study area and shed andesitic volcaniclastic debris into the Stanislaus, Cataract, and Mokelumne paleochannels, mapped as Relief Peak Formation. Similar age-equivalent deposits also occur in the Carson Pass–Kirkwood paleochannel to the north, described by Busby et al. (2008a) and Hagan et al. (2009). Paleorelief and axial gradients were high, with the "paleochannels" actually consisting of rugged canyons with abundant fluvial boulders. The basal fill of the paleochannels consists of Oligocene Valley Springs Formation welded ignimbrites resting on Mesozoic basement along unconformity 1 (Fig. 3). The unconformity at the base of Relief Springs Formation (unconformity 2; Fig. 3) commonly downcuts through Valley Springs Formation to merge with unconformity 1, where Relief Peak Formation paleochannel fill rests directly on Mesozoic basement. Relief Peak Formation paleochannel fill consists of stratified andesitic debris flow and fluvial deposits, representing down-paleochannel reworking of eruptive products, as well as andesitic block-and-ash-flow tuffs, generated by lava dome collapse. Lavas only occur at one locality (The Dardanelles; Busby et al., 2016), and these are basalt, which can flow tens of kilometers from the vent. Inset block diagram shows the area of part B. (B) By 12 Ma, the arc front had swept westward into what is now the Sierra Nevada, and a very large Walker Lane pull-apart basin began to form in the arc axis, referred to as the Sierra Crest–Little Walker pull-apart and volcanic center. The onset of transtensional faulting was marked by deposition of mass-transport deposits in the grabens, consisting of massive debris-flow deposits and debris-avalanche deposits with megaslide blocks of Relief Peak Formation and Valley Springs Formation. Relief Peak Formation and Valley Springs Formation strata were stripped off adjacent horst blocks; for example, see Table Mountain Latite resting directly on basement in the horst block on the front of the block diagram, with older units in the grabens on either side. Mass wasting began by 12.2 ± 0.1 Ma, as shown by the age of an andesite sill intruding mass-transport deposits, and persisted until 10.39 ± 0.18 Ma, as shown by a date on a block-and-ash-flow tuff within a megaslide block beneath Table Mountain Latite. Transtension then triggered eruption of high-K volcanic rocks of the Stanislaus Group, including Table Mountain Latite (this time frame) and lavas and ignimbrites of the Eureka Valley Tuff (next time frame; see part C), by allowing parental magmas with lower degrees of partial melting to ascend (Putirka and Busby, 2007; Putirka et al., 2012). The Table Mountain Latite includes basalt, trachybasaltic andesite, and trachyandesite, and lesser basaltic andesite and andesite lavas erupted from fault-controlled fissures (red inverted V's). The graben-filling Table Mountain Latite (TML) lavas were ponded to thicknesses of up to 400 m. The N-S normal faults (see U and D symbols) are dextral oblique (see arrows), and the NE normal faults are sinistral oblique, consistent with the overall geometry of the fault system, which is a releasing right step (Fig. 4B; Busby et al., 2013a). "Tectono-stratigraphic recycling" continued, with avalanching of Relief Peak Formation megaslide slabs into grabens while they filled with Table Mountain Latite lavas (Fig. 5). Paleochannels were largely destroyed by faulting and avalanching within the pull-apart structure. Buried Stanislaus and Cataract paleochannels are depicted along the east side of the pull-apart basin, where they are preserved on the hanging wall of the Lost Cannon fault and the southernmost East Fork Carson fault (Fig. 2A). There, Valley Springs Formation is overlain by Relief Peak Formation mass-transport deposits, with abundant megaslide slabs of Valley Springs Formation. Along the western margin of the pull-apart basin, the Stanislaus paleochannel was beheaded by faulting ("extinct Stanislaus paleochannel"). Growth faults formed in the Cataract paleochannel but did not dismember it. The Mokelumne paleochannel to the north remained unfaulted.
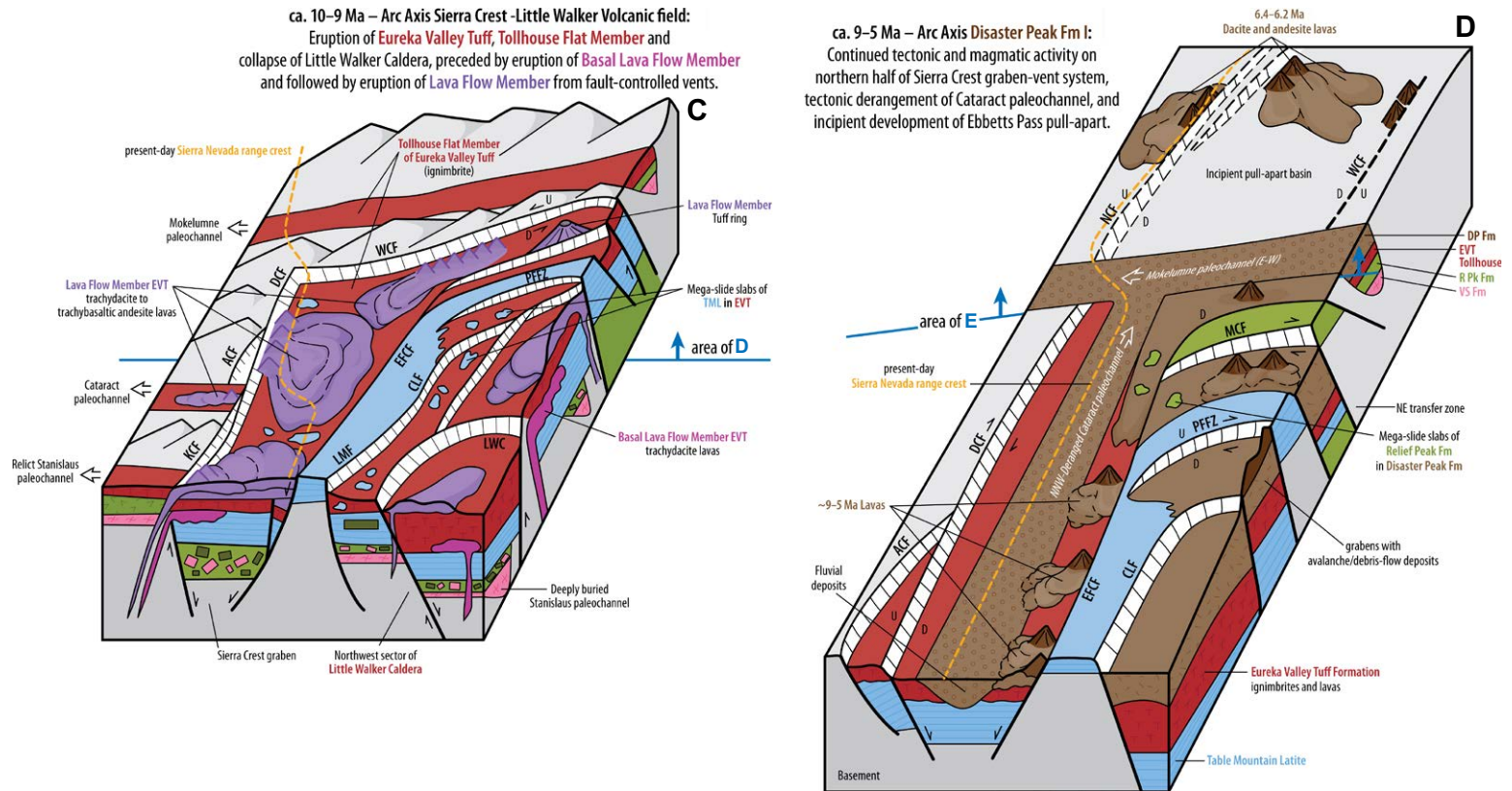
Figure 14 (*continued*). (C) Transtension and volcanism continued in the arc axis, resulting in formation of the Little Walker caldera, which erupted three trachydacite ignimbrites, while lavas continued to erupt across the Sierra Crest–Little Walker volcanic center, evolving to include trachydacites. This time frame shows the period after eruption of Basal Lava Flow Member and Tollhouse Flat Member (Fig. 5), during eruption of the Lava Flow Member. The NW sector of the Little Walker caldera is shown in the bottom-right corner, which formed in the area of maximum transtension. The thickness of the caldera fill is not known (Priest, 1979), nor is it known if it contains slide blocks; it is heavily altered and intruded (Busby's field observations). Due to the great mobility of pyroclastic flows, the Tollhouse Flat Member of the Eureka Valley Tuff (EVT) was deposited in all grabens and paleochannels, including the relict Stanislaus paleochannel, as well as the Mokelumne paleochannel, which has no other Stanislaus Group units. The entire Sierra Crest–Little Walker volcanic center began erupting trachydacite lavas, in addition to continued eruption of basalt to trachyandesite lavas, prior to and after eruption of the Tollhouse Flat Member welded ignimbrite from the caldera. These are shown as Basal Lava Flow Member and Lava Flow Member of the Eureka Valley Tuff (Fig. 5). Lavas of the Eureka Valley Tuff were all erupted from fault-controlled vents, except for those associated with the caldera described by Priest (1979). Widespread eruption of the Lava Flow Member (shown here) was followed by eruptions of the By Day Member welded ignimbrite and Upper Member nonwelded ignimbrite from the Little Walker caldera (not shown here). The last stage of high-K_2O magmatism is recorded by a single black shoshonite lava up to 60 m thick (Dardanelles Formation, not shown), which erupted from a vent along the west side of the Sierra Crest graben and flowed down the Cataract paleochannel. "Tectono-stratigraphic recycling" continued throughout eruption of the Stanislaus Group. After eruption of the Stanislaus Group, volcanism and faulting ended in the southern half of the Sierra Crest–Little Walker volcanic center, so the next time frame shows only the northern half (part D). (D) This time frame shows andesitic magmatism and ongoing subsidence in the northern part of the Sierra Crest–Little Walker volcanic center and pull-apart basin, after hgh-K_2O magmatism ended (the southern half became inactive; see text). For simplicity, all of the members of the underlying Eureka Valley Tuff are generalized into one unit. During this time frame, the Cataract paleochannel (shown in A–C), became deranged from its earlier E-W (Nevadaplano) trend into the approximately N-S Walker Lane Basin trend shown here (described in detail by Busby et al., 2016). We infer that it fed into the Mokelumne paleochannel until that paleochannel got beheaded, as shown in the next time slice (part E). Catastrophic sedimentation continued in the NE transfer zone basins with massive debris-flow deposits. Basalt, basaltic andesite, and andesite lavas erupted from fault-controlled vents with vent facies deposits, and lava domes collapsed to produce block-and-ash-flow tuffs of basaltic andesite to andesite/dacite compositions. Most intrusions are sited along faults. Tectono-stratigraphic recycling continued, as megaslide slabs of older volcanic units were shed into grabens filling with Disaster Peak Formation. Incipient development of the Ebbetts Pass pull-apart basin and volcanic center began in this time frame, with eruption of 6.4–6.2 Ma dacite and andesite lavas from the Noble Canyon fault, shown as relict lavas and megaslide blocks in part E. However, subsidence and volcanism had not yet disrupted the Mokelumne paleochannel in this time frame (Busby et al., 2016). By 5 Ma, the northern part of the Sierra Crest–Little Walker volcanic center and pull-apart became inactive, so the next time frame (part E) shows only the Ebbetts Pass volcanic center and pull-apart.
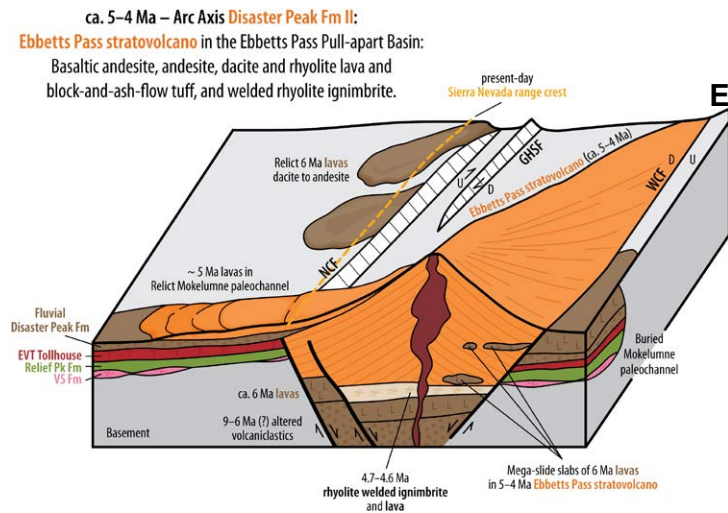
Figure 14 (*continued*). (E) Ebbetts Pass pull-apart basin, with the Ebbetts Pass stratovolcano growing within it. The stratovolcano ultimately filled the basin and built up and westward across the fault that bounded the basin to the west (Noble Canyon fault [NCF] in Fig. 2B). The basal fill consists of altered volcaniclastic rocks inferred to record mass-transport processes during basin inception, and alteration during development of the overlying volcanic center. In the substrate of the 4.6–4.5 Ma stratovolcano, there lies the lower silicic section, including 4.7–4.6 Ma rhyolite welded ignimbrite and lavas (Fig. 5). On the surface, lava emanated from the Ebbetts Pass stratovolcano and escaped the pull-apart basin to flow down the relict Mokelumne paleochannel (Busby et al., 2016). "Stratigraphic recycling" continued, with deposition of mega-slide slabs, including a 6.2 Ma andesite slab recycled from the basin margin. Relative to the Sierra Crest–Little Walker volcanic center, compositions in the Ebbetts Pass volcanic center are more evolved, with rhyolite, more abundant dacite, and only one basalt, showing evidence for a greater degree of crustal contamination and less basalt injection. This may be due to the fact that the Ebbetts Pass pull-apart is much smaller than the Sierra Crest–Little Walker pull-apart basin, with less extension.

A second sample traverse within the pull-apart basin includes (in stratigraphic order, Fig. 2B): (1) a 30-m-thick two-pyroxene andesite lava with trace hornblende (sample MG-08-08; Table 1; Figs. 11A and 13E), and (2) a hornblende two-pyroxene andesite lava with flow breccia (sample MG-08-08; Table 1). The latter is an ~80-m-thick, 300-m-long megaslide block with an age (6.203 ± 0. 011 Ma; Fig. 5) that is much older than strata that lie down section from it.

Silicic intrusions in the core of the Ebbetts Pass stratovolcano in the pull-apart basin (on Silver Peak and Highland Peak [Tdpis]; Fig. 2B) are the youngest dated rocks in the stratovolcano, with a $^{40}Ar/^{39}Ar$ sanidine age of 4.478 ± 0.007 Ma (JHEP-49; Figs. 2B and 5). Although the three closely spaced samples on the flank of Highland Peak are all dacites (JHEP-48, 49, 50; Table 1), modal analyses show they differ, with sample JHEP-49 containing biotite and quartz (Fig. 13G), which are absent from sample JHEP-48 (Fig. 12). Other samples contain sanidine (Fig. 13H). The cliffs on the two peaks also show some variation

in color, which may reflect variations in composition. However, the cliffs are too steep to allow detailed mapping of the intrusions on Highland Peak, and Silver Peak is completely inaccessible. For these reasons, they are generalized as silicic intrusions (Tdpis; Fig. 2B) rather than dacite intrusions.

In the footwall of the Noble Canyon fault (i.e., west of the pull-apart basin), in the Reynolds Peak–Raymond Peak area, strata dip west and are up to 500 m thick (top eroded; Figs. 2B and 10H). This section was deposited when the stratovolcano filled the pull-apart basin, and it represents the youngest preserved strata in the stratovolcano (Fig. 14E). Strata dip uniformly westward south of Reynolds Peak (Fig. 10H), but these pass laterally (northward) into slump folded strata at Reynolds Peak (Fig. 10I). The slump folding indicates sector collapse, perhaps triggered by movements on the Noble Canyon fault. In the part of the section that is not slumped, the lower part of the section is dominated by a reddish black andesite block-and-ash-flow tuff (Fig. 10J), and the upper part of the section is dominated by a light-gray andesite block-and-ash-flow tuff (Fig. 10K; samples CB09-4 and CB09-5, respectively; Table 1). The slumped section contains a basalt peperite intrusion (sample CB09–3; Table 1), which shows very complex mixing with its host volcaniclastic rocks, indicating intrusion while the host was unconsolidated and wet. We infer that this basalt is a flank intrusion that was plumbed up the nearby basin-bounding fault (Noble Canyon fault; Figs. 2B and 14E). This may have contributed to the slumping there, or perhaps it was intruded during a seismic episode on the Noble Canyon fault.

Lavas preserved in erosional remnants of the Mokelumne paleochannel ~6–12 km west of the Ebbetts Pass pull-apart basin (Tdpeps; Fig. 2A) are interpreted to be lavas that were erupted from the Ebbetts Pass stratovolcano and flowed down the relict paleochannel, which had become beheaded by the pull-apart structure (Fig. 14E). Outcrops north of Highway 4 (Fig. 2B) were first mapped as "Miocene Raymond and Silver Peak Andesites of Wilshire (1957)" by Armin et al. (1984), and we concur with this correlation. Additionally, we herein interpret these outcrops as lavas. These lavas are similar to a lava newly mapped as Ebbetts Pass stratovolcano in the Mokelumne paleochannel south of Highway 4 (Fig. 2A; samples CB09-1 and CCB09-2; Table 1). The lava south of Highway 4 forms an ~30-m-high north-facing cliff called Bull Run (fig. 11G *in* Busby et al., 2016). The basal ~5 m section of the lava has unusual thin, wispy, crystal-rich accumulations with both horizontal and vertical orientations, although they are irregular (Figs. 10L, 10M). These wispy accumulations may indicate that crystal-rich magmas mingled with crystal-poor magmas, although the major-element chemistry of the crystal-rich sample (CB09-2; Table 1) is the same as that of the crystal-poor sample (CB09-1; Table 1). It is not understood why the crystal-rich accumulations are oriented in vertical as well as horizontal planes, nor why they are restricted to the basal sixth of the lava.

Intrusions in and around the Ebbetts Pass volcanic center differ from those in and around the Sierra Crest–Little Walker volcanic center by having biotite ± sanidine ± quartz, which are absent in the Sierra Crest–Little Walker volcanic center, except for biotite in the Eureka Valley Tuff (Figs. 8 and 12). This is consistent with the more-evolved compositions of volcanic rocks in the Ebbetts

Pass volcanic center (Table 1). Many of the intrusions in and around the Sierra Crest–Little Walker and Ebbetts Pass volcanic centers are not dated, although maximum ages are provided for most samples by crosscutting relationships (Figs. 8 and 12). However, because the mineralogy of the intrusions matches that of volcanic rocks in each center (Figs. 7, 8, 11, and 12), and the two centers differ, we infer that the intrusions were largely emplaced coeval with volcanism in each of the respective centers.

We tentatively estimate the minimum original volume of the Ebbetts Pass volcanic center at ~270 km³. It is difficult to estimate original volumes of Quaternary Cascades volcanoes, due to glacial erosion (cf. Hildreth, 2007), and the Ebbetts Pass volcanic center has also undergone Alpine erosion, and is even older (Pliocene to late Miocene). To make our estimate, we assumed that the Ebbetts Pass volcanic center completely filled the pull-apart basin, in order for the Ebbetts Pass stratovolcano to build out beyond it, as shown by erosional remnants preserved on the peaks 6–7 km to the NW of the center. The basin fill consists of a lower, sheet-like sequence of lavas and ignimbrites (lower silicic unit) probably deposited along the length and width of the basin, overlain by the Ebbetts Pass stratovolcano, the quaquaversal dips of which suggest it was conical, although it seems likely that some of its volcanic material was funneled northward along the basin (not preserved). Within the pull-apart basin, the central silicic intrusions form the highest units, so only a minimum thickness of the volcanic fill can be estimated there (~1 km). However, the NW flank (top eroded) adds another 500 m to the total minimum thickness, and the center presumably lay hundreds of meters higher than the flank. We therefore estimate a minimum thickness of 2 km. The northward-widening pull-apart basin is an average of 9 km wide (E-W), and the N-S extent is ~15 km. An estimated original volume of ~270 km³ is comparable to that estimated for the Lassen volcanic center in the last 825 k.y. (200 km³; cf. Hildreth, 2007). The Lassen volcanic center is also a good modern analog, because it is a major arc magmatic focus at the rift tip (i.e., in the northernmost Walker Lane pull-apart basin; Busby, 2013; Smith et al., 2016).

Rift Volcanic Rocks

Small basalt and basaltic andesite plugs, most containing olivine phenocrysts (Fig. 13I), are scattered around the region (Fig. 2) but are not associated with mapped faults. We only dated one of these intrusions, which has a $^{40}Ar/^{39}Ar$ plagioclase age of 3.65 ± 0.03 Ma (Fig. 5). The youngest dated mafic volcanic rock in the region is the Columns of the Giants lava on the south side of Highway 108 (mapped as unit Qb on Fig. 2A). This yielded a $^{40}Ar/^{39}Ar$ age of 177 ± 7 ka (Farmer et al., 2013). We discovered a basalt feeder dike for this (sample Qdike 8–19–08; Table 1). These mafic rocks form part of the regional suite of postsubduction magmas (Farmer et al., 2013), which have been interpreted as continental rift magmas (Lange and Carmichael, 1996; Cousens et al., 2011, 2012; Putirka et al., 2012; John et al., 2015b; Putirka and Platt, 2012).

Petrographic Interpretations

While we lack mineral composition data, which would otherwise yield more precise answers, two mineral textures in particular provide some clues as to how magmas might have been processed.

(1) In the now-classic experiments by Tsuchiyama (1985), the sieve (or in his paper "dusty") textures of Figure 9A were demonstrated to be a product of magma mixing: His work showed that in nearly all cases, the sieve areas have high Ca compared to inner, nonsieved cores, and so the texture can be formed by mixing a low-An crystal from a felsic magma into a more mafic, or at least higher-Ca magma, with which the crystal then attempts to equilibrate (Tsuchiyama, 1985). The more coarse "skeletal" plagioclase textures were not reproduced in those experiments, however, and Tsuchiyama (1985) concluded that such skeletal plagioclase represents mixing under conditions of supercooling, as proposed by Kuo and Kirkpatrick (1982). However, in more recent experiments, Iezzi et al. (2014) were able to obtain skeletal plagioclase textures at relatively rapid undercooling with no implicit need for magma mixing, and at the Tequila volcanic field in Mexico, Frey and Lange (2011) were able to link skeletal-type textures to undercooling initiated by magma degassing (rather than magma mixing). Clearly, some of our plagioclase textures are due to magma mixing, but some might also represent near-closed system cooling, or degassing.

(2) Many of our samples are saturated with two pyroxenes, and clinopyroxene (Cpx) often rims orthopyroxene (Opx). This Cpx-on-Opx relationship can come about in different ways, depending upon bulk composition. If these minerals originated from a mafic basaltic parent (>10 wt% MgO), then the Cpx-on-Opx (Fig. 9A) may indicate fractional crystallization of that parent magma at ≥8 kbar pressures. Experimental work by Grove et al. (2003) showed a crossover in phase relationships for such mafic magmas, where Opx crystallization only preceded that of Cpx (by ~50 °C) at high pressures (their fig. 2), and this phase relationship held over a wide range of H_2O contents (0–6 wt% H_2O; their fig. 4). Another possibility, though, is that Opx and Cpx derive from different basaltic magmas. Experimental data indicate that at low pressures, Opx either follows Cpx (Grove et al., 2003) or does not saturate at all (e.g., Barclay and Carmichael, 2004). So another possibility is that Opx grains were derived from basaltic magmas at elevated pressure ranges and mixed with lower-MgO basalts (<8 wt%; e.g., Barclay and Carmichael, 2004) that were near or at Cpx saturation. Yet another possibility is that the parent magmas were more felsic: Blatter and Carmichael's (2001) experiments on magmas having 62–64 wt% SiO_2 (and <6% MgO) could be cosaturated with both Opx and Cpx, where Opx preceded Cpx saturation in the pressure range 0.001 kbar (1 atm) to 3.5 kbar by anywhere from 20 to 100 °C, depending upon bulk composition and pressure. As with plagioclase textures, there are strong
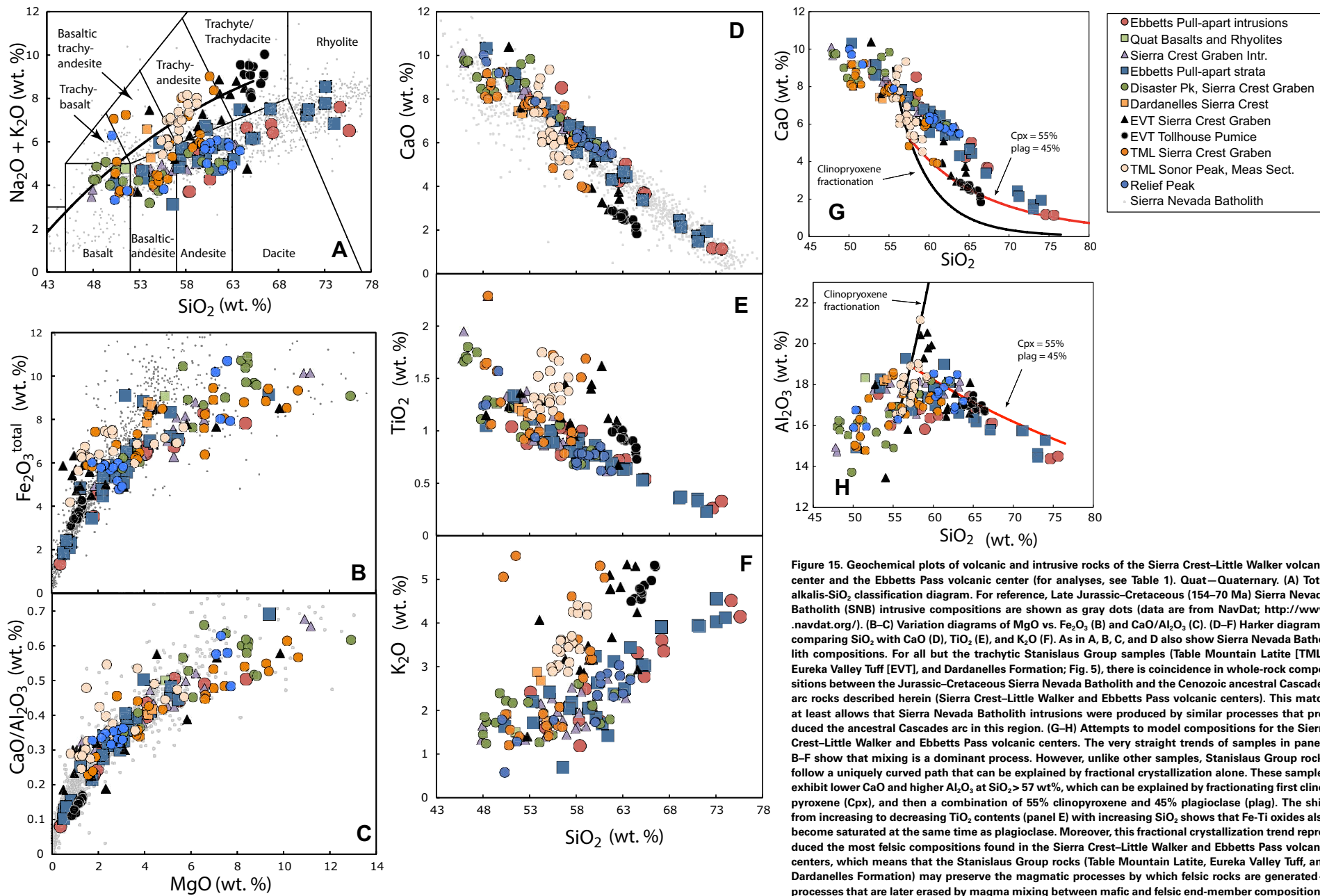
Figure 15. Geochemical plots of volcanic and intrusive rocks of the Sierra Crest–Little Walker volcanic center and the Ebbetts Pass volcanic center (for analyses, see Table 1). Quat—Quaternary. (A) Total alkalis-SiO$_2$ classification diagram. For reference, Late Jurassic–Cretaceous (154–70 Ma) Sierra Nevada Batholith (SNB) intrusive compositions are shown as gray dots (data are from NavDat; http://www .navdat.org/). (B–C) Variation diagrams of MgO vs. Fe$_2$O$_3$ (B) and CaO/Al$_2$O$_3$ (C). (D–F) Harker diagrams, comparing SiO$_2$ with CaO (D), TiO$_2$ (E), and K$_2$O (F). As in A, B, C, and D also show Sierra Nevada Batholith compositions. For all but the trachytic Stanislaus Group samples (Table Mountain Latite [TML], Eureka Valley Tuff [EVT], and Dardanelles Formation; Fig. 5), there is coincidence in whole-rock compositions between the Jurassic–Cretaceous Sierra Nevada Batholith and the Cenozoic ancestral Cascades arc rocks described herein (Sierra Crest–Little Walker and Ebbetts Pass volcanic centers). This match at least allows that Sierra Nevada Batholith intrusions were produced by similar processes that produced the ancestral Cascades arc in this region. (G–H) Attempts to model compositions for the Sierra Crest–Little Walker and Ebbetts Pass volcanic centers. The very straight trends of samples in panels B–F show that mixing is a dominant process. However, unlike other samples, Stanislaus Group rocks follow a uniquely curved path that can be explained by fractional crystallization alone. These samples exhibit lower CaO and higher Al$_2$O$_3$ at SiO$_2$ > 57 wt%, which can be explained by fractionating first clinopyroxene (Cpx), and then a combination of 55% clinopyroxene and 45% plagioclase (plag). The shift from increasing to decreasing TiO$_2$ contents (panel E) with increasing SiO$_2$ shows that Fe-Ti oxides also become saturated at the same time as plagioclase. Moreover, this fractional crystallization trend reproduced the most felsic compositions found in the Sierra Crest–Little Walker and Ebbetts Pass volcanic centers, which means that the Stanislaus Group rocks (Table Mountain Latite, Eureka Valley Tuff, and Dardanelles Formation) may preserve the magmatic processes by which felsic rocks are generated—processes that are later erased by magma mixing between mafic and felsic end-member compositions.

■ GEOCHEMISTRY

Whole-rock major-element compositions from rocks in the Sierra Crest–Little Walker and Ebbetts Pass volcanic centers show that these systems are quite similar, with the notable exception of the Stanislaus Group (Fig. 15), which includes the Table Mountain Latite (lavas), the Eureka Valley Tuff (both ignimbrites and lavas), and the Dardanelles Formation (a single lava). Other volcanic and intrusive units are essentially identical to one another, being mostly calc-alkalic, and ranging from basalt to rhyolite in composition (Fig. 15A), with whole-rock compositions that fall on remarkably straight trends in SiO_2 versus CaO (Fig. 15D), TiO_2 (Fig. 15E), and K_2O (Fig. 15F) diagrams. Such linear trends are indicative of magma mixing, although changes in slope in SiO_2 versus Al_2O_3 (Fig. 15H), for example, require at least three different mixing end members—or, more likely, mixing and fractional crystallization were both important for generating magmatic diversity. At both the Sierra Crest–Little Walker and Ebbetts Pass volcanic centers, the majority of volcanic rocks trace back to similar basaltic parental magmas (Figs. 15A–15F), having ~49% SiO_2 and 12% MgO. However, the parental magmas are certainly not singular in composition, as they would appear to have varying amounts of total Fe_2O_3 (8–11 wt%, projected to 12% MgO) and TiO_2 (1%–2.5% at 49% SiO_2), and K_2O contents vary from 0.7% to 2.0% at 49% SiO_2, and are >5 wt% for the Table Mountain Latite. However, beyond K_2O, the mafic compositions at each volcanic center overlap, indicating that similar parental magmas were delivered to the Sierra Crest–Little Walker and Ebbetts Pass volcanic centers.

The Stanislaus Group samples are a notable exception, as these samples are nearly all trachytic (basaltic trachyandesite to trachydacite), and their trachytic character is mostly a result of higher K_2O (Fig. 15F). These are not the first high-K_2O volcanic rocks to be observed in the Sierra Nevada, and Farmer et al. (2002) presented an interesting model whereby high-K_2O volcanism in the southern Sierra Nevada is a response to the removal of continental lithosphere during "delamination" (e.g., Ducea and Saleeby, 1998). In this model, lithosphere removal allows the heating of specially enriched parts of the lower crust, producing the enriched high-K_2O lavas. We reject this model for several reasons. Perhaps the most important reason is that the first-order response to lithosphere removal, and consequent asthenosphere upwelling, should be an increase in the degree of mantle partial melting, as the lithosphere is replaced by convective mantle, which is the source of mid-ocean-ridge basalt (MORB). The predicted volcanic expression, then, is an increase in the total volume of erupted volcanic materials, with geochemical trends that involve greater melt fractions and an increase in MORB-like (convective) geochemical signatures. However, none of the high-K_2O lavas exhibits these characteristics: Both the central Sierra Nevada Stanislaus Group and the southern Sierra Ne-

vada high-K_2O suites are the products of very low degrees of melt fraction of typical continental mantle lithosphere, rather than a special enriched source (Putirka and Busby, 2007; Putirka et al., 2012). Worse still, lavas erupted after the presumed delamination event—including entrained mantle xenoliths (e.g., the Big Pine volcanic field)—have isotopic signatures that require an ancient continental mantle lithosphere source (Putirka et al., 2012). As shown by Putirka et al. (2012, their fig. 14), the convective mantle does indeed make its appearance, but only to the south and east, beneath the Coso volcanic field, where the north-migrating Mendocino triple junction has had sufficient time to affect the removal of continental mantle lithosphere. We would partially agree with Farmer et al. (2013) that the lithosphere beneath the Sierra Nevada is being heated, but we argue that the lithosphere is degraded slowly, and that high-K_2O volcanism marks the earliest stages of lithosphere degradation, not its removal, which comes much later (e.g., Putirka et al., 2012, their fig. 16).

Our new data support not just a distinct source for the Stanislaus Group, but also a distinct differentiation history compared to other magmas of the Sierra Crest–Little Walker and Ebbetts Pass volcanic centers. As noted in earlier studies (Putirka and Busby, 2007; Putirka et al., 2012), the Table Mountain Latite samples have high concentrations of incompatible trace elements, which can be attributed to low degrees of partial melting. However, the Table Mountain Latite and Eureka Valley Tuff also exhibit a distinct break in slope in TiO_2 (Fig. 15E) and trend to higher Al_2O_3 contents and lower CaO contents (Figs. 15G and 15H). These trends indicate significant clinopyroxene fractionation (Figs. 15G and 15H; see Priest 1979), and the low CaO and lower Al_2O_3 contents of the Eureka Valley Tuff can be produced by adding plagioclase to the crystallization assemblage, at ~58% SiO_2. The major-oxide trends (Fig. 15) also indicate that the Eureka Valley Tuff lavas and Dardanelles Formation lava can be obtained by Table Mountain Latite fractionation, if both plagioclase and Fe-Ti oxides reach saturation in Table Mountain Latite liquids at 60% SiO_2. In contrast, TiO_2 decreases with increasing silica across the entire range of SiO_2 contents (48%–76%) for non–Stanislaus Group samples from the Sierra Crest–Little Walker and Ebbetts Pass volcanic centers; this might not necessarily reflect later Fe-Ti oxide saturation for Stanislaus Group lavas, but instead more complete mixing of the former, or perhaps the preferential eruption of unmixed lavas in the Stanislaus Group. If the contrasts in Fe and Ti are not due to delayed Fe-Ti oxide saturation, then the Stanislaus Group might better capture the crystallization-fractionation processes by which the Sierra Crest–Little Walker and Ebbetts Pass volcanic centers were produced.

The Stanislaus Group magmas appear to be cosanguineous, which supports the interpretation that they represent a single magmatic system, even though lavas of the Stanislaus Group erupted over a much larger area than the caldera-forming ignimbrites (Figs. 2 and 14). We surmise that all these magmas shared a similar magma plumbing system, although this hypothesis is by no means required: Separate plumbing systems may well deliver magmas to similar depths, which then fractionate over similar temperature intervals. In any case, the Table Mountain Latite and Eureka Valley Tuff fall close to a simple fractionation trend, involving only clinopyroxene for the most mafic

samples, and clinopyroxene + plagioclase + Fe-Ti oxides for trachyandesites. In contrast, the remaining (non–Stanislaus Group) Sierra Crest–Little Walker volcanic center samples and all of the Ebbetts Pass volcanic center samples fall on remarkably linear trends, similar to one another but distinct from the Table Mountain Latite and Eureka Valley Tuff. Those linear trends are not matched by the naturally curved trends resulting from fractional crystallization alone, and so they almost certainly represent magma mixing to a degree that was absent for the Table Mountain Latite and Eureka Valley Tuff.

We also find that Tertiary volcanic rocks (excepting the Stanislaus Group) match the major-element compositions of Cretaceous granitic rocks. This match indicates no fundamental difference in the petrologic origin of the Cretaceous plutonic and Tertiary volcanic suites. In such a case, the volcanic systems may indeed provide a better understanding of the genesis of the Sierra Nevada Batholith. For example, Lee et al. (2006) have suggested that Cretaceous plutons may be derived by clinopyroxene + garnet fractionation in the lower crust. However, we see no evidence for the involvement of garnet in the crystallization history of Tertiary Sierra Nevada volcanic rocks. Instead, olivine is found in the most primitive of Tertiary volcanic samples, and clinopyroxene and plagioclase dominate the more felsic samples. In addition, fractionation of olivine + clinopyroxene + plagioclase + Fe-Ti oxides, combined with magma mixing, would explain Tertiary volcanic major-oxide variations. Clearly, whatever processes produced the Tertiary volcanic rocks were capable of producing the Sierran granitic plutons as well.

■ CONCLUSIONS: FEATURES AND PROCESSES COMMON TO TRANSTENSIONAL ARC-RIFT SETTINGS

We conclude with a summary of the evolution of the Sierra Crest–Little Walker and Ebbetts Pass volcanic centers and pull-apart basins (Fig. 14), describing characteristics that should be recognized in other arc-rift settings, and some future directions for research.

Tectono-Stratigraphic Recycling

A key geologic process in the ancestral Cascades arc pull-apart basins is herein referred to as "tectono-stratigraphic recycling": the transfer of megaslide slabs from footwall to hanging-wall blocks in the transtensional arc rift (Figs. 5 and 14). These are referred to as "slabs" rather than "blocks" because they commonly are thin and long (aspect ratios of ~1:5–1:20), with internal layering subparallel to the strata that enclose them. This indicates that the slabs broke off the parent outcrop along bedding planes and slid, relatively intact, rather than tumbling and breaking into equant masses of variable orientation. In some cases, these slabs are relatively easy to recognize; for example, megaslide blocks of white rhyolite welded ignimbrite of the Oligocene Valley Springs Formation are obvious within dark-tan to brown andesitic debris-flow deposits of the Miocene Relief Peak Formation. More difficult to recognize is recycling of Relief Peak Formation andesitic volcaniclastic deposits into Relief Peak Formation debris-avalanche deposits. Most difficult to recognize is the recycling of lava megaslide slabs; these are commonly first identified by anomalously old $^{40}Ar/^{39}Ar$ ages and then confirmed as megaslide slabs through the details of their field relations, including chaotic bedding, with smaller (i.e., meter- to decameter-scale) blocks surrounding the megaslide slabs.

Pull-apart basins (e.g., Fig. 4B) subside more rapidly than any other basin type (Nilsen and Sylvester, 1995). They are steep-walled and deep, with uplifted blocks interspersed with basins in very close proximity, and with rapidly shifting sites of uplift and subsidence (Nilsen and Sylvester, 1995; Mann, 2007). Megaslide blocks in arc-related pull-apart basins are common due to the abundance of tabular, igneous stratigraphic units (lavas and welded ignimbrites) that commonly rest on easily undermined volcaniclastic deposits (debris-flow and fluvial deposits).

Exploitation of Arc Axis by Transtensional Rifting

It has long been recognized that arcs have evolved into rifts in a wide variety of crustal settings (e.g., Yamaji, 1990; Murphy et al., 1990; Lawton and McMillan, 1999; Martín-Barajas et al., 1995; Busby et al., 2006; Centeno-Garcia et al., 2011). This is due to localization of extension or transtension in the thermally weakened arc axis, where rifting succeeds much more rapidly (in millions of years) than it does in intracontinental rifts (which take tens of millions of years; Umhoefer, 2011). The Sierra Crest–Little Walker volcanic center records the onset of Walker Lane transtensional rifting at ca. 12 Ma, through exploitation of the arc axis at a large volcanic center.

Controls of Pull-Apart Size and Magnitude of Extension on Arc Magma Compositions

The formation of the very large Sierra Crest–Little Walker pull-apart in the ancestral Cascades arc triggered rapid ascent of low-degree partial melts at the onset of Walker Lane transtension (Stanislaus Group), causing the outpouring of high-K_2O lava (shoshonite, trachyandesite, and trachybasaltic andesite) as well as basalt. On a smaller scale, more basalt and high-K_2O lava erupted from the southern part of the Sierra Crest–Little Walker pull-apart where transtension was greatest, relative to the northern part, which erupted more andesite and basaltic andesite. This is consistent with the interpretation that the magnitude of extension is important in eruption of low-degree partial melts and primitive melts. The Ebbetts Pass pull-apart, in contrast, is much smaller than the Sierra Crest–Little Walker pull-apart, consistent with the observations that it has only one basalt, few high-K_2O rocks, and a much greater proportion of dacite, and it erupted rhyolites, which are not present in the Sierra Crest–Little Walker pull-apart. We attribute this to a higher degree of crustal contamination

due to slower ascent of magmas in a smaller pull-apart structure. This is consistent with studies in the nearby Bodie Hills (Fig. 1), where minimal extension was accompanied by eruption of intermediate to silicic rocks, few basalts, and only one small-volume high-K_2O lava (John et al., 2012).

All of the ancestral Cascades arc volcanic rocks described here, except for the Stanislaus Group, are compositionally identical to the unconformably underlying Mesozoic plutonic rocks of the Sierra Nevada Batholith; this indicates a similar petrogenesis, by shallow-level fractional crystallization, with no need for deep-seated pyroxenite cumulates. However, the petrogenesis of the Stanislaus Group requires a greater degree of fractionation of clinopyroxene and Fe-Ti oxides, and their major-oxide trends and clinopyroxene-rich modes might be the volcanic expression of processes that lead to pyroxenite cumulates. Such compositions are rare elsewhere in the Cenozoic ancestral Cascades arc (du Bray and John, 2011; du Bray et al., 2013) and the Mesozoic Sierra Nevada Batholith. In the ancestral Cascades arc, these compositions occur within a large pull-apart basin within the arc (Stanislaus Group). A similar example occurs in the Ryukyu arc, where voluminous (~560 km³) late Miocene to Pleistocene high-K "flood andesites" erupted from fissures and filled the Hiatsu "volcano-tectonic depression" (Nagao et al., 1995, 1999; Miyoshi et al., 2010). This distinctive volcanic and geochemical style may be used to infer extreme extension or transtension within ancient arcs where the structural setting might otherwise not be known.

Still unknown, however, is how these magmatic plumbing systems respond to an evolving transtensional field. For example, we have argued previously that the high-K_2O lavas represent the transport of deep-seated, low-degree partial melts (e.g., Putirka et al., 2012). However, most of the high-K_2O lavas have just 3–4 wt% MgO, and so these are clearly not mantle-derived magmas (see Putirka, 2017). If the parent magmas contain >12 wt% MgO, then there has been considerable amounts of fractionation before these lavas reached the surface. Also, mafic rocks are similarly rare in the volcanic suites that preceded and followed the pulses of high-K_2O volcanism. Because the lavas from the various suites are replete with clinopyroxenes, amphiboles, and plagioclase feldspars, they are a perfect target for thermobarometry, and so by measuring their mineral compositions, we can estimate the staging depths (and temperatures) from which these magmas were erupted. Our current model is that the evolutionary pattern of fractional crystallization was shallow-deep-shallow, as the system erupted lavas that transition from low-K_2O to high-K_2O and then back to low-K_2O compositions. However, the evolution of a transtensional system may well impose a permanent change on the plumbing system or in some way affect how magmas are transported to the surface, or perhaps even eruption-triggering mechanisms (e.g., Putirka, 2017). In Putirka et al. (2012), we also showed that subduction-related geochemical signatures linger well past the end of subduction processes. The post-transtension system may similarly establish shallow crustal reservoirs that did not exist prior to the onset of transtension, but that remain connected to deep-seated conduits that continue to feed thermal energy to shallow depths. Mineral compositions will allow us to determine whether transtensional stress regimes continue to influence volcanic activity long after their stress regimes have passed.

Unzipping of a Ribbon Continent by Rift Tip Propagation in the Arc Axis

In some cases, a continental rift may exploit the length of the arc axis simultaneously, as in the case of the Gulf of California (Lizarralde et al., 2007). There, stalling of a large subducting (Farallon) microplate offshore of Baja California resulted in plate capture at ca. 12 Ma (Stock and Lee, 1994). A distinctly different geologic record has been created by subduction zone microplate interactions offshore of California. There, the Walker Lane transtensional rift tip has propagated northward with time in the ancestral Cascades arc axis since ca. 12 Ma, in concert with northward migration of the Mendocino triple junction (Busby, 2013; Smith et al., 2016). The study presented herein, of two pull-apart basins in the ancestral Cascades arc, provides local-scale confirmation of this regional-scale interpretation. In ancient arc-rift terranes, regional age patterns of the arc-to-rift transition (simultaneous vs. time-transgressive) may be used to help reconstruct the geologic record of microplate subduction.

Structural Controls on Volcanic Plumbing Systems and Coeval Surface Processes

Much attention has been paid to magmatic plumbing systems at active volcanoes by using geophysical and geochemical methods. However, the geologic contexts of continental arcs have been neglected relative to the study of their geochemical characteristics (Hildreth, 2007). Our geologic observations reveal the structural controls on magmatic plumbing systems at eroded extinct volcanoes, and their relation to coeval surface processes (Fig. 14). This required construction of detailed geologic maps, using the geochemical, petrographic, and geochronological data presented herein. We hope that the study presented herein convinces future workers of the importance of integrating laboratory data with detailed geologic mapping, which is the only way we might ever understand the interplay among tectonics, volcanic styles, and magma chemistry.

REFERENCES CITED

Argus, D.F., and Gordon, R.G., 1991, Current Sierra Nevada–North America motion from very long baseline interferometry: Implications for the kinematics of the western United States: Geology, v. 19, p. 1085–1088, https://doi.org/10.1130/0091-7613(1991)019<1085:CSNNAM>2.3.CO;2.
Armin, R.A., John, D.A., and Moore, W.J., 1984, Geologic Map of the Markleeville 15-Minute Quadrangle with Quaternary Geology by John C. Dohrenwend: U.S. Geological Survey Miscellaneous Investigations Series Map I-1474, scale 1:62,500.

Barclay, J., and Carmichael, I.S.E., 2004, A hornblende basalt from western Mexico: Water-saturated phase relations constrain a pressure-temperature window of eruptability: Journal of Petrology, v. 45, p. 485–506, https://doi.org/10.1093/petrology/egg091.

Bateman, P.C., and Wahrhaftig, C., 1966, Geology of the Sierra Nevada, in Bailey, E.H., ed., Geology of Northern California: California Division of Mines Bulletin 190, p. 107–172.

Blatter, D.L., and Carmichael, I.S.E., 2001, Hydrous phase equilibria of a Mexican high-silica andesite: A candidate for a mantle origin?: Geochimica et Cosmochimica Acta, v. 65, p. 4043–4065, https://doi.org/10.1016/S0016-7037(01)00708-6.

Bormann, J., Hammond, W.C., Kreemer, C., and Blewitt, G., 2016, Accommodation of missing shear in the Central Walker Lane, western North America: Constraints from dense GPS measurements: Earth and Planetary Science Letters, v. 440, p. 169–177, https://doi.org/10.1016/j.epsl.2016.01.015.

Brem, G.F., 1977, Petrogenesis of Late Tertiary Potassic Volcanic Rocks of the Sierra Nevada and Western Great Basin [Ph.D. thesis]: Riverside, California, University of California, 361 p.

Busby, C.J., 2012, Extensional and transtensional continental arc basins: Case studies from the southwestern United States, in Busby, C., and Azor, A., eds., Tectonics of Sedimentary Basins: Recent Advances: Wiley-Blackwell, p. 382–404, https://doi.org/10.1002/9781444347166.ch19.

Busby, C.J., 2013, Birth of a plate boundary at ca. 12 Ma in the ancestral Cascades arc, and implications for transtensional rift propagation, Walker Lane: Geosphere, v. 9, p. 1147–1160, https://doi.org/10.1130/GES00928.1.

Busby, C.J., and Putirka, K., 2009, Miocene evolution of the western edge of the Nevadaplano in the central and northern Sierra Nevada: Paleocanyons, magmatism and structure, in Ernst, G., ed., The Rise and Fall of the Nevadaplano: International Geology Review, v. 51, no. 7–8, p. 671–701.

Busby, C.J., Fackler Adams, B., Mattinson, J., and De Oreo, S., 2006, View of an intact oceanic arc, from surficial to mesozonal levels: Cretaceous Alisitos Arc, Baja California, Mexico: Journal of Volcanology and Geothermal Research, v. 149, p. 1–46, https://doi.org/10.1016/j.jvolgeores.2005.06.009.

Busby, C.J., Hagan, J.C., Putirka, K., Pluhar, C.J., Gans, P.B., Wagner, D.L., Rood, D.H., DeOreo, S.B., and Skilling, I., 2008a, The ancestral Cascades arc: Cenozoic evolution of the central Sierra Nevada (California) and the birth of the new plate boundary, in Wright, J.E., and Shervais, J.W., eds., Ophiolites, Arcs, and Batholiths: A Tribute to Cliff Hopson: Geological Society of America Special Paper 438, p. 331–378, https://doi.org/10.1130/2008.2438(12).

Busby, C.J., DeOreo, S.B., Skilling, I., Hagan, J.C., and Gans, P.B., 2008b, Carson Pass–Kirkwood paleocanyon system: Implications for the Tertiary evolution of the Sierra Nevada, California: Geological Society of America Bulletin, v. 120, p. 274–299, https://doi.org/10.1130/B25849.1.

Busby, C.J., Koerner, A.A., Melosh, B.L., Andrews, G.D.M., and Hagan, J.C., 2013a, The Sierra Crest graben-vent system: A Walker Lane pull-apart in the ancestral Cascades arc: Geosphere, v. 9, p. 736–780, https://doi.org/10.1130/GES00670.1.

Busby, C.J., Hagan, J.C., and Renne, P., 2013b, Initiation of Sierra Nevada range front–Walker Lane faulting at ca. 12 Ma in the Ancestral Cascades arc: Geosphere, v. 9, no. 5, p. 1125–1146, https://doi.org/10.1130/GES00927.1.

Busby, C.J., Andrews, G.D.M., Koerner, A.K., Brown, S.R., Melosh, B.L., and Hagan, J.C., 2016, Progressive derangement of ancient (Mesozoic) E-W Nevadaplano paleochannels into modern (Miocene–Recent) NNW trends in the Walker Lane belt, central Sierra Nevada: Geosphere, v. 12, p. 135–175, https://doi.org/10.1130/GES01182.1.

Carlson, C.W., 2017, Kinematics and Transfer Mechanisms of Strain Accommodation at the Transition between the Northern and Central Walker Lane, Western Nevada [Ph.D. thesis]: Reno, Nevada, University of Nevada, 217 p.

Carlson, C.W., and Faulds, J., 2014, Geologic mapping at the northern terminus of the central Walker Lane, western Nevada: Kinematics and strain transfer mechanisms in an evolving transform boundary: Geological Society of America Abstracts with Programs, v. 46, no. 6, p. 156.

Carlson, C.W., and Faulds, J., 2015, Reference directions, rotations and magnetostratigraphy: Utilization of Oligocene ignimbrite paleomagnetism to better understand Walker Lane tectonics, western Nevada, USA: San Francisco, California, American Geophysical Union, Fall Meeting 2015, abstract GP31A–1365.

Carlson, C.W., and Faulds, J.E., 2016, Translation vs. rotation: The battle for enigmatic dextral-shear accommodation in the Walker Lane, western Nevada, USA: Geological Society of America Abstracts with Programs, v. 48, no. 7, abstract 117–10.

Carlson, C.W., Pluhar, C.J., Glen, J.M.G., and Farner, M.J., 2013, Kinematics of the west-central Walker Lane: Spatially and temporally variable rotations evident in the late Miocene Stanislaus Group: Geosphere, v. 9, no. 6, p. 1530–1551, https://doi.org/10.1130/GES00955.1.

Cashman, P., and Fontaine, S.A., 2000, Strain partitioning in the northern Walker Lane, western Nevada and northeastern California: Tectonophysics, v. 326, no. 1–2, p. 111–130, https://doi.org/10.1016/S0040-1951(00)00149-9.

Cashman, P.H., Trexler, J.H., Muntean, T.W., Faulds, J.E., Louie, J.N., and Oppliger, G.L., 2009, Neogene tectonic evolution of the Sierra Nevada–Basin and Range transition zone at the latitude of Carson City, Nevada, in Oldow, J.S., and Cashman, P.H., eds., Late Cenozoic Structure and Evolution of the Great Basin–Sierra Nevada Transition: Geological Society of America Special Paper 447, p. 171–188, https://doi.org/10.1130/2009.2447(10).

Cashman, P.H., Trexler, J.H., Widmer, M.C., and Queen, S.J., 2012, Post–2.6 Ma tectonic and topographic evolution of the northeastern Sierra Nevada: The record in the Reno and Verdi basins: Geosphere, v. 8, p. 972–990, https://doi.org/10.1130/GES00764.1.

Centeno-Garcia, E., Busby, C., Busby, M., Talavera, O., and Gehrels, G., 2011, Evolution of the Cretaceous Guerrero terrane along the Mexican margin, from extensional arc through retroarc to continental arc settings: Geological Society of America Bulletin, v. 123, no. 9/10, p. 1776–1797, https://doi.org/10.1130/B30057.1.

Clark, W.B., and Evans, J.R., 1977, Mines and Mineral Resources of Alpine County: California Division of Mines and Geology Technology and Engineering, 48 p.

Cousens, B., Henry, C.D., Harvey, B.J., Brownrigg, T., Prytulak, J., and Allan, J.F., 2011, Secular variations in magmatism during a continental arc to post-arc transition: Plio-Pleistocene volcanism in the Lake Tahoe/Truckee area, northern Sierra Nevada, California: Lithos, v. 123, p. 225–242, https://doi.org/10.1016/j.lithos.2010.09.009.

Cousens, B., Henry, C.D., and Gupta, V., 2012, Distinct mantle sources for Pliocene–Quaternary volcanism beneath the modern Sierra Nevada and adjacent Great Basin, northern California and western Nevada, USA: Geosphere, v. 8, p. 562–580, https://doi.org/10.1130/GES00741.1.

Crafford, A.E.J., 2007, Geologic Map of Nevada: U.S. Geological Survey Data Series 249, 1 CD-ROM, 46 p., 1 plate, http://pubs.usgs.gov/ds/2007/249.

Curtis, G.H., 1954, Mode of Origin of Pyroclastic Debris in the Mehrten Formation of the Sierra Nevada: University of California Publications in Geological Sciences, v. 29, p. 453–501.

Dixon, T.H., Miller, M., Farina, F., Wang, H., and Johnson, D., 2000, Present-day motion of the Sierra Nevada block and some tectonic implications for the Basin and Range Province, North American Cordillera: Tectonics, v. 19, p. 1–24, https://doi.org/10.1029/1998TC001088.

Dong, S., Gulsen, U., Wesnousky, S.G., Maloney, J., Kent, G., and Driscoll, N., 2014, Strike-slip faulting along the Wassuk Range of the northern Walker Lane, Nevada: Geosphere, v. 10, p. 40–48, https://doi.org/10.1130/GES00912.1.

du Bray, E.A., and John, D.A., 2011, Petrologic, tectonic, and metallogenic evolution of the ancestral Cascades magmatic arc, Washington, Oregon, and northern California: Geosphere, v. 7, p. 1102–1133, https://doi.org/10.1130/GES00669.1.

du Bray, E.A., John, D.A., and Cousens, B.L., 2014, Petrologic, tectonic and metallogenic evolution of the southern segment of the ancestral Cascades magmatic arc, California and Nevada: Geosphere, v. 10, no. 1, p. 1–39, https://doi.org/10.1130/GES00944.1.

Ducea, M., and Saleeby, J., 1998, A case for delamination of the deep batholithic crust beneath the Sierra Nevada, California: International Geology Review, v. 40, p. 78–93, https://doi.org/10.1080/00206819809465199.

Farmer, G.L., Glazner, A.F., and Manley, C.R., 2002, Did lithospheric delamination trigger late Cenozoic potassic volcanism in the southern Sierra Nevada, California?: Geological Society of America Bulletin, v. 114, p. 754–768, https://doi.org/10.1130/0016-7606(2002)114<0754:DLDTLC>2.0.CO;2.

Farmer, G.L., Glazner, A.F., Kortemeier, W.T., Cosca, M.A., Jones, C.H., Moore, J.E., and Schweickert, R.A., 2013, Mantle lithosphere as a source of postsubduction magmatism, northern Sierra Nevada, California: Geosphere, v. 9, no. 5, p. 1102–1124, https://doi.org/10.1130/GES00885.1.

Faulds, J.E., and Henry, C.D., 2008, Tectonic influences and temporal evolution of the Walker Lane: An incipient transform along the evolving Pacific–North American plate boundary, in Spencer, J.E., and Titley, S.R., eds., Ores and Orogenesis: Circum-Pacific Tectonics, Geologic Evolution, and Ore Deposits: Arizona Geological Society Digest, v. 22, p. 437–470.

Ferranti, L., Oldow, J.S., Geissman, J.W., and Neil, M.M., 2009, Flattening strain during coordinated slip on a curved fault array, Rhodes Salt Marsh extensional basin, central Walker Lane, west-central Nevada, in Oldow, J.S., and Cashman, P.H., eds., Late Cenozoic Structural

and Evolution of the Great Basin–Sierra Nevada Transition: Geological Society of America Special Paper 447, p. 189–214.

Fleck, R.J., duBray, E.A., John, D.A., Vikre, P.G., Cosca, M.A., Snee, L.W., and Box, S.E., 2015, Geochronology of Cenozoic Rocks in the Bodie Hills, California and Nevada: U.S. Geological Survey Data Series 916, 26 p.

Frey, H.M., and Lange, R.A., 2011, Phenocryst complexity in andesites and dacites from the Tequila volcanic field, Mexico: Resolving the effects of degassing vs. magma mixing: Contributions to Mineralogy and Petrology, v. 162, p. 415–445, https://doi.org/10.1007/s00410-010-0604-1.

Garrison, N., Busby, C.J., Gans, P.B., Putirka, K., and Wagner, D.L., 2008, A mantle plume beneath California? The mid-Miocene Lovejoy flood basalt, northern California, in Wright, J., and Shervais, J., eds., Ophiolites, Arcs and Batholiths: Geological Society of America Special Paper 438, p. 551–572, https://doi.org/10.1130/2008.2438(20).

Gledhill, T., Pluhar, C.J., Johnson, S.A., Lindeman, J.R. and Petronis, M.S., 2016, A kinematic model for vertical-axis rotation within the Mina deflection of the Walker Lane: American Geophysical Union Abstract GP31B-1300.

Gorny, C., Busby, C., Pluhar, C., Hagan, J., and Putirka, K., 2009, An in-depth look at distal Sierra Nevada paleochannel fill: Drill cores through the Table Mountain Latite near Knight's Ferry, in Ernst, G., eds., The Rise and Fall of the Nevadaplano: International Geology Reviews, v. 51, no. 9–11, p. 824–842.

Grove, T.L., Elkins-Tanton, L.T., Parman, S.W., Chatterjee, N., Muntener, O., and Gaetani, G., 2003, Fractional crystallization and mantle-melting controls on calc-alkaline differentiation trends: Contributions to Mineralogy and Petrology, v. 145, p. 515–533, https://doi.org/10.1007/s00410-003-0448-z.

Hagan, J.C., Busby, C.J., Putirka, K., and Renne, P.R., 2009, Cenozoic paleocanyon evolution, ancestral Cascades arc volcanism, and structure of the Hope Valley–Carson Pass region, Sierra Nevada, California: International Geology Review, v. 51, p. 777–823, https://doi.org/10.1080/00206810903028102.

Henry, C.D., 2008, Ash-flow tuffs and paleovalleys in northeastern Nevada: Implications for Eocene paleogeography and extension in the Sevier hinterland, northern Great Basin: Geosphere, v. 4, p. 1–35, https://doi.org/10.1130/GES00122.1.

Henry, C.D., Hinz, N.H., Faulds, J.E., Colgan, J.P., John, D.A., Brooks, E.R., Cassel, E.J., Garside, L.J., Davis, D.A., and Castor, S.B., 2012, Eocene–early Miocene paleotopography of the Sierra Nevada–Great Basin–Nevadaplano based on widespread ash-flow tuffs and paleovalleys: Geosphere, v. 8, p. 1–27, https://doi.org/10.1130/GES00727.1.

Hildreth, W., 2007, Quaternary Magmatism in the Cascades—Geologic Perspective: U.S. Geological Survey Professional Paper 1744, 125 p.

Huber, N.K., 1983a, Preliminary Geologic Map of the Dardanelles Cone Quadrangle, Central Sierra Nevada, California: U.S. Geological Survey Miscellaneous Field Map MF-1436, scale 1:62,500.

Huber, N.K., 1983b, Preliminary Geologic Map of the Pinecrest Quadrangle, Central Sierra Nevada, California: U.S. Geological Survey Miscellaneous Field Studies Map MF-1437, scale 1:62,500, 1 sheet.

Hunter, L.E., Howle, J.F., Rose, R.S., and Bawden, G.W., 2011, LiDAR-assisted identification of an active fault near Truckee, California: Bulletin of the Seismological Society of America, v. 101, no. 3, p. 1162–1181, https://doi.org/10.1785/0120090261.

Iezzi, G., Mollo, S., Shahini, E., Cavallo, A., and Scarlato, P., 2014, The cooling kinetics of plagioclase feldspar as revealed by electron microprobe mapping: The American Mineralogist, v. 99, p. 898–907, https://doi.org/10.2138/am.2014.4626.

Jayko, A.S., and Bursik, M., 2012, Active transtensional intracontinental basins: Walker Lane belt in the western Great Basin, in Busby, C., and Azor, A., eds., Recent Advances in Tectonics of Sedimentary Basins: Wiley-Blackwell, p. 226–248, https://doi.org/10.1002/9781444347166.ch11.

John, D.A., 2001, Miocene and early Pliocene epithermal gold-silver deposits in the northern Great Basin, western United States: Characteristics, distribution, and relationship to magmatism: Economic Geology and the Bulletin of the Society of Economic Geologists, v. 96, p. 1827–1853, https://doi.org/10.2113/gsecongeo.96.8.1827.

John, D.A., du Bray, E.A., Blakely, R.J., Fleck, R.J., Vikre, P.G., Box, S.E., and Moring, B.C., 2012, Miocene magmatism in the Bodie Hills volcanic field, California and Nevada: A long-lived eruptive center in the southern segment of the ancestral Cascades arc: Geosphere, v. 8, p. 44–97, https://doi.org/10.1130/GES00674.1.

John, D.A., du Bray, E.A., Henry, C.D., and Vikre, P.G., 2015a, Cenozoic magmatism and epithermal gold-silver deposits of the southern ancestral Cascade arc, western Nevada and eastern California, in Pennell, W., and Garside, L.J., eds., New Concepts and Discoveries: Geological Society of Nevada 2015 Symposium Proceedings: Reno, Nevada, Geological Society of Nevada, p. 611–645.

John, D.A., du Bray, E.A., Box, S.E., Vikre, P.G., Rytuba, J.J., Fleck, R.J., and Moring, B.C., 2015b, Geologic Map of the Bodie Hills, California and Nevada: U.S. Geological Survey Scientific Investigations Map 3318, 64 p., 2 sheets, scale 1:50,000.

Keith, W.J., Dohrenwend, J.C., Guisso, J.R., and John, D.A., 1982, Geologic Map of the Carson-Iceberg and Leavitt Lake Roadless Areas, Central Sierra Nevada, California: U.S. Geological Survey Report MF-1416-A, scale 1:62,500.

Kent, G.M., Babcock, J.A., Driscoll, N.W., Harding, A.J., Seitz, G.G., Dingler, J.A., Gardner, J.V., Goldman, C.R., Heyvaert, A.C., Gayes, P., Karlin, R., Mayer, L.A., Morgan, C.W., Owen, L.A., and Richards, R.C., 2005, A 60 k.y. record of extension across the western boundary of the Basin and Range Province: Estimate of slip rates from offset shoreline terraces and a catastrophic slide beneath Lake Tahoe: Geology, v. 33, p. 365–368, https://doi.org/10.1130/G21230.1.

King, N.M., Hillhouse, J.W., Gromme, S., Hausback, B.P., and Pluhar, C.J., 2007, Stratigraphy, paleomagnetism, and anisotropy of magnetic susceptibility of the Miocene Stanislaus Group, central Sierra Nevada and Sweetwater Mountains, California and Nevada: Geosphere, v. 3, p. 646–666, https://doi.org/10.1130/GES00132.1.

Koerner, A.K., Busby, C.J., Putirka, K., and Pluhar, C.J., 2009, New evidence for alternating effusive and explosive eruptions from the type section of the Stanislaus Group in the "Cataract" palaeocanyon, central Sierra Nevada: International Geology Review, v. 51, p. 962–985, https://doi.org/10.1080/00206810903028185.

Kreemer, C., Blewitt, G., and Hammond, W.C., 2009. Geodetic constraints on contemporary deformation in the northern Walker Lane: 2. Velocity and strain rate tensor analysis, in Oldow, J.S., and Cashman, P.H., eds., Late Cenozoic Structure and Evolution of the Great Basin–Sierra Nevada Transition: Geological Society of America Special Paper 447, p. 17–31, https://doi.org/10.1130/2009.2447(02).

Kuo, L.C., and Kirkpatrick, R.J., 1982, Pre-eruption history of phyric basalts from DSDP Legs 45 and 46: Evidence from morphology and zoning patterns in plagioclase: Contributions to Mineralogy and Petrology, v. 79, p. 13–27, https://doi.org/10.1007/BF00376957.

Lange, R.A., and Carmichael, I.S.E., 1996, The Aurora volcanic field, California-Nevada: Oxygen fugacity constraints on the development of andesitic magma: Contributions to Mineralogy and Petrology, v. 125, p. 167–185, https://doi.org/10.1007/s004100050214.

Lawton, T.F., and McMillan, N.J., 1990, Arc abandonment as a cause for passive continental rifting: Comparison of the Jurassic Mexican Borderland rift and the Cenozoic Rio Grande rift: Geology, v. 27, p. 779–782, https://doi.org/10.1130/0091-7613(1999)027<0779:AAAACF>2.3.CO;2.

Lee, C.-T., Cheng, X., and Horodyskyj, U., 2006, The development and refinement of continental arcs by primary basaltic magmatism, garnet pyroxenite, accumulation, basaltic recharge, and delamination: Insights from the Sierra Nevada, California: Contributions to Mineralogy and Petrology, v. 151, p. 222–242, https://doi.org/10.1007/s00410-005-0056-1.

Lee, J., Stockli, D.F., Owen, L.A., Finkel, R.C., and Kislitsyn, R., 2009a, Exhumation of the Inyo Mountains, California: Implications for the timing of extension along the western boundary of the Basin and Range Province and distribution of dextral slip rates across the Eastern California shear zone: Tectonics, v. 28, TC1001, https://doi.org/10.1029/2008TC002295.

Lee, J., Garwood, J., Stockli, D., and Gosse, J., 2009b, Quaternary faulting in Queen Valley, California-Nevada: Implications for kinematics of fault slip transfer in the Eastern California shear zone–Walker Lane Belt: Geological Society of America Bulletin, v. 121, p. 599–614, https://doi.org/10.1130/B26352.1.

Lindgren, W., 1911, The Tertiary Gravels of the Sierra Nevada of California: Washington D.C., U.S. Geological Survey, 222 p.

Lizarralde, D., Axen, G.J., Brown, H.E., Fletcher, J.M., Gonzalez-Fernandez, A., Harding, A.J., Steven Holbrook, W., Kent, G.M., Paramo, P., Sutherland, F., and Umhoefer, P.J., 2007, Variation in styles of rifting in the Gulf of California: Nature, v. 448, p. 466–469, https://doi.org/10.1038/nature06035.

Mann, P., 2007, Global catalogue, classification and tectonic origins of restraining- and releasing bends on active and ancient strike-slip fault systems, in Cunningham, W.D., and Mann, P., eds., Tectonics of Strike-Slip Restraining and Releasing Bends: Geological Society of London Special Publication 290, p. 13–142, https://doi.org/10.1144/SP290.2.

Martín-Barajas, A., Stock, J.M., Layer, P., Hausback, B., Renne, P., and Lopez-Martinez, M., 1995, Arc-rift transition volcanism in the Puertecitos Volcanic Province, northeastern Baja California, Mexico: Geological Society of America Bulletin, v. 107, p. 407–424, https://doi.org/10.1130/0016-7606(1995)107<0407:ARTVIT>2.3.CO;2.

Miyoshi, M., Shimono, M., Hasenaka, T., Sano, T., Mori, Y., and Fukuoka, T., 2010, Boron systematics of Hiatsu and Kirishima basaltic rocks from southern Kyushu, Japan: Geochemical Journal, v. 44, p. 359–369, https://doi.org/10.2343/geochemj.1.0076.

Murphy, J.B., Keppie, J.D., Dostal, J., and Hynes, A.J., 1990, The geochemistry and petrology of the Late Precambrian Georgeville Group: A volcanic arc-rift succession in the Avalon terrane of Nova Scotia, in D'Lemos, R.S., Strachan, R.A., and Topley, C.G., eds., The Cadomian Orogeny: Geological Society of London Special Publication 51, p. 383–393.

Nagao, T., Hase, Y., Ikawa, T., Nagamine, S., Sakaguchi, K., Yamamoto, M., Shuto, K., and Hayashida, K., 1995, Characteristics of andesites forming lava plateaus in Kyushu, SW Japan: Proposal of "flood andesite": Geological Society of Japan Memoir 44, p. 155–164.

Nagao, T., Hase, Y., Nagamine, S., Kakubuchi, S., and Sakaguchi, K., 1999, Late Miocene to middle Pleistocene Hisatsu volcanic rocks generated from heterogeneous magma sources: Evidence from temporal-spatial variation of distribution and chemistry of the rocks: Journal of Mineralogy, Petrology and Economic Geology, v. 94, p. 461–481, https://doi.org/10.2465/ganko.94.461.

Nagorsen-Rinke, S., Lee, J., and Calvert, A., 2013, Pliocene sinistral slip across the Adobe Hills, eastern California–western Nevada: Kinematics of fault slip transfer across the Mina deflection: Geosphere, v. 9, p. 37–53, https://doi.org/10.1130/GES00825.1.

Nilsen, T.H., and Sylvester, A.G., 1995, Strike slip basins, in Busby, C.J., and Ingersoll, R.V., eds., Tectonics of Sedimentary Basins: Blackwell Science, p. 425–456.

Noble, D.C., Slemmons, D.B., Korringa, M.K., Dickinson, W.R., Al-Rawi, Y., and McKee, E.H., 1974, Eureka Valley Tuff, east-central California and adjacent Nevada: Geology, v. 2, p. 139–142, https://doi.org/10.1130/0091-7613(1974)2<139:EVTECA>2.0.CO;2.

Noble, D.C., Korringa, M.K., Church, S.E., Bowman, H.R., Silberman, M.L., and Heropoulos, C., 1976, Elemental and isotopic geochemistry of nonhydrated quartz latite glasses from the Eureka Valley Tuff, east-central California: Geological Society of America Bulletin, v. 87, p. 754–762, https://doi.org/10.1130/0016-7606(1976)87<754:EAIGON>2.0.CO;2.

Oldow, J.S., 1992, Late Cenozoic displacement partitioning in the northwestern Great Basin, in Craig, S.D., ed., Structure, Tectonics, and Mineralization of the Walker Lane: Walker Lane Symposium Proceedings Volume: Reno, Nevada, Geological Society of Nevada, p. 17–52.

Oldow, J.S., 2003, Active transtensional boundary zone between the western Great Basin and Sierra Nevada block, western U.S. Cordillera: Geology, v. 31, p. 1033–1036, https://doi.org/10.1130/G19838.1.

Oldow, J.S., Kohler, G., and Donelick, R.A., 1994, Low-angle displacement transfer system linking the Furnace Creek and Walker Lane fault zones, west-central Nevada: Geology, v. 22, p. 637–640, https://doi.org/10.1130/0091-7613(1994)022<0637:LCETIT>2.3.CO;2.

Oldow, J.S., Aiken, C.L.V., Hare, J.L., Ferguson, J.F., and Hardyman, R.F., 2001, Active displacement transfer and differential block motion within the central Walker Lane, western Great Basin: Geology, v. 29, p. 19–22, https://doi.org/10.1130/0091-7613(2001)029<0019:ADTADB>2.0.CO;2.

Oldow, J.S., Geissman, J.W., and Stockli, D.F., 2008, Evolution and strain reorganization within late Neogene structural stepovers linking the central Walker Lane and northern Eastern California shear zone, western Great Basin: International Geology Review, v. 50, p. 270–290, https://doi.org/10.2747/0020-6814.50.3.270.

Oldow, J.S., Elias, E.A., Prestia, V.I., Ferranti, L., and McClelland, W.C., 2009, Late Miocene to Pliocene synorogenic deposition during upper-plate fragmentation in the Silver Peak extensional complex, west-central Great Basin, in Oldow, J.S., and Cashman, P.H., eds., Late Cenozoic Structure and Evolution of the Great Basin–Sierra Nevada Transition: Geological Society of America Special Paper 447, p. 275–312, https://doi.org/10.1130/2009.2447(14).

Petronis, M.S., Geissman, J.W., and McIntosh, W.C., 2004, Transitional field clusters from uppermost Oligocene volcanic rocks in the central Walker Lane, western Nevada: Physics of the Earth and Planetary Interiors, v. 141, no. 3, p. 207–238, https://doi.org/10.1016/j.pepi.2003.12.004.

Petronis, M.S., Geissman, J.W., Oldow, J.S., and McIntosh, W.C., 2007, Tectonism of the southern Silver Peak Range: Paleomagnetic and geochronologic data bearing on the Neogene development of a regional extensional complex, central Walker Lane, Nevada, in Till, A.B., Roeske, S.M., Sample, J.C., and Foster, D.A., eds., Exhumation Associated with Continental Strike-Slip Fault Systems: Geological Society of America Special Paper 434, p. 81–106, https://doi.org/10.1130/2007.2434(05).

Petronis, M.S., Geissman, J.W., Oldow, J.S., and McIntosh, W.C., 2009, Late Miocene to Pliocene vertical-axis rotation attending development of the Silver Peak–Line Mountain displacement transfer zone, west-central Nevada, in Oldow, J.S., and Cashman, P.H., eds., Late Cenozoic Structure and Evolution of the Great Basin–Sierra Nevada Transition: Geological Society of America Special Paper 447, p. 215–254.

Petronis, M.S., Grondin, D., Castillo, G., Shields, S., Lindline, J., Romero, B., and Pluhar, C.J., 2016, The eastern Mono basin transtensional zone: New paleomagnetic and $^{40}Ar/^{39}Ar$ data bearing on the timing and extent of vertical axis block rotation associated with intercontinental deformation: San Francisco, California, American Geophysical Union, Fall Meeting 2016, abstract GP31B–1302.

Pluhar, C., Deino, A., King, N., Busby, C., Hausback, B., Wright, T., and Fischer, C., 2009, Lithostratigraphy, magnetostratigraphy, geochronology and radiometric dating of the Stanislaus Group, CA, and age of the Little Walker caldera, in Ernst, G., ed., The Rise and Fall of the Nevadaplano: International Geology Reviews, v. 51, no. 9–11, p. 873–899.

Priest, G.R., 1979, Geology and Geochemistry of the Little Walker Volcanic Center, Mono County, California [Ph.D. thesis]: Corvallis, Oregon, Oregon State University, 311 p.

Putirka, K.D., 2017, Down the crater: Where magmas are stored and why they erupt: Elements, v. 13, p. 11–16, https://doi.org/10.2113/gselements.13.1.11.

Putirka, K., and Busby, C.J., 2007, The tectonic significance of high K_2O volcanism in the Sierra Nevada, California: Geology, v. 35, no. 10, p. 923–926, https://doi.org/10.1130/G23914A.1.

Putirka, K., and Platt, B., 2012, Basin and Range volcanism as a passive response to extensional tectonics: Geosphere, v. 8, no. 6, p. 1274–1285, https://doi.org/10.1130/GES00803.1.

Putirka, K., Jean, M., Cousens, B., Sharma, R., Torres, G., and Carlson, C., 2012, Cenozoic volcanism in the Sierra Nevada and Walker Lane, California, and a new model for lithosphere degradation: Geosphere, v. 8, p. 265–291, https://doi.org/10.1130/GES00728.1.

Ransome, F.L., 1898, Some Lava Flows on the Western Slope of the Sierra Nevada, California: U.S. Geological Survey Bulletin 9, 71 p.

Renne, P.R., Swisher, C.C., Deino, A.L., Karner, D.B., Owens, T., and DePaolo, D.J., 1998, Intercalibration of standards, absolute ages and uncertainties in $^{40}Ar/^{39}Ar$ dating: Chemical Geology, v. 145, p. 117–152, https://doi.org/10.1016/S0009-2541(97)00159-9.

Renne, P.R., Balco, G., Ludwig, K.R., Mundil, R., and Min, K., 2011, Joint determination of ^{40}K decay constants and $^{40}Ar*/^{40}K$ for the Fish Canyon sanidine standard, and improved accuracy for $^{40}Ar/^{39}Ar$ geochronology [Reply]: Geochimica et Cosmochimica Acta, v. 75, p. 5097–5100, https://doi.org/10.1016/j.gca.2011.06.021.

Roelofs, A., 2004, Tertiary Magmatism near Sonora Pass: Arc and Non-Arc Magmatism in the Central Sierra Nevada, California [M.S. thesis]: Chapel Hill, North Carolina, University of North Carolina, 73 p.

Ryall, A.S., and Priestly, K., 1975, Seismicity, secular strain, and maximum magnitude in the Excelsior Mountains area, western Nevada and eastern California: Geological Society of America Bulletin, v. 86, p. 1585–1592, https://doi.org/10.1130/0016-7606(1975)86<1585:SSSAMM>2.0.CO;2.

Slemmons, D.B., 1953, Geology of the Sonora Pass Region [Ph.D. thesis]: Berkeley, California, University of California, 222 p.

Slemmons, D.B., 1966, Cenozoic Volcanism of the Central Sierra Nevada, California, in Bailey, E.H., ed., Geology of Northern California: California Division of Mines and Geology Bulletin 170, p. 199–208.

Smith, K.D., Keny, G.M., von Seggern, D.P., Driscoll, N.W., and Eisses, A., 2016, Evidence for Moho–lower crustal transition depth diking and rifting of the Sierra Nevada microplate: Geophysical Research Letters, v. 43, p. 10,738–10,744, https://doi.org/10.1002/2016GL070283.

Steiger, R.H., and Jäger, E., 1977, Subcommission on Geochronology: Convention on the use of decay constants in geo- and cosmochronology: Earth and Planetary Science Letters, v. 36, p. 359–362, https://doi.org/10.1016/0012-821X(77)90060-7.

Stock, J.M., and Lee, J., 1994, Do microplates in subduction zones leave a geological record?: Tectonics, v. 13, p. 1472–1487, https://doi.org/10.1029/94TC01808.

Stockli, D.F., Dumitru, T.A., McWilliams, M.O., and Farley, K.A., 2003, Cenozoic tectonic evolution of the White Mountains, California and Nevada: Geological Society of America Bulletin, v. 115, p. 788–816, https://doi.org/10.1130/00167606(2003)115<0788:CTEOTW>2.0.CO;2.

Tincher, C.R., and Stockli, D., 2009, Cenozoic volcanism and tectonics in the Queen Valley area, Esmeralda County, western Nevada, in Oldow, J.S., and Cashman, P.H., eds., Late Cenozoic

Structure and Evolution of the Great Basin–Sierra Nevada Transition: Geological Society of America Special Paper 447, p. 225–274.

Tsuchiyama, A., 1985, Dissolution kinetics of plagioclase in the melt of the system diopside-albite-anorthite, and origin of dusty plagioclase in andesites: Contributions to Mineralogy and Petrology, v. 89, p. 1–16, https://doi.org/10.1007/BF01177585.

Umhoefer, P.J., 2011, Why did the southern Gulf of California rupture so rapidly?: Oblique divergence across hot, weak lithosphere along a tectonically active margin: GSA Today, v. 21, no. 11, p. 4–10, https://doi.org/10.1130/G133A.1.

Unruh, J.R., Humphrey, J., and Barron, A., 2003, Transtensional model for the Sierra Nevada frontal fault system, eastern California: Geology, v. 31, p. 327–330, https://doi.org/10.1130/0091-7613(2003)031<0327:TMFTSN>2.0.CO;2.

Wakabayashi, J., 2013, Paleochannels, stream incision, erosion, topographic evolution, and alternative explanations of paleoaltimetry, Sierra Nevada, California: Geosphere, v. 9, no. 2, p. 191–215, https://doi.org/10.1130/GES00814.1.

Wesnousky, S.G., 2005, The San Andreas and Walker Lane fault systems, western North America: Transpression, transtension, cumulative slip and the structural evolution of a major transform plate boundary: Journal of Structural Geology, v. 27, no. 8, p. 1505–1512, https://doi.org/10.1016/j.jsg.2005.01.015.

Wesnousky, S.G., Bormann, J.M., Kreemer, C., Hammond, W.C., and Brune, J.N., 2012, Neotectonics, geodesy, and seismic hazards in the northern Walker Lane of western North America: Thirty kilometers of crustal shear and no strike-slip?: Earth and Planetary Science Letters, v. 329–330, p. 133–140, https://doi.org/10.1016/j.epsl.2012.02.018.

Wilshire, H.G., 1957, Propylitization of Tertiary volcanic rocks near Ebbetts Pass, Alpine County, California: University of California Publications in Geological Sciences, v. 32, no. 41, p. 243–271, scale 1:68,500.

Yamaji, A., 1990, Rapid intra-arc rifting in Miocene northeast Japan: Tectonics, v. 9, p. 365–378, https://doi.org/10.1029/TC009i003p00365.